AKUSTIKA

odborný časopis o akustice a vibracích

Volume 50
July
2026

Studio D - akustika s.r.o.

CONTENT/OBSAH

PARTICULAR ANALYSIS OF SOUND SIGNALS ON DEVICE YAMAHA PSR E463

[a)] Tomas Barot, [a)] Ladislav Rudolf, [b)] Marek Kubalcik, [a)] Radek Krpec

[a)] Faculty of Education, University of Ostrava,
Frani Sramka 3, Ostrava, Czech Republic,
tomas.barot@osu.cz, ladislav.rudolf@osu.cz, radek.krpec@osu.cz

[b)] Faculty of Applied Informatics, Tomas Bata University,
Nad Stranemi 4511, Zlin, Czech Republic, kubalcik@utb.cz

ABSTRACT

The mathematical statistics fulfils a significant role in our lives. The multidisciplinary impact can be seen in a wide spectrum of areas e.g. engineering, medicine, humanity sciences. In this article, the particular analysis of sound signals is presented. The proposed analyses are bound on device Yamaha PSR E463. The methods of mathematical induction are utilized on data of software Audacity. The spectral density function is measured. The confidence intervals of descriptive aspects of them are achieved. The normality of data of spectral density signals is proposed. Autocorrelations, cross correlations of spectral density functions are drawn. In accordance of normality of data, then the multiple sample tests ANOVA or Kruskal-Wallis's test are used. For purposes of paired testing of two spectral density functions, the Mann-Whitney test or Wilcoxon paired test is used. The main idea of the article can transfer, that particular statistical analysis can be useful and suitable tool, how to understand the context of the applied acoustics.

1. INTRODUCTION

The mathematical statistics [1-12] fulfils a significant role in our lives. The multidisciplinary impact can be seen in a wide spectrum of areas e.g. engineering [13-24], medicine [25], humanity sciences [26-38]. The difference is based on statistical significance level alpha [39]. For purposes of quantitative humanity science research is determined alpha as 0.05. In an area of engineering is 0.01 and in medicine is 0.001.

In the quantitative research, the p-value [40] is obtained. The p-value is then compared with the statistically significant level alpha. If the p-value is greater than alpha, then the zero hypothesis is failed to be rejected. In the opposite case, the zero hypothesis is rejected in favour of the alternative hypothesis. The hypotheses can be focused on testing the normality of data [41], determination of confidence intervals [42], paired testing [43], two-sample or higher-sample tests [44].

In this sense of testing hypotheses, the paired comparation [43] can be useful. If data fulfils the normality [41], then the paired T-test [43] is used. In the opposite case, the Wilcoxon paired test [43] is applied. In the acoustic research, the comparison of two signals can be appropriate. Where the normality test [41] is Shapiro-Wilk test.

The declaration of included frequencies can be obtained in the form of spectral density functions [45]. This information can help to understand the background of structure of the sound signals [46-50]. This data can be achieved in the form of exported table in the sound software e.g. Audacity [51].

In this article, the particular analysis of sound signals is presented, as cannot be widely seen. The proposed analyses are bound on device Yamaha PSR E463. The methods of mathematical induction are utilized on data of software Audacity and provided in the statistical software PAST Statistics 5.0.

The spectral density function [45] is measured. The confidence intervals of descriptive aspects [42] of them are achieved. The normality of data [41] of spectral density signals [45] is proposed.

For purposes of obtained data of signal boundness, the autocorrelations [52], cross correlations [53] of spectral density functions are drawn. In accordance of normality of data, then the multiple sample tests ANOVA or Kruskal-Wallis's test [44] are used. For purposes of paired testing of two spectral density functions, the paired T-test or Wilcoxon paired test is used.

The main idea of the article can transfer, that particular statistical analysis can be useful and suitable tool, how to understand the context of the applied mathematics.

2. METHODS

The methodology background is based on the principles, which can be seen in the frame of the quantitative research [1-12]. In the case of presented methods, the system of comparison the p-value [40] with the significance level [39] is utilized. With regards to these comparisons, the acceptation or rejection of a zero hypothesis is appeared. Whether the p-value is greater than statistically significance level, then the zero hypothesis is accepted. In the opposite case, the zero hypothesis is rejected in favour of the alternative hypothesis. In the humanities areas [26-38], the level is 0,05. In the engineering sciences [13-24], the level is 0,01. And, in the medicine [25], the level is 0,001. Before testing the hypotheses, the normality [41] of input data must be measured. For these purposes, the Shapiro-Wilk or Anderson-Darling test [41] is applied. For the normal distributed data and for non-normal distributed data, the other tests of hypotheses are used. Whether data fulfils the normality assumption, the parametrical test are used. In the opposite case, the non-parametrical tests are proceeded. In the article, tests of normality, two and higher sample tests [44], two sample paired tests [43] are processed. For two sample tests, are T+F test or Mann-Whitney test [44] are considered. For higher sample test, the ANOVA or the Kruskal-Wallis [44] tests are bounded. For two sample paired tests, the paired T test or the Wilcoxon paired test [43] are used.

In the software Audacity [51], the spectral density function [45] of input sound signals [46-50] is measured. The spectral density functions can characterize and analyse the included obtained frequencies of proposed signals. The accords C dur, D dur, F dur and a mol are further analysed for the change repertoire – for a piano, for a flute and for a saxophone. Each tool is measured alone, and the global comparison is offered. The source of signals is the Yamaha keyboard PSR 463, which is connected with the computer by the USB connection. From the Audacity software, data is exported to the text format, which includes two columns: the frequency and the spectral density function. Then data can be imported to the software MS Excel and to the software PAST Statistics.

The analysis in MS Excel is the graphical interpretation of the spectral density functions across the tools and accords. In the software PAST Statistics, the normality tests [41], bootstrap statistical characteristics [42] considered on the confidence intervals, the autocorrelation functions [52], the cross-correlation functions [53] and the cluster analysis [54] is processed.

At first, the spectral density functions are drawn in plots in MS Excel, for pairs C dur & D dur, C dur & F dur, C dur & a mol in case of input sound of the piano, the flute and the saxophone. These pairs are analysed in software PAST Statistics on the normality, bootstrap pointers on the confidence sense, Mann-Whitney test and Wilcoxon paired test. For the considered pairs, the autocorrelation and cross-correlation function is drawn by PAST. Then these pairs of autocorrelation functions are compared by the Wilcoxon paired test after analysis of normality.

For the accords C dur, D dur, F dur and a mol, the tools piano, flute and saxophone are considered as higher samples of the spectral density functions. Therefore, the Kruskal-Wallis test is applied. For the descriptive characteristics of tools, the cluster analysis for each accord is then provided. On the plot of this cluster analysis the neighbourhood sources can be classified. All these tests are computed in the software PAST Statistics 5.0, which is free available.

3. RESULTS AND DISCUSSION

In this section, source signals from piano (Subsection 3.1), flute (Subsection 3.2) and saxophone (Subsection 3.3) are analysed using by the spectral density functions. These spectral density functions are further compared using by Wilcoxon paired tests. In the next step, the autocorrelation function of the spectral density functions is drawn and compared also by the Wilcoxon paired tests. In the subsections **3.1 – 3.3**, the pairs of spectral density functions of signals C dur & D dur, C dur & F dur, C dur & a mol are analysed. In the **Subsection 3.4**, the global analysis is proposed in favour of Kruskal-Wallis test comparisons and the cluster analysis.

3.1. PIANO

For the source signal of piano, the bootstrap confidence intervals can be seen in **Table 1** for C & D Dur. For these accords the spectral density functions (**Figure 1**) are similar on the statistically significant level 0.05, which can be achieved after provided Mann-Whitney (**Table** 3) and Wilcoxon paired test (**Table 4**). Normality tests (**Table 2**) are negative.

	C Dur	Lower conf.	Upper conf.	**D Dur**	Lower conf.	Upper conf.
N	**511**	511	511	**511**	511	511
Mean	**-104,538**	-106,1708	-102,9397	**-103,889**	-105,5252	-102,3242
Std. error	**0,81259**	0,7347702	0,883549	**0,817785**	0,7416558	0,8858625
Variance	**337,4148**	275,8824	398,9166	**341,7427**	281,0772	401,0084
Stand. dev	**18,36885**	16,76404	20,12708	**18,48628**	16,91245	20,16552
Median	**-113,983**	-114,2116	-113,819	**-113,897**	-114,3619	-113,635
Skewness	**1,852378**	1,561453	2,107275	**1,739381**	1,476253	1,978305
Kurtosis	**2,447188**	1,049602	3,504339	**2,038577**	0,8378013	2,993161

Tab. 1. Bootstrap Confidence Intervals for C & D Dur.

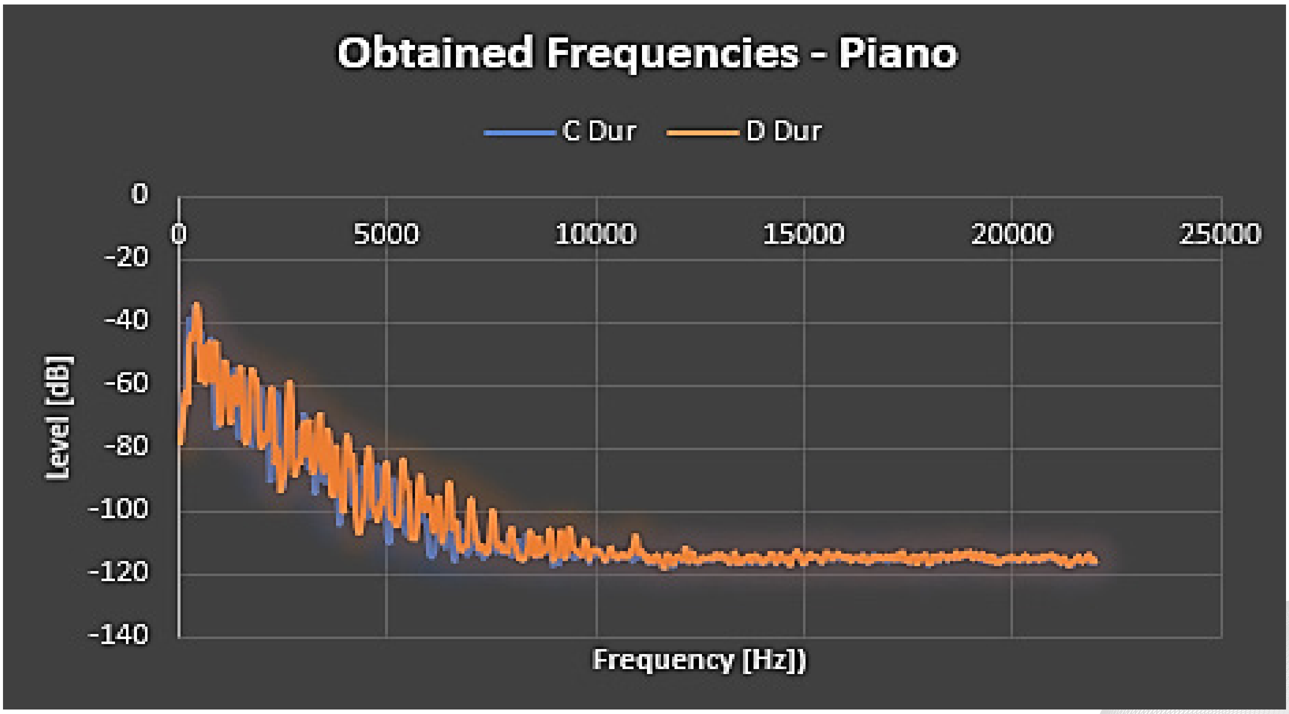

Fig. 1. Spectral Density Functions of C Dur & D Dur

	C Dur	D Dur
N	511	511
Shapiro-Wilk	0,66	0,6885
p(normal)	1,16E-30	1,28E-29
Anderson-Darling	74,19	66,71
p(normal)	8,59E-140	9,24E-130
p(Monte Carlo)	0,0001	0,0001
Lilliefors L	0,3161	0,2895
p(normal)	0,0001	0,0001
p(Monte Carlo)	0,0001	0,0001
Jarque-Bera JB	414,3	341,9
p(normal)	1,06E-90	5,67E-75
p(Monte Carlo)	0,0001	0,0001

Tab. 2. Achieved Negative Normality Tests

C Dur	**D Dur**		
N:	511	N:	511
Mean rank:	253,23	Mean rank:	258,27
Mann-Whitney test for stochastic equality			
U :	1,28E+05		
z :	0,54619	p (equal):	0,58493
Monte Carlo permutation:	p (equal):	0,5847	

Tab. 3. Mann-Whitney Test with Confirmation of Similarities of C&D Dur

For the spectral density functions of C & D Dur were drawn the autocorrelation functions (**Figure 2**) and one cross-correlation function (**Figure 3**). Here can be seen similarities, which can be seen also in the **Table 5** as achieved results of Wilcoxon paired test.

C Dur	**D Dur**		
N:	511		
Mean:	-104,54	Mean:	-103,89
Median:	-113,98	Median:	-113,9
Wilcoxon test for stochastic equality :			
W :	62167		
Normal appr. z :	-0,97051	p (equal):	**0,33179**
Monte Carlo (n=99999):	p (equal):	0,33299	
Exact test not executed (N>22)			
Vargha-Delaney A effect size:	0,5029 (small)		

Table 4. Wilcoxon Paired Test with Confirmation of Similarities of C&D Dur

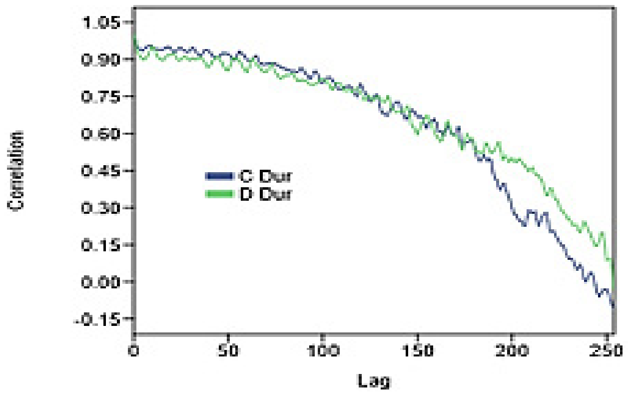

Fig. 2. Autocorrelation Functions of C & D Dur Signals

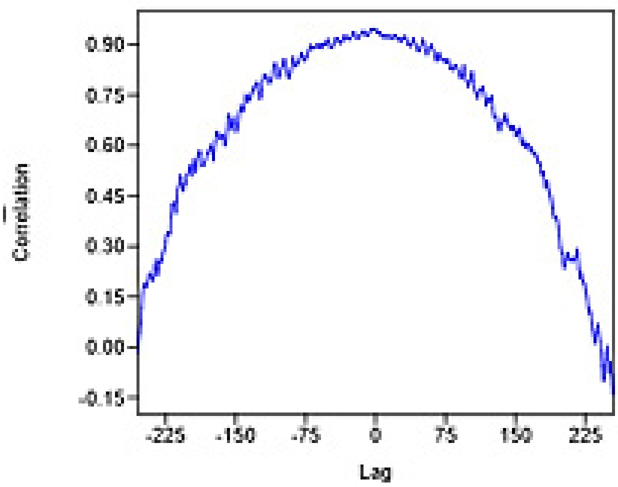

Fig. 3. Cross-Correlation Function of C & D Dur Signals

For the spectral density functions of C & F Dur (**Figure 4**), and C Dur & a mol (**Figure 5**) did not identified the similarities using by Mann-Whitney (p-value 0,00052204) and Wilcoxon paired tests (p-value 3,8997E-32). Also, similarities across the autocorrelation functions (**Figure 6 - 7**) were not obtained (p-value < 0,05).

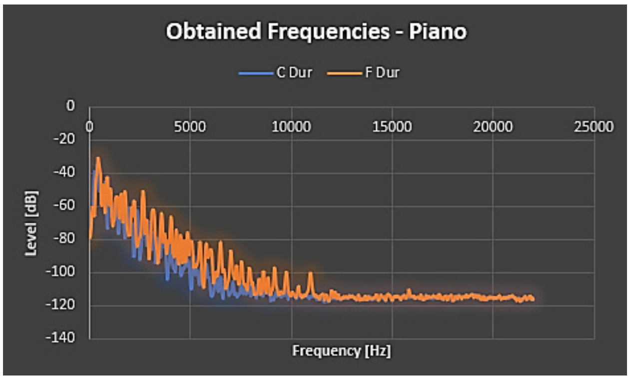

Fig. 4. Spectral Density Functions of C & F Dur

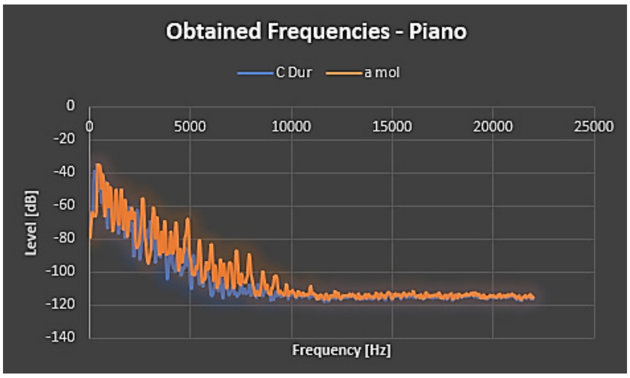

Fig. 5. Spectral Density Functions of C Dur & a mol

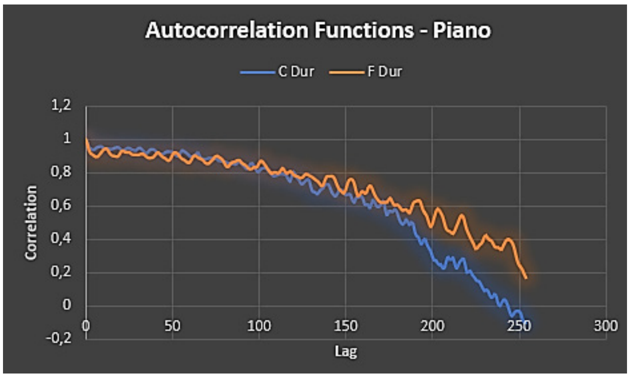

Fig. 6 Autocorrelation Functions of Spectral Density Function of C Dur & F Dur

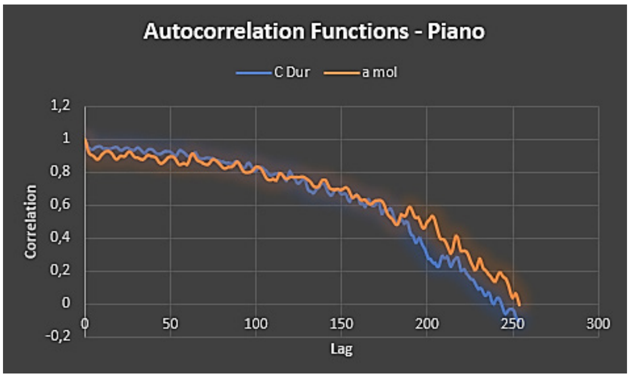

Fig. 7. Autocorrelation Functions of Spectral Density Function of C Dur & a mol

3.1. FLUTE

For the spectral density functions of C & D Dur (**Figure 8**), C & F Dur (**Figure 9**), and C Dur & a mol (**Figure 10**) did not identified the similarities using by Mann-Whitney (p-value <0,05) and Wilcoxon paired tests (p-value <0,05). Also, similarities across the autocorrelation functions (**Figure 11 - 13**) were not obtained (p-value < 0,05).

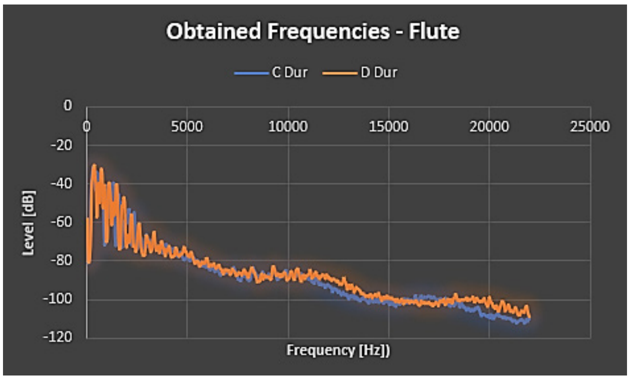

Fig. 8. Spectral Density Functions of C & D Dur

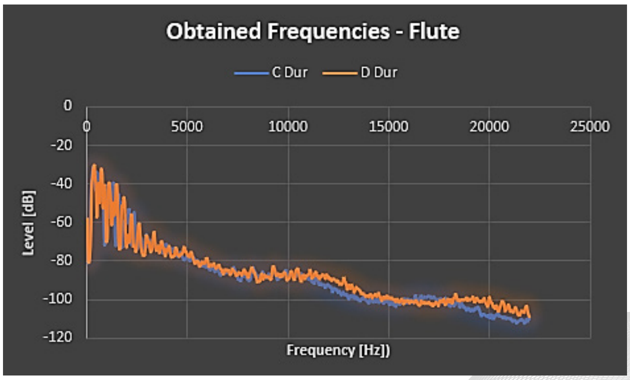

Fig. 9. Spectral Density Functions of C & F Dur

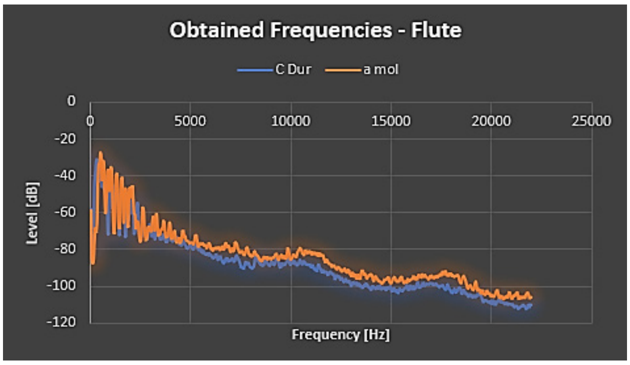

Fig. 10. Spectral Density Functions of C Dur & a mol

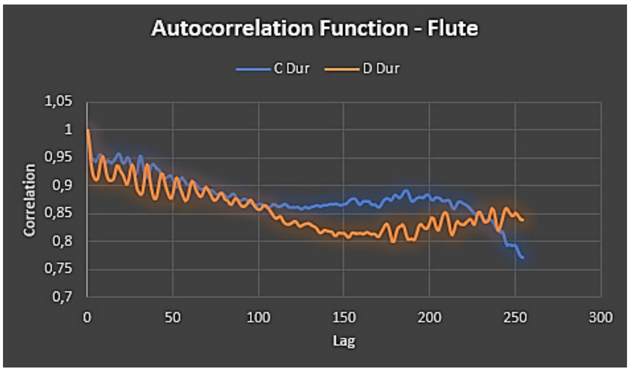

Fig. 11. Autocorrelation Functions of Spectral Density Function of C & D Dur

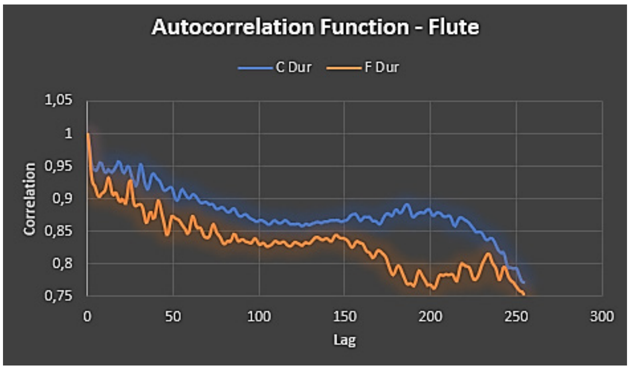

Fig. 12. Autocorrelation Functions of Spectral Density Function of C & F Dur

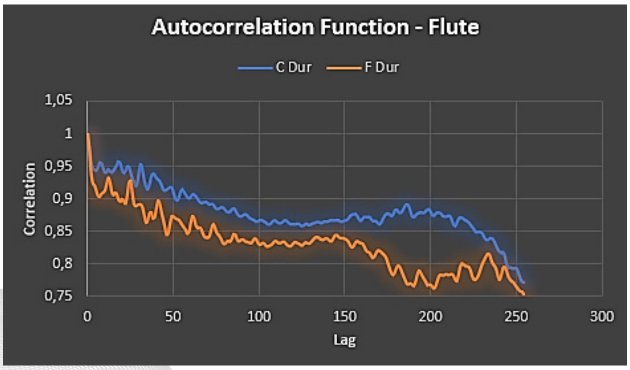

Fig. 13. Autocorrelation Functions of Spectral Density Function of C Dur & a mol

3.3. SAXOPHONE

For the spectral density functions of C & D Dur (**Figure 14**), C & F Dur (**Figure 15**), and C Dur & a mol (**Figure 16**) did not identified the similarities using by Mann-Whitney (p-value <0,05) and Wilcoxon paired tests (p-value <0,05). Also, similarities across the autocorrelation functions (**Figure 17 - 19**) were not obtained (p-value < 0,05).

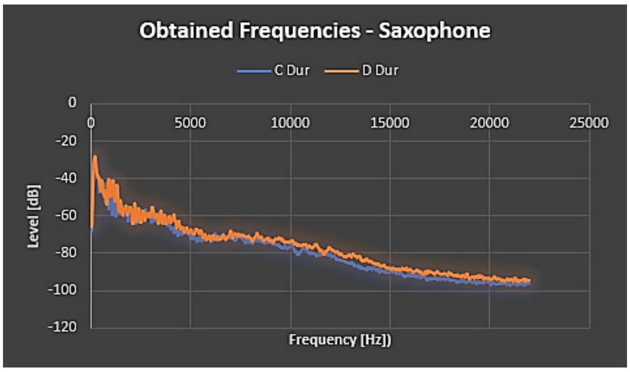

Fig. 14. Spectral Density Functions of C & D Dur

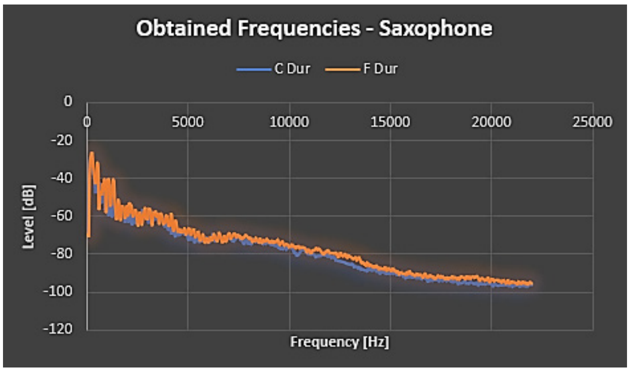

Fig. 15. Spectral Density Functions of C & F Dur

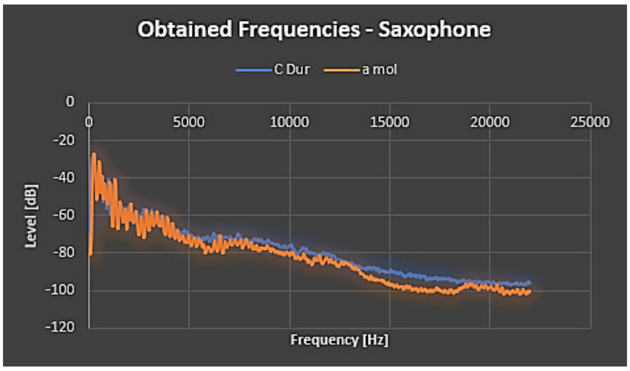

Fig. 16. Spectral Density Functions of C Dur & a mol

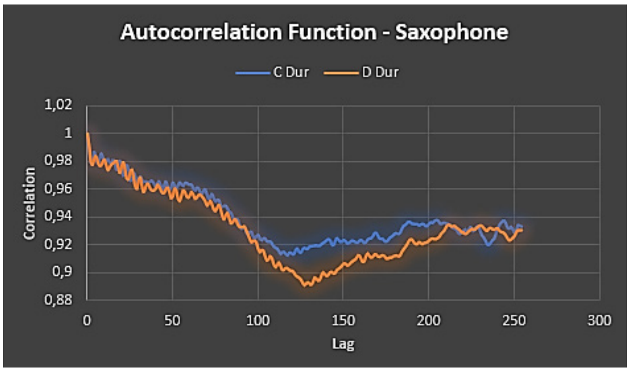

Fig. 17. Autocorrelation Functions of Spectral Density Function of C & D Dur

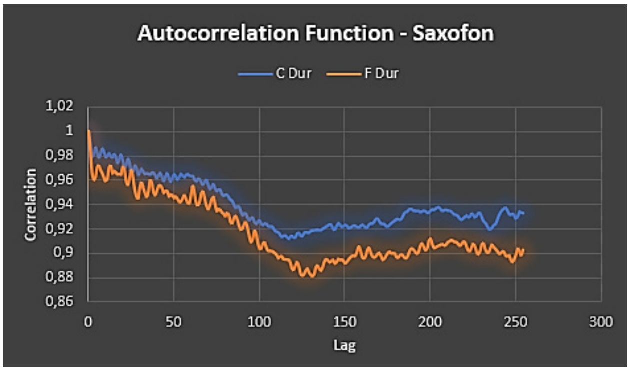

Fig. 18. Autocorrelation Functions of Spectral Density Function of C & F Dur

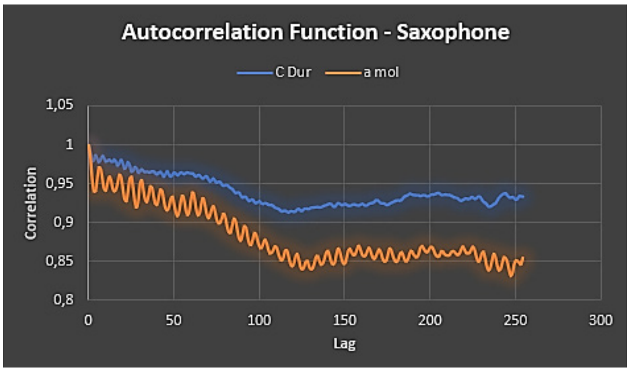

Fig. 19. Autocorrelation Functions of Spectral Density Function of C Dur & a mol

3.4. GLOBAL ANALYSIS

For the spectral density functions of C Dur (**Figure 20**), D Dur (**Figure 21**), F Dur (**Figure 22**) and a mol (**Figure 23**), the differences across source of signals Piano, Flute and Saxophone were compared using by Kruskal-Wallis tests with result of p-value <0,05.

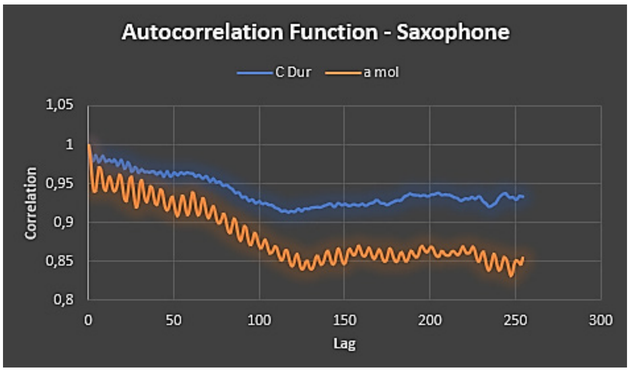

Fig. 20. Spectral Density Functions of Sources across C Dur

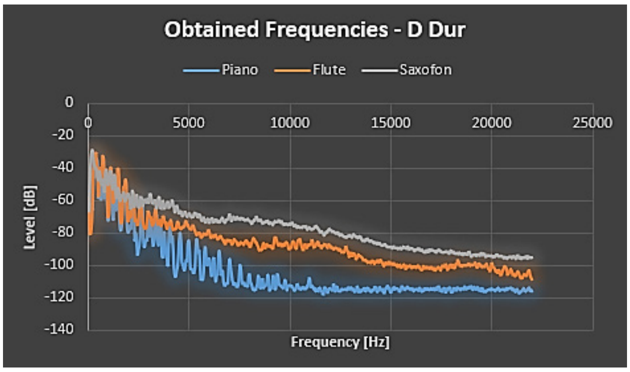

Fig. 21. Spectral Density Functions of Sources across D Dur

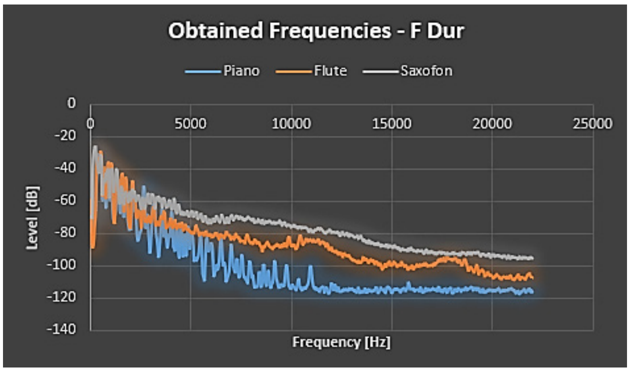

Fig. 22. Spectral Density Functions of Sources across F Dur

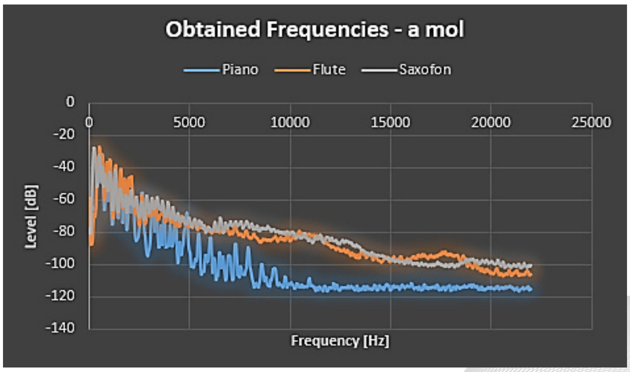

Fig. 23. Spectral Density Functions of Sources across a mol

The similarities of sound sources across accords can be systematically drawn using by Cluster analysis (**Figure 24**), where the Euclidean distances was measured. Positively, the groups are corresponding the aim of this work.

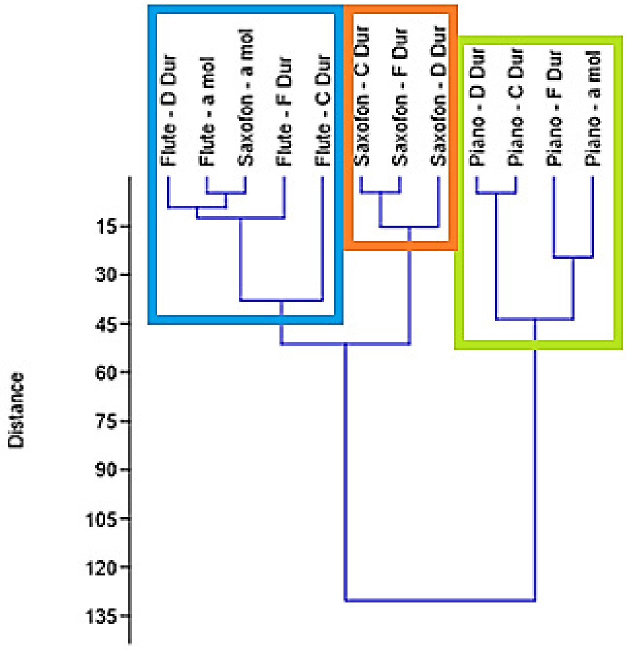

Fig. 24. Cluster Analysis Across Sound Sources and Accords

4. CONCLUSION

Across signal sources of device Yamaha PSR E463 (Piano, Flute, Saxophone), the statistically significant similarities were identified on the significance level 0,05. The particularly based signals were accords C Dur, D Dur, F Dur and a mol. The spectral density functions of these signals were measured by the software Audacity. The autocorrelation functions of spectral densities were computed using by software PAST Statistics 5.0, when all statistical tests were also provided in this tool. **Similarities** were identified by **Piano C & D Dur**, where p-value was > 0,05. The bootstrap confidence intervals were measured for the spectral density function, also the normality of data was presented. The similarities were identified using by the Mann-Whitney and Wilcoxon paired tests. Also, the positive result was achieved by comparison of autocorrelation functions of spectral density functions. Repeatedly, the Wilcoxon paired test obtained positive results. Other sound sources across accords were **negative** with statistical computations of described tests on the p-value < 0,05. In the sense of global comparison, also the outputs were in the Kruskal-Wallis test rejected. More positively, the cluster analysis was obtained, where the sources across accords were grouped systematically. The main idea of this article was to point on possibilities of the statistical computations in the area of processing the sound signals.

References

1. Shitakova O, Guskov A, Gorbacheva N, Orlov, R, Sidorina T. Mathematical statistics in research: pedagogical aspect. Professional education in the modern world. 2025; 15: 324-334. doi:10.20913/2618-7515-2025-2-14

2. Binh C, Tran BD, Hung H, Phuong T, Quynh N. Textbook of Probability Theory and Mathematical Statistics. 2025.

3. Wang Y. The Application of Probability Theory and Mathematical Statistics in Economic Life. Highlights in Business Economics and Management. 2025; 55: 19-23. doi:10.54097/30a36f34.

4. Lewis L. Solving a Research Problem in Mathematical Statistics with AI Assistance. 2025. doi:10.48550/arXiv.2511.18828.

5. Cejes J. Mathematical modeling approach in teaching Statistics and Probability. International Journal of Science and Research Archive. 2025; 16: 839-851. doi:10.30574/ijsra.2025.16.2.2382.

6. Kumar D. Foundations and Applications of Mathematical Statistics: A Theoretical and Prac-

tical Perspective. Knowledgeable Research A Multidisciplinary Journal. 2025; 4: 34-41. doi:10.57067/pq8w3n17.

7. Behera J. Foundations of Mathematical Analysis for Statistics. 2025

8. Fanolong F, Hamdi S. Designing Contextual Mathematical Literacy Task to Enhance Junior High School Students' Understanding of Statistics. International Journal of Mathematics And Computer Research. 2025; 13. doi:10.47191/ijmcr/v13i11.11.

9. Shcherbatykh S, Lykova K, Igonina E, Simonovskaya G. Development of cognitive mobility when teaching probability theory and mathematical statistics to students using digital solutions. Perspectives of science and Education. 2025; 74: 175-192. doi:10.32744/pse.2025.2.12.

10. Velkoska A, Marina N, Hristov A, Sandjakoska, L. Mathematical-Statistics-with-examples-in-R. 2025.

11. Egamov M, Sharipov E, Shodiev S, Abdiraxmonov A. Application of mathematical modeling in probability theory and mathematical statistics. E3S Web of Conferences. 2024; 583. doi:10.1051/e3sconf/202458306017.

12. Ballani F, Stoyan D. Statistics for simulated assemblies of particles from mathematical models. Granular Matter. 2025; 27. doi:10.1007/s10035-025-01519-6.

13. Ryohei K. Generalized Statistics on Lattices. Physical Review X. 2025;16. doi:10.1103/6k88-w52n.

14. Mitchell H. Robust Statistics. 2025. doi:10.1007/978-3-662-71023-4_12.

15. Puts M, Salgado D. Leveraging Machine Learning for Official Statistics. 2025. doi:10.1007/978-3-032-10004-7_2.

16. Feng Y, Xue H, Li Y, Cheng M, Kobayashi R, Hsin PS, Chen YA. Anyonic membranes and Pontryagistatistics. 2025. doi:10.48550/arXiv.2509.14314.

17. Madusanka HKS. Statistics Jumpstart for Agricultural Research. 2025. doi:10.5281/zenodo.17697097.

18. Takada Y, Izumi K. Machine Learning for the Production of Official Statistics: Density Ratio Estimation using Biased Transaction Data for Japanese labor statistics. 2025. 10.48550/arXiv.2510.24153.

19. Kurisu D, Okamoto Y, Otsu T. Random sets from the perspective of metric statistics. 2025. doi:10.48550/arXiv.2511.13440.

20. Namburi JC. Statistics in 3d gravity from knots and links. Journal of High Energy Physics. 2025. doi:10.1007/JHEP12(2025)139.

21. Magiera J. UAV Classification Based on Statistics of RF Transmissions. Applied Sciences. 2026; 16: 499. doi:10.3390/app16010499.

22. Dai Z, Tseng L, Faeth G. Velocity Statistics of Round, Fully-Developed, Buoyant Turbulent Plumes. 2025: 47-54. doi:10.1115/IMECE1994-0609.

23. Lee M, Haiman Z, Pandey S, Genel S. The Effect of Intrinsic Alignments on Weak-lensing Statistics in Hydrodynamical Simulations. The Astrophysical Journal. 2025; 996: 36. doi:10.3847/1538-4357/ae1ca7.

24. Yilmaz D. Sustainability in the Cosmetics Industry: Environmental Impacts, Statistics, and Solutions. 2025. doi:10.58830/ozgur.pub862.c3490.

25. Sterba A, Sedova P, Brown R, Stehlik A, Bryndziar T, Cimflova P, Zvolsky M, Belaskova S, Kovacova I, Bednarik, J, Mikulik R. Predictors of spontaneous intracerebral hemorrhage mortality: a community-based study in Brno, Czech Republic. Acta neurologica Belgica. 2024; 124. doi:10.1007/s13760-024-02612-y.

26. Vaclavik M, Tomasek M, Cervenkova I, Baarova B. Analysis of Quality Teaching and Learning from Perspective of University Students. Education Sciences. 2022; 12: 1-11. doi:10.3390/educsci12110820.

27. Vaclavik M, Sikorova Z, Cervenkova I. Analysis of Independences of Normality on Sample Size with Regards to Reliability. 2019. doi:10.1007/978-3-030-31362-3_29.

28. Burkovicova R, Simik O. Preschool Teachers and Digital Technologies: Evidence of a U-Shaped Experience Effect. International Journal of Instruction. 2026; 19: 705-718. doi:10.29333/iji.2026.19136a.

29. Simik O. Analysis of Visual Components in Czech History Textbooks for Lower Grades of Elementary Schools. 2021. doi:10.1007/978-3-030-80346-9_10.

30. Simik O. Learning Tasks in Natural Science Textbooks as a Tool for Pupil´s Development of Scientific Literacy. ACTA UNIVERSITATIS MATTHAEI BELII. 2025; 15.

31. Kargerova P, Gobelova T, Simlova Z, Seberova A. The WANDA Reflective Method as a Tool for Improving Teachers' Well-being. Revija za elementarno izobraževanje. 2025; 18: 169. doi:10.18690/rei.5403.

32. Harsa P, Merica M, Gregor T, Kaplanova A, Kufa T, Brenova M. Bossing - problematic and pathological interactions at workplace in public healthcare sector. Psychiatrie pro praxi. 2023; 24: 156-160. doi:10.36290/psy.2023.029.

33. Jandacka D, Skypala J, Plesek J, Urbaczka J, Golian M, Burda M, Sustek J, Zahradnik D, Elavsky S, Jandackova V, Selbie S, Silvernail J, Hamill J. Biomechanical insights into Achilles tendinopathy risk and protection in runners: a large prospective study 4HAIE. British Journal of Sports Medicine. bjsports-2025. 2025. doi:10.1136/bjsports-2025-110260.

34. Farana R, Brtva P, Irwin G, Newell K. Neck Angle in the Handstand Changes the Pattern of Multi-Joint Variability. Journal of motor behavior. 2025; 57: 1-9. doi:10.1080/00222895.2025.2558711.

35. Nian Z, Chudy S. International comparative study of standards for new teacher's professional development. e-Pedagogium. 2022; 22: 36-50. doi:10.5507/epd.2022.003.

36. Zavodna M, Havlaskova T, Javorcik T, Kostolanyova K. Hybrid Learning Through the Eyes of Current Lower Secondary School Teachers: A Pilot Study. European Conference on e-Learning. 2025; 24: 379-384. doi:10.34190/ecel.24.1.3802.

37. Barot T, Kostolanyova K, Simonova I, Javorcik T, Krpec R, Kubalcik M. Chi-Squared Test Particularly Modified by Paired Test. System Design in Software Engineering. 2025. doi:10.1007/978-3-031-94770-4_31

38. Korenova L, Krpec R, Barot T. Digital Technologies in Primary Mathematics Education: Insights from Future Teachers' Portfolios. European Conference on e-Learning. 2024; 23(1):197-208. doi:10.34190/ecel.23.1.2929

39. Barot T, Vaclavik M, Seberova A. Particular Analysis of Regression Effect Sizes Applied on Big Data Set. Proceedings of the Computational Methods in Systems and Software. 2024. doi:10.1007/978-3-031-53552-9_18

40. Barot T, Lackova L. Confirmation of Cybernetical Modelling in Applied Research of Resilience. Informatics and Cybernetics in Intelligent Systems. 2021. doi:10.1007/978-3-030-77448-6_24

41. Vaclavik M, Sikorova Z, Barot T. Skewness in Applied Analysis of Normality. Advances in Intelligent Systems and Computing. 2020. doi:10.1007/978-3-030-63319-6_86

42. Zaragoza A, Guillermo A. Descriptive statistics manual. Definition and exercises. 2025. doi:10.62486/978-628-97230-1-4.

43. Barot T, Krpec R, Kubalcik M. Applied Quadratic Programming with Principles of Statistical Paired Tests. Advances in Intelligent Systems and Computing. 2019. doi:10.1007/978-3-030-31362-3_27

44. Kutac P, Jandacka D, Elavsky S, Uchytil J, Bunc V, Krajcigr M, Barot T. The effect of regular running on the bone tissue of middle-aged men and women. The Journal of sports medicine and physical fitness. 2024; 64(5). doi:10.23736/S0022-4707.23.15279-0

45. Barot T, Rudolf L, Bernat M. Spectral Density Functions Compared by Wilcoxon Paired Test. 21st Century Computer Science - Challlenges and Dilemmas. 2025: 137-145.

46. Zhang X. Spectral statistics and wave-chaos transition in three-dimensional acoustic cavities. Chinese Physics B. 2026. doi:10.1088/1674-1056/ae3555.

47. Limon J, Kamruzzaman ARM, Rahman M, Hussain S. Vehicular Sound and Its Consequence on Sound Pollution in Industrial and Commercial Zone of Sylhet City. Feni University Journal. 2026; 3: 31-42. doi:10.3329/fuj.v3i1.86547.

48. Troshkina O, Troshkin A, Gnatiuk L, Shevchenko L, Novoselchuk N. Sound studies of the architectural environment: urban soundscape and sound semantics. Landscape Architecture and Art. 2026; 27: 18-24. doi:10.22616/j.landarchart.2025.27.02.

49. Rittenschober T, Decloux A. Localization and Sound Power Estimation of Sound Sources in Industrial Plants using the Sound Field Scanning Method. INTER-NOISE and NOISE-CON Congress and Conference Proceedings. 2025; 272: 462-474. doi:10.3397/IN_2025_1070999.

50. Rindel J. Sound insualtion measurements according to ISO standards. Noise News International. 2025: 27-31.

51. Fikri S, Kirom M,, Al-Furqaan D. Audacity: Learning Media Design in Listening Skills for Arabic Special Development Program. International Journal of Arabic Language Teaching. 2024; 6: 1-18. doi:10.32332/ijalt.v6i01.7935.

52. Barot T, Burgsteiner H, Kolleritsch W. Comparison of Discrete Autocorrelation Functions with Regards to Statistical Significance. Advances in Intelligent Systems and Computing. Applied Informatics and Cybernetics in Intelligent Systems. 2020. doi:10.1007/978-3-030-51974-2_24

53. Barot T, Rudolf L, Kubalcik M. Applied Analysis of Differences by Cross-Correlation Functions. Proceedings of the Computational Methods in Systems and Software. 2024. doi:10.1007/978-3-031-53552-9_19

54. Backhaus K, Erichson B, Gensler S, Weiber R, Weiber T. Cluster Analysis. 2025. doi:10.1007/978-3-658-47931-2_8.

Ing. Tomáš Barot, Ph.D.

He works at University of Ostrava. His area is applied statistics and application in education. He is an associate professor. He publishes in applied statistics and in educational sciences. He teaches the courses bound with the international Erasmus+ students

doc. Ing. Ladislav Rudolf, Ph.D.

He works at University of Ostrava. His area is energetic systems. He is an associate professor. He publishes in mathematical statistics and in educational sciences.

Prof. Ing. Marek Kubalčík, Ph.D.

He works at Tomas Bata University in Zlin. His area is applied process control and design. He is a professor. He publishes in applied technical science.

RNDr. Radek Krpec, Ph.D.

He works at University of Ostrava. His area is applied statistics. He is an associate professor. He publishes in applied statistics and in educational sciences. He teaches the courses bound on statistics and general mathematics.

ROOM ACOUSTIC MEASUREMENT METHODS IN THE PAST, PRESENT AND FUTURE, INCLUDING THE IMPORTANCE OF THE ISO 3382 SERIES

Jens Holger Rindel

Odeon A/S, DTU Science Park, Diplomvej Bldg, 381, DK-2800 Kgs. Lyngby, Denmark,
jhr@odeon.dk

ABSTRACT

The measurement of reverberation time in a room was introduced by W.C. Sabine a few years before 1900 with the purpose to handle acoustic problems in a lecture theatre. The sound source was organ pipes at the seven octave frequencies from 63 Hz to 4000 Hz. Later, the measurements were greatly improved by using interrupted white noise emitted by a loudspeaker and a microphone connected to a level recorder that could display the decay curve. This led to the first international standard on reverberation time measurements in 1963, intended for laboratory measurements of the sound absorption coefficient of materials. In 1975 appeared another international standard intended for reverberation time measurements, primarily in rooms for speech and music. A revision in 1997 introduced the impulse response as a basis for room acoustic measurements. This opened up for derivation of other room acoustic parameters than the reverberation time, and this again led to a better understanding of how to design good rooms for music and speech. Some types of rooms are not sufficiently characterised by the reverberation time, and for that reason a new standard appeared in 2012 with a measurement method specifically intended for open-plan offices. Future development of room acoustic measurements may include faster and more reliable methods, better methods to overcome problems at low frequencies, a method to handle the influence the high-frequency problem of varying temperature and humidity of the air, and new ways to derive three-dimensional information on the sound reflections in a room.

1. INTRODUCTION

This paper presents a brief overview of room acoustic measurements and how the methods have developed during the last 125 years. The emphasis is on the major milestones that mark significant improvements. During the last 60 years, international standards on measurement methods have played an important role for promoting new and improved methods. The list of references is made with the intention to point at the origin of the measurement methods and the room acoustic parameters.

2. THE EARLY DAYS OF ROOM ACOUSTIC MEASUREMENTS

Wallace C. Sabine (1868-1919) is known as founder of room acoustic measurements around 1900. He introduced the concept of reverberation time, defined as the time for the sound intensity in a room to decay to 1/1.000.000 of the initial intensity after a sound source is turned off [1]. The measurements were performed with specially constructed organ pipes as sound sources and a chronograph (stopwatch) to measure the audible decay time. The organ pipes were of the type gemshorn, which have a strong fundamental tone and relatively weak overtones. Sabine could calculate the reverberation time related to 60 dB decay by a very clever method. He used four identical sets of organ pipes, and could then measure the audible decay time using one, two, three or all four organ pipes as the sound source. This gave different results because the initial energy was different. For example, the initial sound level is 6 dB higher with four organ pipes compared to one organ pipe; thus, the reverberation time is ten times the difference in audible decay time for the two measurements [1]. The frequencies of the organ pipes were at seven octaves from 64 Hz to 4096 Hz, corresponding to the music tones C. Later, more organ pipes with the tones E and G were included, so measurements could be made in approximately onethird octave intervals. This was meant for laboratory measurements of sound absorption of materials [2].

C. Sabine. He explains: "During the 1930s the stop watch and ear method was replaced by relay-controlled chronometers (acoustic clocks) operating in conjunction with frequency oscillators, amplifiers, loudspeakers, attenuators, and microphones" [3]. The methods using a loudspeaker emitting periodic varying tones, a microphone and oscillograph are described in the book by Vern O. Knudsen

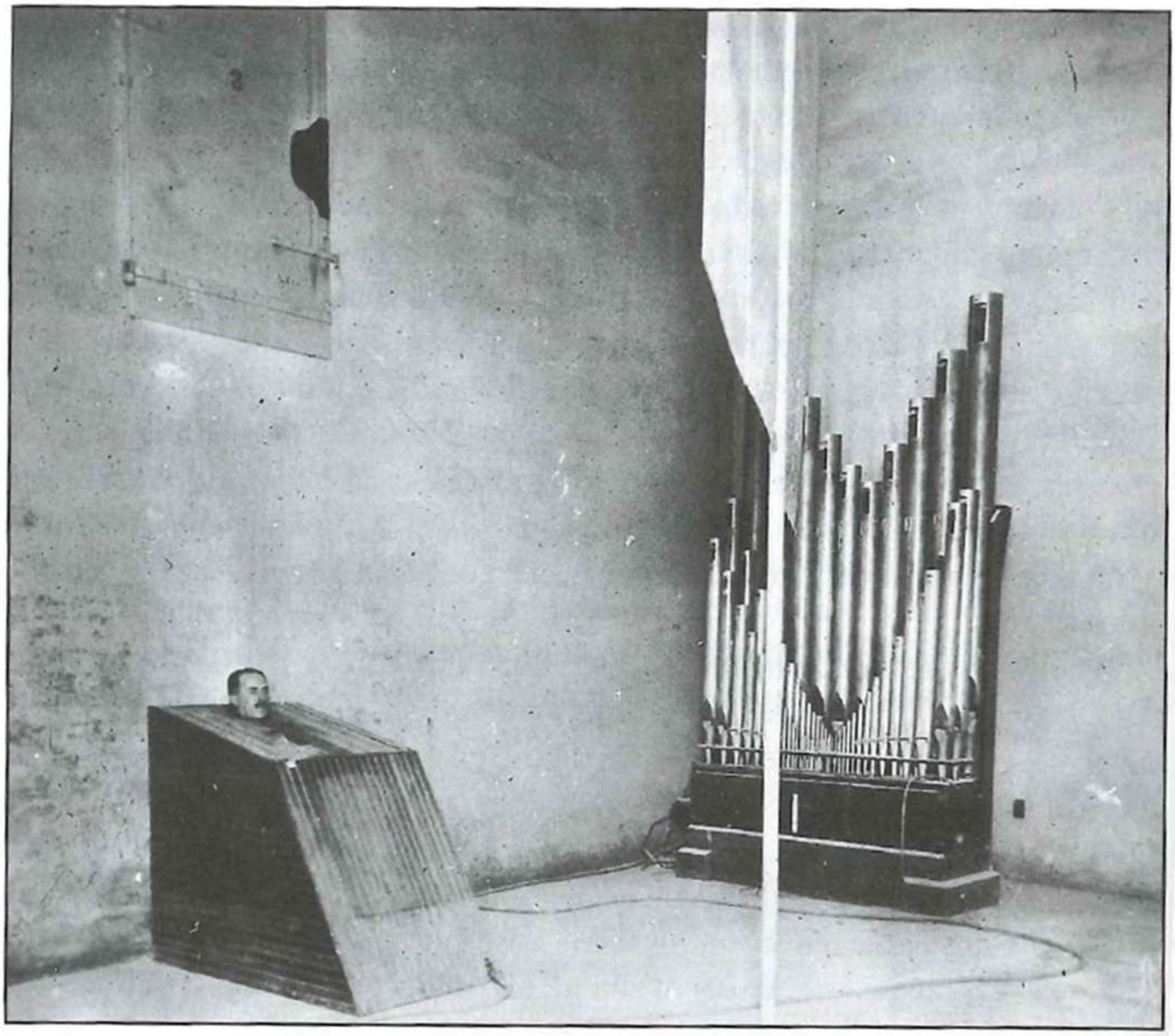

Fig. 1: Conducting an absorption test in the reverberation chamber, 1919. From Kopec [2] p. 64.

In Figure 1 is seen the setup for an absorption test in the large reverberation chamber at the Riverbank laboratories. The operator is sitting in a box in order to minimize the absorption from clothing. The rotating fan seen in the photo was used to increase the diffusion. Paul E. Sabine continued the work with acoustic measurements after the death of Wallace

[4, Chapter VII]. An example of a warble-tone signal and measured decay curves are seen in Figure 2.

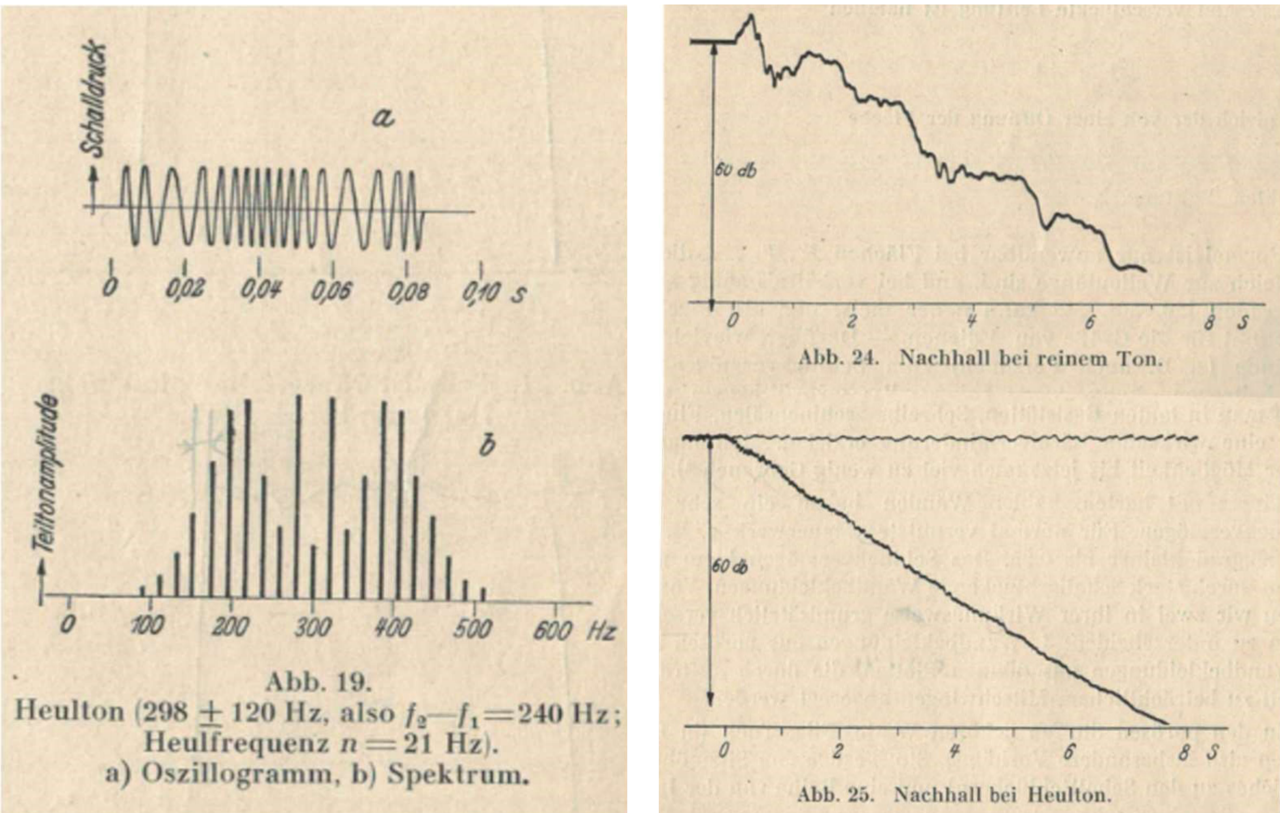

Fig. 2: Measurement using a warble-tone. Left: The time- and frequency function of the signal. Right: Decay curves with a single frequency (upper part) or with the warble tone (lower part). From Schoch [5].

Field measurements of reverberation time were also made with (portable) organ pipes and stop-watch until around 1930. However, in 1934 measurements were made in the old Philharmonic Hall of Berlin (destroyed during the second world war) using for the first time a symphony orchestra as the sound source [6]. The music from the very first bars of the Beethoven Coriolanus overture was used as the sound signal. This particular music starts with some tutti cords in fortissimo, followed by pauses long enough to evaluate the reverberation time, see Figure 3. This implies, that the measurements could be made with the audience present. Reverberation times with and without an audience were reported in (approximate) octave bands from 125 Hz to 2 kHz. The 4 kHz band was measured, but no results were reported due to insufficient signal-to-noise level. Measurements with pistol shots (a start revolver) were also taken into use [6].

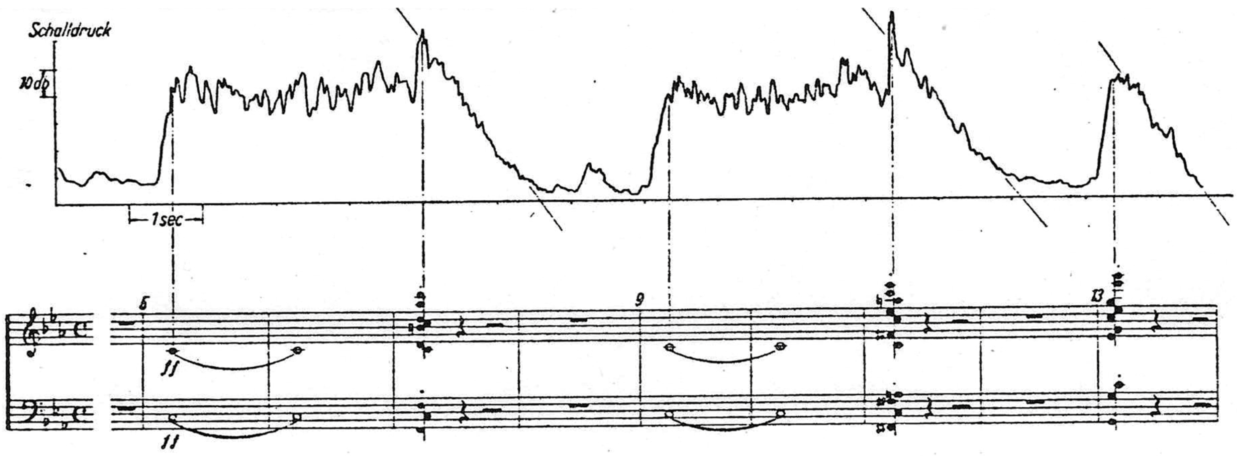

Figure 3: Decay curves in 500 Hz band measured 1934 in the old Philharmonie, Berlin, using a symphony orchestra as sound source. The music was Beethoven's Coriolanus overture, and the hall was with full audience. From Meyer & Jordan [6].

The registration of the decay curves was very difficult in the 1930s. For the concert hall measurements was used a technique, where the signal from the microphone was sent through a filter and a logarithmic amplifier to a movable mirror. A light beam was directed via the mirror towards a slowly rotating cylinder, which was covered with a phosphorescing layer. The curve that was made by the light beam was visible for long enough time to allow redrawing on paper.

A milestone in room acoustic measurements is the level recorder with a high-speed, logarithmic potentiometer. The first level recorder was made by Neumann around 1940, and from 1943 an improved model by Brüel & Kjær became widespread as an unavoidable part of the acoustic measurement equipment [7].

3. FIRST MEASUREMENT STANDARDS

ISO/R 354 recommendation was the first international standard for measuring the absorption coefficient of materials in a reverberation chamber [8]. It was published in 1963, five years after an American ASTM standard with similar contents [9]. A loudspeaker was used to emit the sound, either a warble tone or white noise. The sound was interrupter to get the decay. A microphone was connected to cathode ray tube or a level recorder. From this could be derived the decay rate (dB/s) or the reverberation time. The reading was taken from the part of the decay curve between -5 dB and -35 dB (or less) from the start of the decay curve. Measurements were made in octave bands or one-third octave bands from 100 Hz to 4000 Hz.

4. MEASUREMENT OF REVERBERATION TIME IN AUDITORIA

Since the first measurement standard ISO/R 354 was made for laboratory testing of materials, it soon became clear that there was a need for another standard directed towards field measurements, especially for auditoria. Such a standard was published in 1975 as ISO 3382 [10]. It described measurements made with loudspeakers and interrupted noise, and it also opened for other methods using organ pipes, blank pistol shots, or an orchestra as the sound source. The description of source and receiver positions were adapted to typical auditoria or concert halls. The derivation of reverberation time from the decay curve was the same as in ISO/R 354. The frequency range was one-third octave bands from 125 Hz to 4000 Hz. If the decay curve was not close to a straight line, two reverberation times were to be reported for the early and the late part of the decay, respectively.

There are several remarkable matters in this standard. One is the use of one-third octave bands. While this made sense for the measurement of absorption coefficients, it is more problematic for measurements of reverberation time in auditoria. Among acousticians working with concert halls, it was common practice to measure in octave bands and often to look at the average of two or three octave bands. The wider bandwidth was in order to obtain results that were not too sensible to variations in measurement positions.

Another remarkable matter in the standard is the possibility to use a pistol shot. It had become common to measure with pistol shots and derive the reverberation time directly from the squared impulse response, see Figure 4. However, already in 1965, Schroeder had shown how to derive a correct decay curve by backwards integration of the squared impulse response [12]. Without this integration, the results could be wrong, especially if the decay curve deviated much from an exponential decay. The example in Figure 5 shows the squared impulse response and the integrated impulse response measured in a concert hall.

The measurement method with the integrated squared impulse response is a milestone in room acoustic measurements. While the interrupted noise signal is stochastic and has to be repeated several times, the integrated impulse response remains the same if repeated. Schroeder had shown that the decay curve of the latter is the same as the ensemble average of an infinite number of interrupted noise signals [12]. While the interrupted noise method has remained a common method for laboratory measurements, the integrated impulse response has become the preferred method for field measurements because it is time-consuming and accurate.

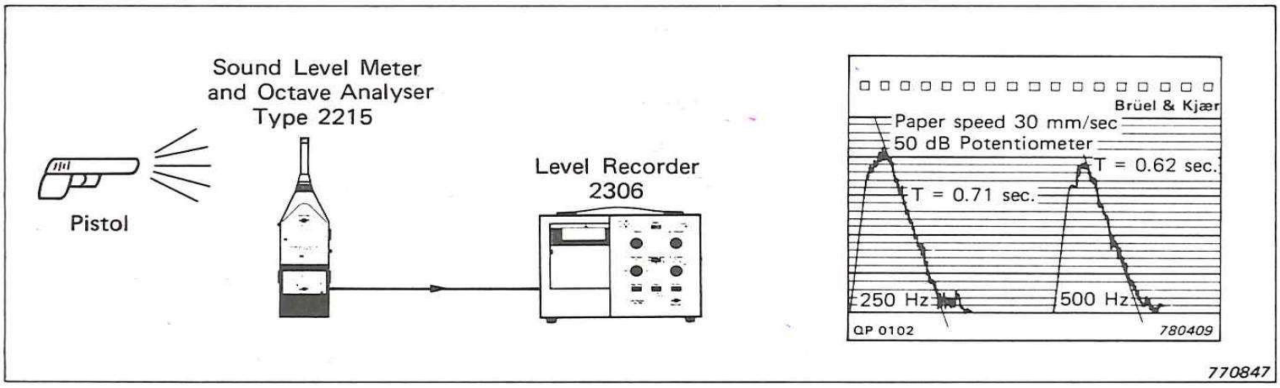

Figure 4: Set-up for measurement of reverberation time with the pistol shot method. From Fig. 6.1 in Ginn [11].

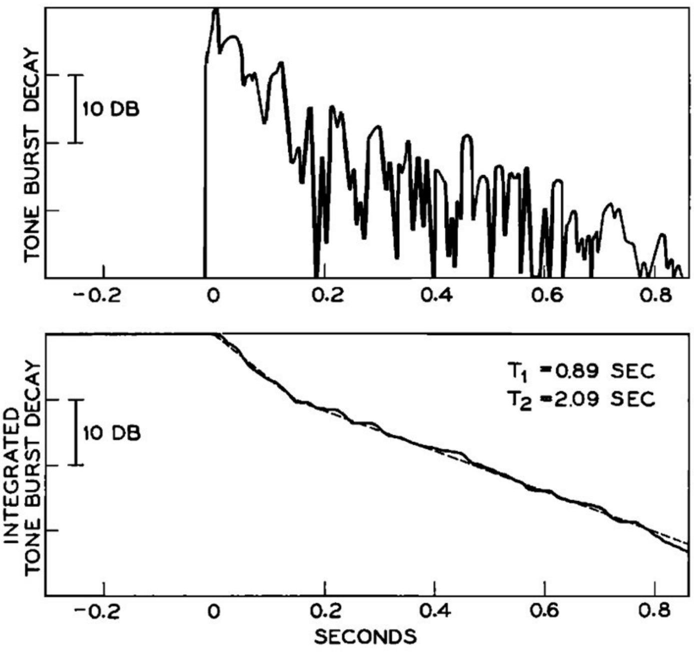

Figure 5: Measured squared impulse response (tone burst decay) and corresponding integrated impulse response (decay curve). A one-third octave band filter centred at 167 Hz was applied. Two different reverberation times have been derived, T1 from the upper 10 dB and T2 from the lower part of the curve. From Schroeder [12].

5. IMPROVED MEASUREMENT METHODS

5.1. INTEGRATED IMPULSE RESPONSE METHOD

The second edition of ISO 3382 was published in 1997 with several improvements [13]. The introduction states: "The intention is to make it possible to compare reverberation time measurements with higher certainty, and to promote the use of and consensus in measurement of the newer measures." The scope includes this sentence: "It is not restricted to auditoria or concert halls; it is also applicable to rooms intended for speech and music or where noise protection is a consideration."

The standard makes a clear distinction between two alternative methods for measuring the reverberation time: The interrupted noise method or the integrated impulse response method. The decay directly after excitation with a pistol shot or other impulse sources should only be used for survey purposes and is not recommend for accurate evaluation of the reverberation time. Impulse responses can be generated with loudspeakers using signals with Maximum Length Sequence (MLS), chirps or linear sweeps.

The measurement of impulse response opens up for the derivation of several other room acoustic parameters, and such parameters are included in informative annexes of the standard. Most of these new parameters had been developed since the 1950s, especially in relation to the use of scale models for acoustic design of auditoria, see Jordan chapters 4, 9, and 11 in [14]. The room acoustic parameters in this edition of the standard are listed in Table 1. The lateral energy fraction (LF) requires a figure-of-eight microphone, and the inter-aural cross correlation (IACC) requires measurement with a dummy head.

Name	Symbol	Unit	Description	Origin
Sound strength	G	dB	Total sound level relative to 10 m in free field	Lehmann [15]
Early decay time	EDT	s	Reverberation time derived from the first 10 dB	Jordan [16]
Early-to-late index	C50, C80	dB	Ratio of early to late sound energy in dB (Clarity)	Reichard [17]
Definition	D_{50}	-	Ratio of early to total sound energy (Deutlichkeit)	Thiele [18]
Centre time	T_S	ms	Time of gravity of the squared impulse response (Schwerpunktzeit)	Kürer [19]
Lateral energy fraction	LF	-	Ratio of early lateral energy to early total energy	Barron [20]
Inter-aural cross correlation coefficient	IACC	-	Maximum of normalised inter-aural cross correlation function	Damaske [21]

Table 1: Auditorium measures derived from impulse responses, ISO 3382 Annex A and B [13].

5.2. LINEAR REGRESSION REPLACES MANUAL ESTIMATE OF DECAY RATE

The standard of 1997 states that the measurements of reverberation time in concert halls should be made in octave bands from 63 Hz to 4 kHz, while one-third octave bands from 100 Hz to 5 kHz can be used in other kinds of rooms. All reverberation parameters (EDT, T_{20}, and T_{30}) shall be determined from the slope of linear regression line within the evaluation range. For reverberation time this is a clear improvement from earlier manual methods, but for early decay time (EDT) this is more problematic as shown by Bradley [22]. For nearly 30 years, the EDT had been derived from the two points at 0 dB and -10 dB on the decay curve, neglecting the irregularities that are often seen in the first part of the decay curve, see Jordan [14, page 70]. While the difference between the two evaluation methods for EDT is negligible in long distances from the source, the difference can be very significant in positions close to the source. EDT is known to be a good measure of perceived reverberance, but the research behind this was based on the two-point EDT (before 1997).

Due to the fact that the air attenuation can influence the measurement results at frequencies above 500 Hz, the standard requires temperature and relative humidity in the room during the measurements to be included in the test report. These should be measured to an accuracy of ± 1 °C and ± 5 %, respectively.

5.3. SPEECH TRANSMISSION INDEX

In Annex A of the 1997 edition of the standard is mentioned in a note, that the Speech Transmission Index (STI) can also be used to determine the speech intelligibility, but this is a special measuring technique not covered in the standard. A simplified version of the method using only signals at 500 Hz and 2000 Hz is the Rapid Speech Transmission Index (RASTI). Brüel & Kjær produced portable equipment for these measurements, consisting of a speech transmitter (Type 4225) and a speech receiver (Type 4419). The method is based on a series of complicated modulation transfer functions, but the measurement result is simple and easy to understand. For many years, the RASTI measurements became quite popular as a supplement to other room acoustic measurements. However, in the 2011 edition of the measurements standard [23], the RASTI method was declared obsolete and was not be used. Also, the STI method has problems in relation to room acoustic measurements, mainly because the method is not sensible to echoes [24].

5.4. SINE SWEEP MEASUREMENTS

An early example of measuring with sine sweep signals was the series of concert hall measurements from 1984 by Gade & Rindel [25]. A linear sine sweep that covered one octave band was used and scaled in time and frequency for the six octave bands from 125 Hz to 4 kHz, see Figure 6. The response measured in the room was converted to an impulse response by convolution with the original sine sweep signal.

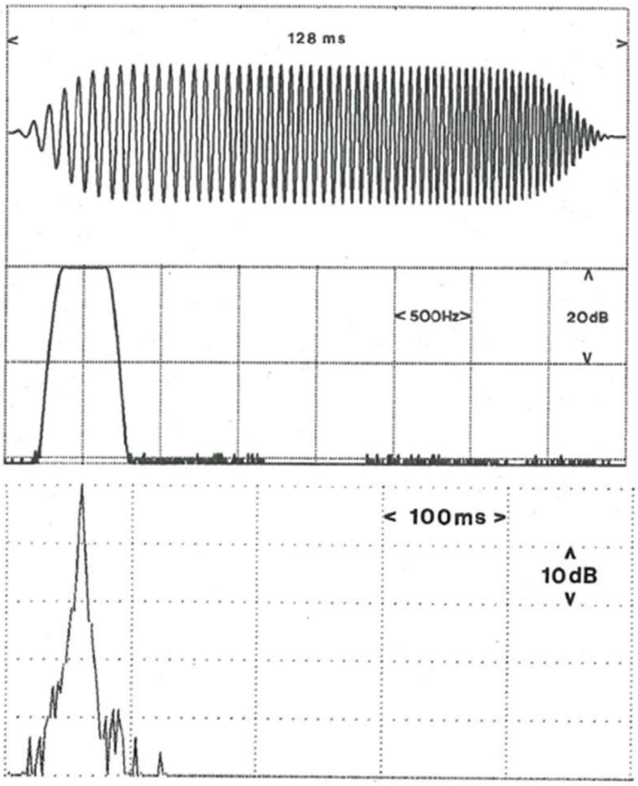

Figure 6: Sine sweep signal covering one octave, here shown for the 500 Hz octave band. Top: Signal in time domain.

Middle: Signal in frequency domain. Bottom: Impulse response after convolution. After Gade & Rindel [25].

6. RECENT DEVELOPMENTS IN ROOM ACOUSTIC MEASUREMENTS

6.1. PERFORMANCE SPACES IN ISO 3382-1

For reasons to be explained in the next section 6.2, it was decided that the room acoustic measurement standard should be divided into two parts (and later three parts). Part 1 from 2009 [26] was in fact a 3rd edition of the previous ISO 3382 standard. This new edition had some minor changes, mainly in the annexes on various room acoustic parameters.

Annex A was extended with information on JND (just noticeable difference) [27] and the late lateral energy level, a new parameter related to the perceived listener envelopment. It is measured as the lateral energy level after 80 ms using a calibrated figure-of-eight microphone and is based on research by Bradley & Soulodre [28].

A new Annex C was added with the parameters Early Support (ST_{Early}) and Late Support (ST_{Late}) for the acoustic conditions at the orchestra platform. The former is related to the musicians' ability to hear each other, while the latter is related to the musicians' perceived reverberance. Both are measured in the distance of 1.0 m from the acoustic centre of an omnidirectional sound source. These parameters are based on research by Gade [29].

6.2. ORDINARY ROOMS IN ISO 3382-2

In 2001 the technical committee on acoustics ISO/TC 43 received a New Work Item Proposal (ISO/TC 43/SC 2 N 638) that recommend to divide ISO 3382 into two parts. Part 1 should be for performance spaces as the existing standard, while Part 2 should deal with "the measurement of reverberation time in rooms in general. Examples are living rooms, classrooms, workshops, stairwells, and industrial halls". ISO 3382-2 [30] is supposed to be a reference standard for building acoustic measurements and other standards where reverberation time is a part of the measurements. The part 2

of the standard deals with reverberation time, only. Both the interrupted noise method and the integrated squared impulse response method are described. The evaluation range for derivation of the reverberation time can be 20 dB or 30 dB, with a preference for 20 dB for various reasons, as explained in the introduction to the standard.

Concerning the number of source and receiver positions and other technical details, the part 2 of the standard distinguishes between three levels of measurement accuracy: survey, engineering, and precision. The precision method is meant for testing laboratories, especially for the measurement of the absorption coefficient of materials. Two annexes are included, one for the measurement uncertainty, and the other one with definition of "measures that quantify the degree of nonlinearity and the degree of curvature of the decay curve. These measures may be used to give warnings when the decay curve is not linear, and consequently the result should be marked as less reliable and not having a unique reverberation" [30]. The origin of these quality measures is the work of Bodlund in 1984 for a Nordtest method [31]. He elaborated on the possibilities of using a computer for pression measurements in a laboratory with the interrupted noise method. He also introduced ensemble averaging as an attractive alternative to arithmetic averaging of reverberation times.

6.3. OPEN PLAN OFFICES IN ISO 3382-3

A second New Work Item Proposal (ISO/TC 43/SC 2 N 889) was proposed in 2007 that recommend establishing a new part 3 to the ISO 3382 series. The reason was acoustical problems in open plan spaces (offices, schools), and the recognition that the reverberation time was not sufficient or useful for characterizing open plan spaces. The proposal stated that "there is reasonable agreement that other types of measurements such as rate of spatial decay of sound pressure levels, speech transmission index and background noise levels are needed for a more complete evaluation of the performance of open plan spaces".

The measurement of spatial decay in large spaces had already been taken into use in industrial halls, see ISO 14257 [32]. The possibilities of using the speech transmission index (STI) in relation to open plan offices had been suggested by several researchers [33, 34]. Finally, the ISO 3382-3 [35] was published with the title limited to open plan offices.

Several new measures were defined, four of them being mandatory:

distraction distance r_D

spatial decay rate of A-weighted sound pressure level of speech, $D_{2,S}$ · A-weighted sound pressure level of speech at 4 m, $L_{p,A,S,4\,m}$ · average A-weighted background noise level, $L_{p,A,B}$.

The distraction distance r_D is derived from STI measurements performed on a line of receivers with increasing distances from an omni-directional source. The distance where

STI is estimated to decrease below 0,5 is defined as the distraction distance. The sound source must emit a noise signal at specified sound power and spectrum that represents speech sound. This new part of the standard did not solve the acoustical problems in open plan offices. However, it did establish a very important common reference for research in the field of acoustics of open plan offices. The acoustical problems in open plan offices are much more complicated than ordinary noise control. It is more like an optimisation problem, and how use the new parameters is still under discussion [36].

A second edition of ISO 3382-3 was published in 2022 [37] with minor changes. Most important is the addition of another parameter, the comfort distance (r_C). This is defined as the distance from the omni-directional source, where the Aweighted sound pressure level of speech decreases below 45 dB.

7. FUTURE MEASUREMENT METHODS

7.1. REVISION OF ISO 3382-1

ISO 3382-1 is currently being revised and some of the ideas for future changes may be unveiled. Most importantly, it will be emphasised that the standard is not only for music rooms, but also includes rooms for speech and open-air performance spaces. It will be made clear which of the room acoustic measures are relevant in rooms for speech, especially classrooms. Some new room acoustic parameters may be suggested, such as an echo-parameter and the acoustic efficiency, both of them most relevant for open-air performance spaces [38].

A new method for normalisation of the measurements to a standard atmosphere (20 °C, 50 % RH) is also being discussed.

7.2. MEASUREMENT OF MODAL REVERBERATION TIMES

The problem of measuring reverberation time at low frequencies (< 100 Hz) in small rooms (< 200 m^3) is still a challenge. One idea is to measure the reverberation time of single modes. Instead of a conventional statistical approach, the source and microphone positions can be chosen strategically in order to separate one low-frequency mode at a time [39]. This is best applied to rectangular rooms, where the modal pattern of the modes is well known.

7.3. APPLICATION OF CEPSTRUM ANALYSIS

Flutter echoes and the spectral colouration due to periodic sound reflections are easy to hear but difficult to measure objectively. A method that has proven useful, especially for colouration issues, is the application of the so-called cepstrum analysis [40]. This is the inverse Fourier transform of the logarithm of the spectrum. The spectrum is derived as the Fourier transform of the impulse response. Peaks in the cepstrum indicate a periodicity in the spectrum, which is typical for the colouration.

7.4. MEASUREMENTS WITH A 3D FIELD MICROPHONE

The 3D distribution of the sound reflections in a receiver position can measured by replacing the omnidirectional microphone with a number of cardioid capsules, three orthogonal intensity probes, or some other microphone array. The measured signal can be transformed into first order ambisonics signals (B-format) or higher order ambisonics signals with addition of more microphones in the array. This technique can be used to measure the spatial room impulse response (SRIR) and to visualise the directions of reflections in the measured impulse response as a hedgehog pattern [41-42].

However, the use of 3D field microphones opens up for several other applications. The measured signal can be transferred into a figure-of-eight signal and a simultaneous omni-directional signal for deriving the lateral energy parameters in ISO 3382-1. By application of a head-related transfer function (HRTF) the measured signal can also be transferred into a binaural room impulse response (BRIR), thus replacing a dummy head for the measurement of the IACC parameter.

7.5. APPLICATION OF SOUND INTENSITY AND PARTICLE VELOCITY

Further application of the above-mentioned technique is to measure two different impulse responses, the traditional one based on sound pressure and another one based on the 3D sound intensity. Thus, a dynamic diffusion curve (DDC) can be derived from the difference between the two decay curves [43]. The DDC is a measure of the amount of non-directional energy as a function of the decay level. This technique is very efficient for analysing the degree of diffusivity and for detecting echoes and flutter echoes in a room. It has also been suggested for evaluation of the acoustical quality of reverberation rooms [44].

The simultaneous measurement of sound pressure and particle velocity opens up for improvements of measurements in reverberation rooms, that are used for measuring the absorption coefficients of materials. With current technique, it is a significant problem that the diffusivity in the room is compromised when the test material is installed. With the possibility to measure both the potential energy density and the kinetic energy density, the total energy density can be achieved. This may offer more accurate and robust measurement results, because the total energy density varies very little throughout the room. This applies to the steady-state sound as well as to the decaying sound field. This is the basis for a detailed measurement method that has been described in a US patent by Hanyu [45].

REFERENCES

1. W.C. Sabine, Reverberation, The American Architect, 1900. Paper No. 1 in Collected Papers on Acoustics, Harvard University Press, 1922.

2. J.W. Kopec, The Sabines at Riverbank, Woodbury, New York, 1997.

3. P.E. Sabine, Architectural Acoustics: Its Past and Its Possibilities, J. Acoust. Soc. Am. 11, 1939, 21-28 [4] V.O. Knudsen, Architectural Acoustics, John Wiley & Sons, New York, 1932.

4. A. Schoch, Die Physikalischen und Technischen Grundlagen der Schalldämmung im Bauwesen, Hirzel Verlag, Leipzig, 1937.

5. E. Meyer and V.L. Jordan, Nachhallzeiten von Konzerträumen und Schallschluckung der Zuhörerschaft, Elektrische Nachrichten-technich (E.N.T.) 12, 1935, 213220.

6. P.V. Brüel and U. Ingård, A new high speed level recorder, J. Acoust. Soc. Am. 21(2), 1949, 91-93.

7. ISO/R 354, Measurement of absorption coefficients in a reverberation room, International Organization for Standardization, Geneva, 1963.

8. ASTM C423, Standard Test Method for Sound Absorption and Sound Absorption Coefficients by the Reverberation Room Method, 1958.

9. ISO 3382, Measurement of reverberation time in auditoria, International Organization for Standardization, Geneva, 1975.

10. K.B. Ginn, Architectural Acoustics, Brüel & Kjær, Denmark, 1978.

11. M.R. Schroeder, New Method of Measuring Reverberation Time, J. Acoust. Soc. Am. 37, 1965, 409-412.

12. ISO 3382 (Ed. 2), Measurement of reverberation time in auditoria with reference to other acoustical parameters, International Organization for Standardization, Geneva, 1997.

13. V.L. Jordan, Acoustical Design of Concert Halls and Theatres, Applied Science Publishers, London, 1980.

14. P. Lehmann, Über die Ermittlung raumakustischer Kriterien und deren Zusammenhang mit subjektiven Beurteilungen der Hörsamkeit, Dissertation TU Berlin, 1976.

15. V.L. Jordan, Room Acoustics and Architectural Acoustics Development in Recent Years, Appl. Acoustics 2, 1969, 217-235.

16. W. Reichard, O. Abdel Alim, W. Schmidt, Definition und Messgrundlage eines objektiven Masses zur Ermittlung der Grenze zwischen brauchbarer und unbrauchbarer Durchsichtigkeit bei Musikdarbietung, Acustica 32, 1975, 126-137.

17. R. Thiele, Richtungsverteilung und Zeitfolge der Schallrückwürfe in Räumen, Acustica 3, 1953, 291-302.

18. R. Kürer, Zur Gewinnung von Einzahlkriterien bei Impulsmessungen in der Raumakustik, Acustica 21, 1969, 370372.

19. M. Barron, The subjective effects of first reflections in concert halls – the need for lateral reflections, J. Sound Vib. 15, 1971, 475-494.

20. P. Damaske, Subjektive Untersuchung von Schallfeldern, Acustica 19, 1967, 199.

21. J.S. Bradley, Review of objective room acoustics measures and future needs, Appl. Acoustics 72, 2011, 713-720.

22. IEC 60268-16 (Ed. 4), Sound system equipment – Part 16: Objective rating of speech intelligibility by speech transmission index, International Electrotechnical Commission, Geneva, 2011.

23. J.H. Rindel, A note on meaningful acoustical parameters for open-air theatres. Acta Acustica 7, 2023, 20.

24. A.C. Gade and J.H. Rindel, Akustik i danske koncertsale. Publikation nr. 22, Laboratoriet for Akustik, DTH, Lyngby, 1984.

25. ISO 3382-1, Acoustics - Measurement of room acoustic parameters - Part 1: Performance spaces, International Organization for Standardization, Geneva, 2009.

26. I. Bork, Report on the 3rd Round Robin on Room Acoustical Computer Simulation – Part II: Calculations, Acta Acustica/Acustica 91, 2005, 753-763.

27. J.S. Bradley and G.A. Soulodre, Objective measures of listener envelopment. J. Acoust. Soc. Am. 98, 1995, 2590– 2597.

28. A.C. Gade, Investigations of musicians' room acoustic conditions in concert halls. Part II: Field experiments and synthesis of results, Acta Acustica/Acustica 69, 1989, 249-262

29. ISO 3382-2, Acoustics - Measurement of room acoustic parameters - Part 2: Reverberation time in ordinary rooms, International Organization for Standardization, Geneva, 2008.

30. K. Bodlund, Reverberation time measurements according to the interrupted noise method – Precision methods for computer-controlled equipment, NORDTEST Tech Report 026, National Testing Institute, Borås, Sweden, 1984.

31. ISO 14257, Acoustics - Measurement and parametric description of spatial sound distribution curves in workrooms for evaluation of their acoustical performance, International Organization for Standardization, Geneva, 2001.

32. V. Hongisto, A model predicting the effect of speech of varying intelligibility on work performance, Indoor Air 15(6), 2005, p. 458-68.

33. C.B. Pop, C.B. and J.H. Rindel, Speech privacy in open-plan offices, Proceedings of Inter-Noise 2005, Rio de Janeiro, Brazil, 2005.

34. ISO 3382-3, Acoustics - Measurement of room acoustic parameters - Part 3: Open plan offices, International Organization for Standardization, Geneva, 2012.

35. J.H. Rindel, Open plan office acoustics – a multidimensional optimization problem. Proceedings of DAGA 2018, Munich, 2018.

36. ISO 3382-3 (Ed. 2), Acoustics - Measurement of room acoustic parameters - Part 3: Open plan offices, International Organization for Standardization, Geneva, 2022.

37. J.H. Rindel, A note on meaningful acoustical parameters for open-air theatres. Acta Acustica 7, 2023, 20. DOI:

38. 10.1051/aacus/2023015.

39. A. Prato, F. Casassa, A. Schiavi, Reverberation time measurements in non-diffuse acoustic field by the modal reverberation time, Appl. Acoustics 110, 2016, 160-169.

40. J.H. Rindel, Detection of Colouration in Rooms by use of Cepstrum Technique. Proceedings of DAGA 2016, Aachen, 2016.

41. D. Protheroe and B. Guillemin, 3D impulse response measurements of spaces using an inexpensive microphone array, International Symposium on Room Acoustics, ISRA 2013, Toronto, Canada, 2013.

42. S.V.Amengual Gari, W. Lachenmayr, E. Mommertz, Spatial analysis and auralization of room acoustics using a tetrahedral microphone, JASA Express Letters, J. Acoust. Soc. Am. 141(4), 2017.

43. C.L. Christensen & J.H. Rindel: Diffusion in concert halls analysed as a function of time during the decay process. Proceedings of the Institute of Acoustics, Vol. 33, Pt. 2, 2011, 98-105.

44. M. Nolan, M. Berzborn, E. Fernandez-Grande, Isotropy in decaying reverberant sound fields, J. Acoust. Soc. Am. 148(2), 2020, 1077-1088.

45. T. Hanyu, Acoustic energy measurement device, and acoustic performance evaluation device and acoustic information measurement device using the same, United States Patent No. US 8,798,955 B2, 2014.

Jens Holger Rindel
Professor emeritus, MSc, PhD
Senior researcher, Odeon A/S, Denmark
Senior acoustic consultant, Multiconsult, Norway

Short CV

2017

Jens Holger Rindel, b. 1947 in Copenhagen, Denmark. M.Sc. 1971 (civil engineering), Ph.D. 1977, both from the Technical University of Denmark. Until 2008 Professor in acoustics at the Technical University of Denmark. Senior researcher at the Norwegian Building Research Institute (1998-99). Visiting professor at the University of Sydney, the Nihon University, Japan, and the University of Auckland, New Zealand. Coordinator of European research projects (CAHRISMA, ERATO, DOREMI) and convenor of several ISO and CEN working groups. Author of textbooks, design guides in architectural acoustics, and more than 160 scientific papers. Short courses and master classes in architectural acoustics. Fellow of IOA and ASA. Since 2012 working part time with Odeon A/S and part time senior consultant in Multiconsult, Norway.

Work addresses:

Odeon A/S, Scion-DTU
Diplomvej 381
DK-2800 Kgs. Lyngby
Denmark

Multiconsult
Nedre Skøyen vei 2
P.O. Box 265 Skøyen
N-0213 Oslo
Norway

Telephone:

+45-5122 9870
+47-9801 5949

E-mail: jhr@odeon.dk, jehr@multiconsult.no

SOUND REFLECTIONS

Jens Holger Rindel

Odeon A/S, DTU Science Park, DK-2800 Kgs. Lyngby, Denmark, jhr@odeon.dk

ABSTRAKT

The present paper is a review of the author's work on sound reflections covering a span of years starting from 1982. After a study of the reflection properties of curved surfaces, the diffraction effects related to single reflectors was studied, both theoretically and experimentally. The main result was a characteristic frequency above which the sound reflection is fully efficient as long as the reflection point is within the reflecting surface. Next, the array of reflectors was studied, and again the characteristic frequency was found useful as a design parameter, but here as an upper frequency limit for reliable reflections. The design principle was successfully applied in a concert hall in Copenhagen. Recently, the reflection of a spherical sound wave emitted from a point source has been studied and a theoretical model has been developed. An application of this model is for the sound propagation over an area with sound absorbing properties like those of a seated audience in a large auditorium.

1. INTRODUCTION

A general model of sound reflection from a surface is shown in Figure 1.

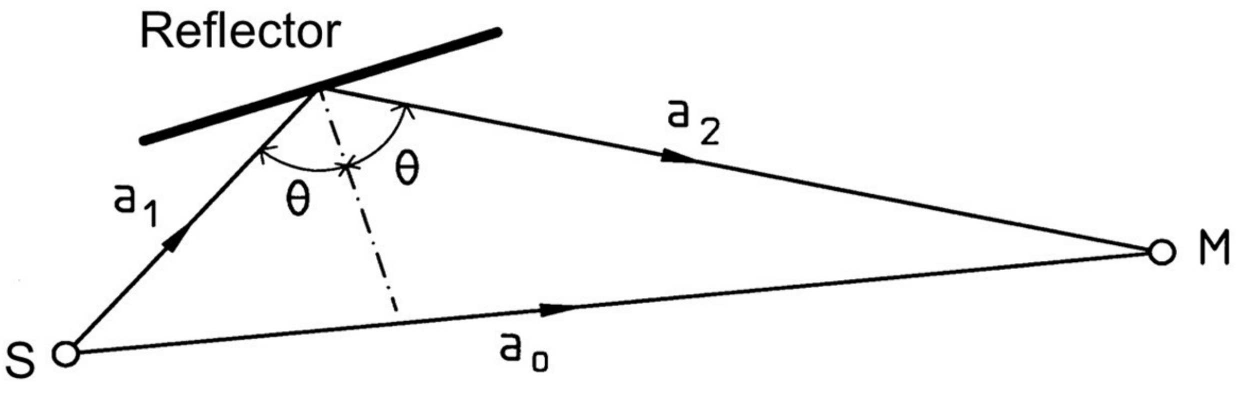

Fig. 1: Distances and angles related to the sound reflection from a surface. Sound is emitted from a point source (S) and the receiver point is M.

The attenuation of the reflected sound relative to the direct sound is:

$$DL = L_{refl} - L_{dir} = DL_a + DL_m + DL_k + DL_s \quad \text{(dB)} \tag{1}$$

where the four attenuation terms are related to distance (a), absorption due to the material (m), curvature of the surface (k), and finite size of reflector (s). The attenuation terms are usually negative corresponding to the reflected sound pressure level being lower than the direct sound pressure level.

The attenuation due to distance DL_a is -6 dB per doubling of the distance due to the energy spread on the surface of a sphere:

$$\Delta L \quad = 20\,\lg \frac{\qquad}{(\qquad)} \qquad \text{(dB)} \tag{2}$$

If the angle-dependent absorption coefficient of the material is α_θ, the reflected sound energy is $(1 - \alpha_\theta)$ times the incident sound energy, and the attenuation due to the material DL_m is:

$$\Delta L \quad = 10\,\lg(1 - \alpha\,) \qquad \text{(dB} \tag{3}$$

The characteristic distance a* is defined as the harmonic average of the two distances from the reflection point to the source (a_1) and to the receiver (a_2):

$$a^* = \frac{\qquad}{(4)} \tag{4}$$

2. REFLECTION FROM A CURVED SURFACE

From a geometrical analysis of the reflection of a sound wave from a curved surface with radius R, the attenuation due to curvature is found to be [1]:

$$\Delta L \quad = -10\,\lg\; 1 + \frac{a^*}{R\cos\theta} \qquad \text{(dB)} \tag{5}$$

By convention R is negative for a concave surface and positive for a convex surface. The formula (5) is illustrated in Figure 2, and it is noted that the sound is always attenuated when reflected from a convex surface. However, in case of a concave surface, the sound pressure level can be increased due to a focusing effect.

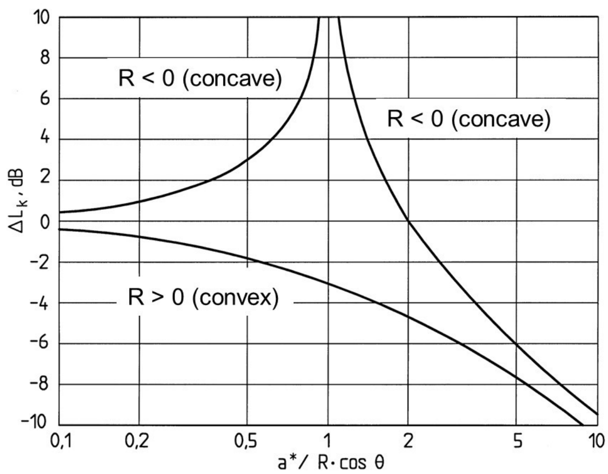

Fig. 2: The attenuation due to curvature.

3. SINGLE REFLECTORS AND DIFFRACTION EFFECTS

The attenuation of a sound reflection from a rectangular plate can be calculated by the Kirchhoff-Fresnel approximation as presented by the author in 1986 [2]. The solution implies a transformation of variables into u and v, which are orthogonal directions on the surface of the plate, see Figure 3. The origo of this coordinate system is the geometrical reflection point. In one direction, the variable is u:

$$u = \sqrt{\frac{2}{\lambda}\left(\frac{1}{a} + \frac{1}{a}\right)} \cdot \xi \tag{6}$$

where λ is the wavelength, a_1 and a_2 are the distances (see Figure 1) and ξ is the distance from the reflection point. So, if the width of the plate is 2b and the distance from the reflection point on the plate to the nearest edge is e, we have for u_1 that ξ = e cos θ and for u_2 that ξ = (2b – e) cos θ.

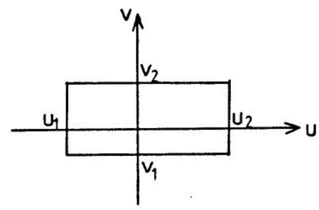

Fig. 3: The parameters u_1, u_2, v_1, and v_2 that correspond to distances from the reflection point to the edges of the reflecting plate.

The attenuation of the reflection due to diffraction is:

$$\Delta L \quad = 10\,\lg(K \cdot K\,) \qquad \text{(dB)} \tag{7}$$

where the coefficients K_1 and K_2 represents the two orthogonal directions of the plate. They are calculated by means of the Fresnel integrals C(x) and S(x), and for the first direction we get:

$$K = \_ \qquad C(u\,) - C(u\,) \qquad + S(u\,) - S(u\,) \tag{8}$$

and similarly for K_2 with the v_1 and v_2 parameters.

The result in Eqn. (8) can be visualised with the Cornu's spiral, which is the graph created when C(x) and S(x) are displayed as abscissa and ordinate, respectively, see Figure 4 a. An example of a low frequency is $u_2 = -u_1 = 0.7$ (red arrow in Figure 4). The length of the arrow is proportional to the amplitude of the sound pressure in the reflected sound wave. A very high frequency or infinitely large plate is represented by $u_2 = -u_1 \rightarrow \infty$. This yields the coefficient $K_1 = 1$, and thus the attenuation $DL_s = 0$ dB (blue arrow in Figure 4).

The results show that the sound is reflected efficiently at high frequencies althought with some fluctuations, but the sound is attenuated below a certain frequency. This led to the introduction af the characteristic frequency f_g for a single reflector:

$$f = \frac{c\, a^*}{2\, S \cos\theta} \quad \text{(Hz)} \tag{9}$$

Measurements in the large anechoic chamber at DTU were made using an impulse gating technique [3]. The set-up is seen in Figure 5.

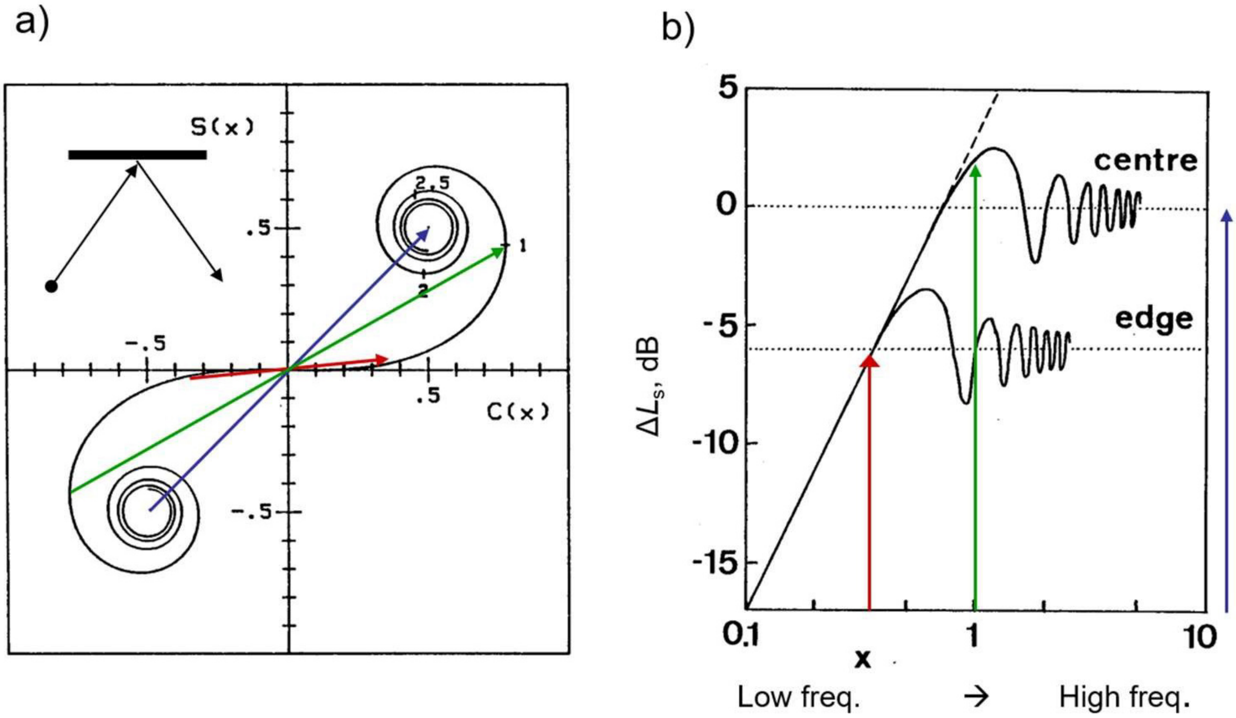

Figure 4: Attenuation due to diffraction of sound reflection from a plate. a) The Cornu's spiral and reflection point in the centre of the plate; low frequency (red arrow), middle frequency (green arrow), high frequency limit (blue arrow).
b) Attenuation in dB for reflection point in centre or on the edge.

Fig. 5: Set-up in anechoic chamber foe measurement of sound reflection from a single reflecting plate.

and an example of the measurement results are seen in Figure 6. The agreement between the measurement results and the calculations with the Kirchhoff-Fresnel approximation is in general very good. Only, at frequencies below c. 125 Hz the measurements deviate from the predictions, probably due to limitations in the measurement technique.

The conclusion from the study of single reflectors is that the characteristic frequency f_g should be as low as possible in order to reflect a wide frequency range. This means that the reflector plates should be as large as possible.

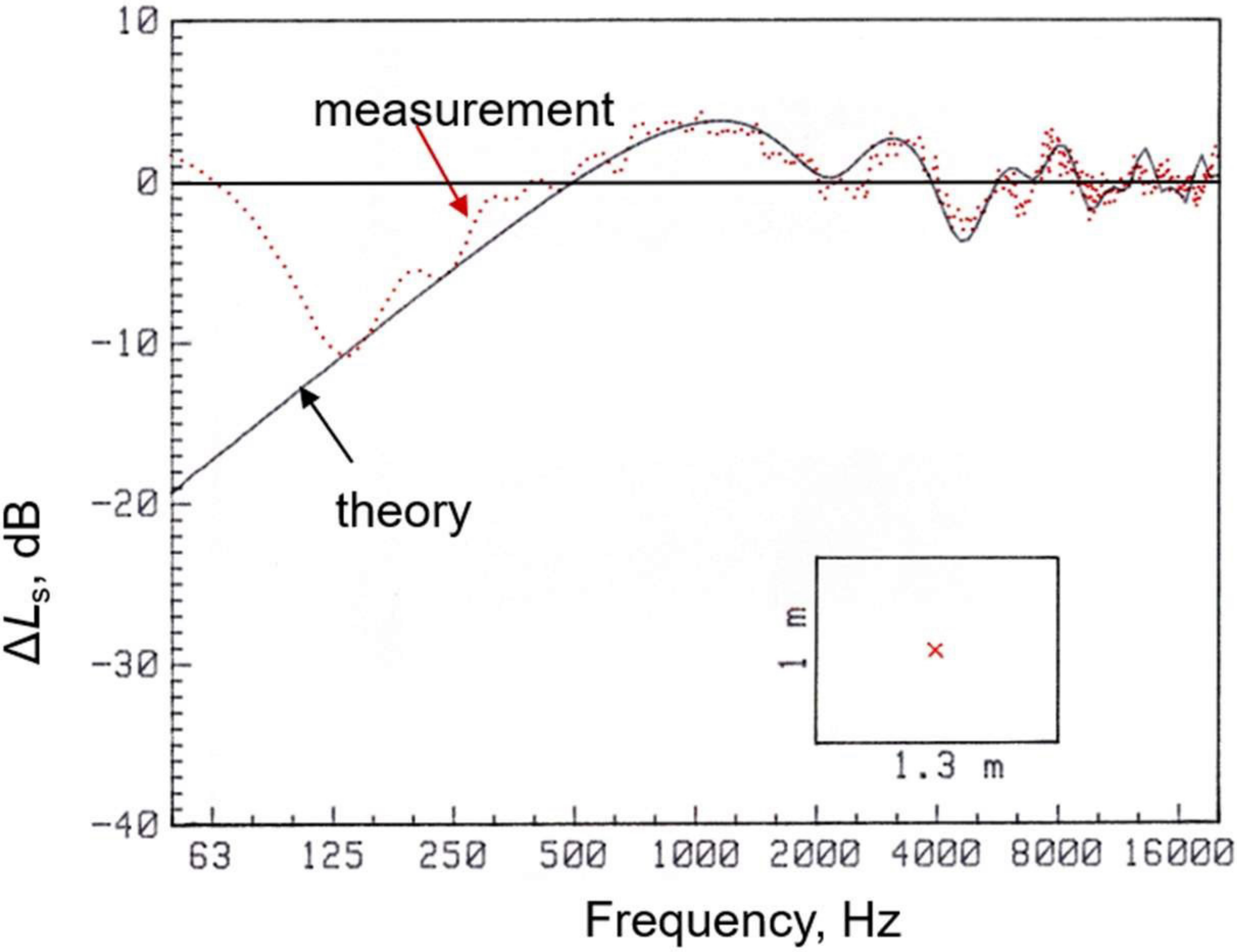

Figure 6: Measured and calculated attenuation of sound reflection from a rectangular plate. Angle of incidence θ = 30°, a1 = a2 = 3.0 m. Adapted from [3].

4. ARRAY OF REFLECTORS

The study of sound reflections was continued with investigations on arrays of reflectors. The theoretical model based on the Kirchhoff-Fresnel approximation was extended to a two-dimensional pattern of rectangular reflector plates, see Figure 7 and 8.

The theoretical model for the reflector array can explain that all the plates work together at low frequencies, and the result is comparable to that for a very large reflector. However, for middle and high frequencies the reflection is dominated by that from the particular plate on which the geometrical reflection point is located. The other plates contribute less and

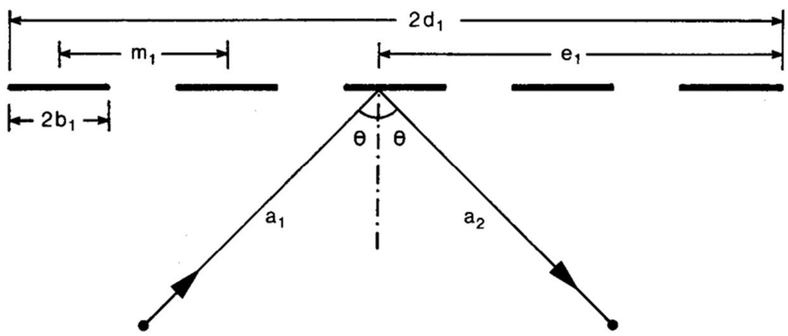

Figure 7: A reflector array with five rows of reflector plates. In incident and reflected sound are indicated as rays.

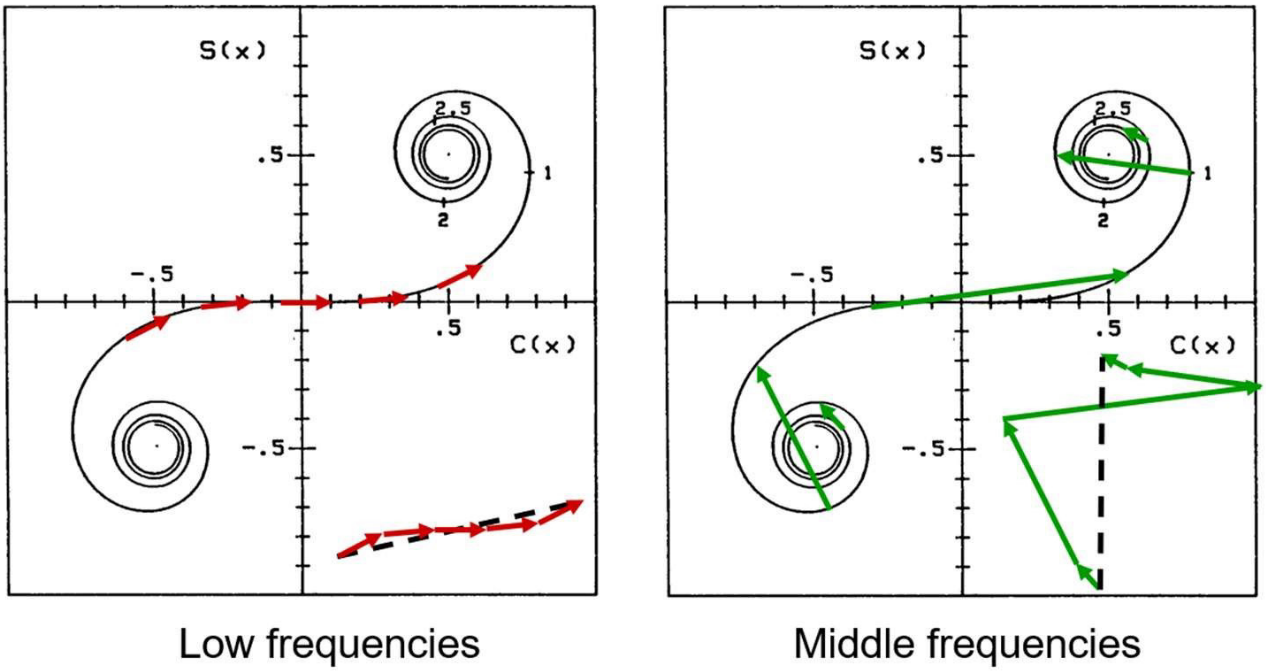

Fig. 8: Application of the Cornu's spiral for a reflector array with five rows as in Figure 7. At low frequencies the contributions from each row are approximately in phase. At middle frequencies the contributions add like vectors due to different phase.

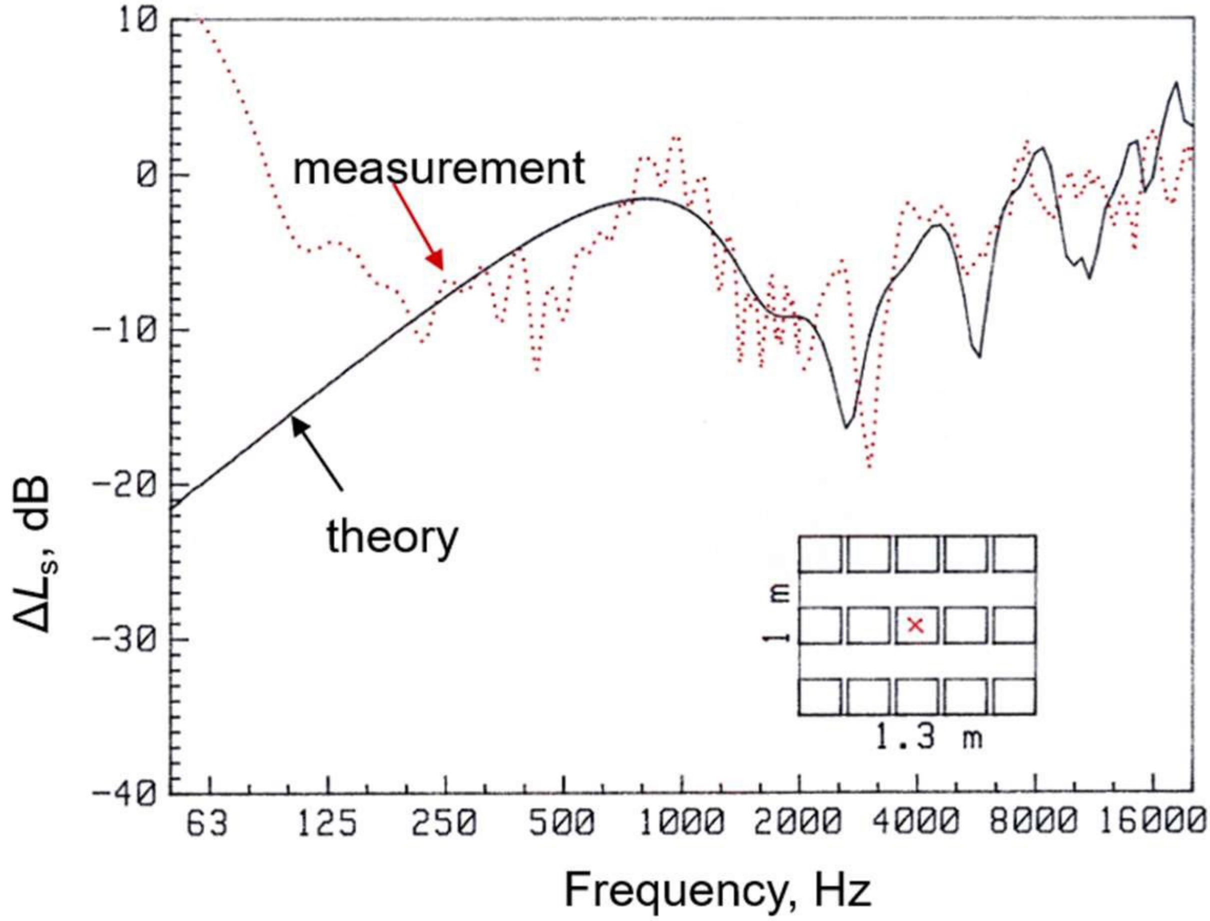

*Fig. 9: Measured and calculated attenuation of sound reflection from a reflector array. Plate dimensions 0.23 m * 0.20 m. Angle of incidence θ = 30°, a1 = 3.0 m, a2 = 2.0 m. Adapted from [3].*

with different phase, see Figure 8. The theoretical model was compared with measurements, and one example is seen in Figure 9.

Further analysis of reflector arrays was presented in 1990 [4]. The calculation results were compared with the characteristic frequency for a single plate, Eqn. (9) and one example is seen in Figure 10. Above the characteristic frequency the results vary depending on the exact position of the reflection point. If the reflection point is located between the plates, the high frequency reflection is weak and rapidly decreasing with frequency. Below the characteristic frequency, the results are quite stable and the position of the reflection point is not so important. Actually, the low frequencies are reflected quite well, and the level has been shown to depend on the density, i.e. how close the plates are together in the array.

It was found that the characteristic frequency f_g for the plates in the reflector array is also relevant for a reflector panel, but with a very different meaning. While f_g shall be as low as possible for a single reflector, the opposite is true for a reflector array. The best and most even reflection over a wide frequency range is obtained with a reflector array consisting of many small plates. At frequencies above f_g the reflections can vary significantly with small movements of the receiver position, see Figure 10.

The design principle was applied for the acoustical refurbishment of the concert hall in Copenhagen, originally used by the Danish Radio, but today taken over by the Royal Academy of Music. As seen in Figure 11, 61 slightly bent reflector plates are arranged in five rows, and each reflector has the dimensions 1.8 m * 0.8 m. With $a_1 = a_2 = 7.07$ m and θ = 45°, the characteristic frequency is f_g = 1200 Hz. More details can be found in [5].

Unfortunately, this design principle for a reflector array is seldomly followed. In several newly designed concert halls it is seen that the reflector array over the orchestra podium is designed with a few, very large reflectors. It seams like the fundamental difference between single reflectors and a reflector array is not understood.

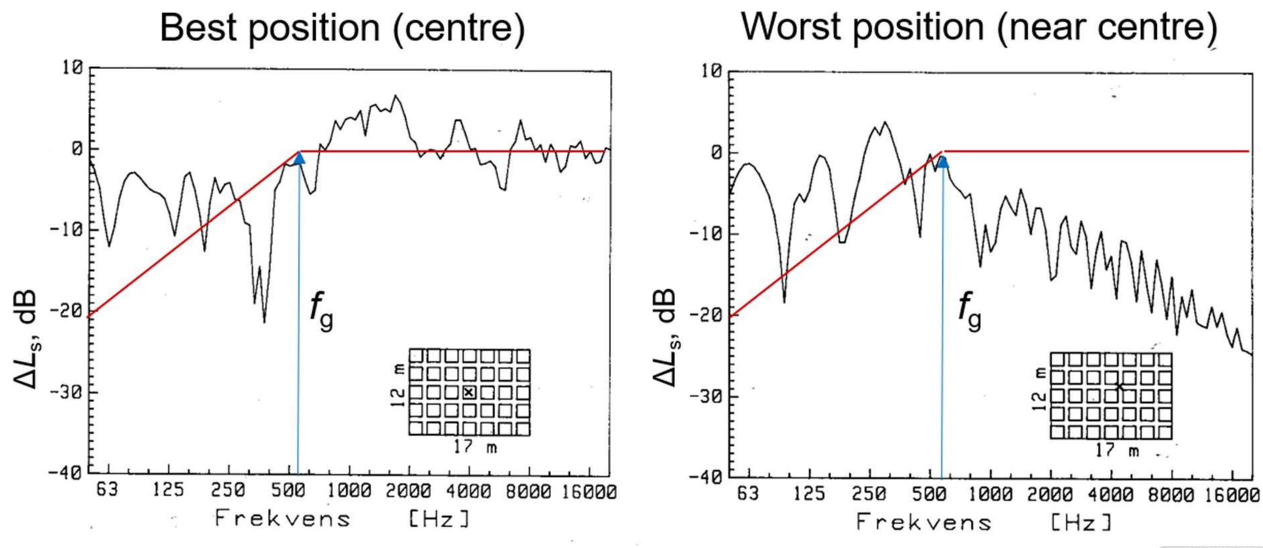

*Fig. 10: Calculation results for a reflector panel. Left with reflection point in centre of the middle plate. Right with the reflection point between plates, but near the middle of the array. Plate dimension 1.8 m * 1.8 m. Density of array = 50 %, Angle of incidence θ = 30°, a1 = a2 = 7.1 m. The characteristic frequency for a single plate is indicated. Adapted from [4].*

Fig. 11: Photo from the concert hall after the new reflector array and new wall reflectors were installed in 1989.

5. REFLECTION OF SOUND IN NON-SPECULAR DIRECTION

The sound reflection from a rectangular plate was further studied in 2004 by the application of a result derived for the sound transmission though a rectangular opening [6]. The directional sound radiation was averaged over frequency bands of one octave. The frequency dependent parameter is ka, where k is the angular wave number and a is one-half the side of a square with the same area as the plate. An example of calculated sound reflection is shown in Figure 12 for the angle of incidence 60° relative to the normal of the plate. While the sound reflection is within a narrow wedge for ka high, the reflection is broadening into a wider fan of directions when ka decreases. For ka = ¼ the reflection is nearly omnidirectional within a half-sphere. For comparison is shown in dotted line the Lambert's law for a diffuse reflection.

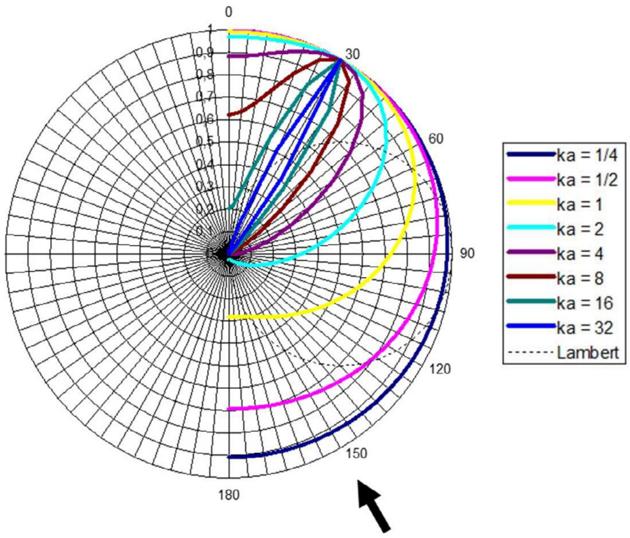

Fig. 12: Directivity of sound reflection in octave bands for a plane sound wave incident in the direction indicated by the arrow. The reflecting plane is in the vertical axis (0 to 180 degrees). The frequency parameter is ka.

6. SPHERICAL WAVE REFLECTION

Sound reflections are usually calculated with the assumption that the incident sound is a plane wave, even if the source is a point source in a well-defined distance from the reflecting surface. It has been known for a long time (at least since 1951) that a spherical sound wave gives reflections that can deviate significantly from those generated by a plane wave. This has been studied for decades in connection with outdoor sound propagation, but still the spherical wave reflection is seldomly applied in room acoustics. One reason for this might be that the mathematics involved is quite heavy. Also, solutions found in the literature mostly assume that the reflecting surface has infinite area.

Figure 13 is an example of the sound emitted from a point source in a height h_s above a surface. Using the image source method, the reflected sound can be treated as the sound emitted from the image source and transmitted through the surface to the receiver point. The total sound pressure in the receiver point is the sum of the sound pressures of the two sound waves. The result is strongly dependent on the phase difference between the two sound pressures, and this is not only due to the different length of propagation, but also due to the phase shift at the reflection.

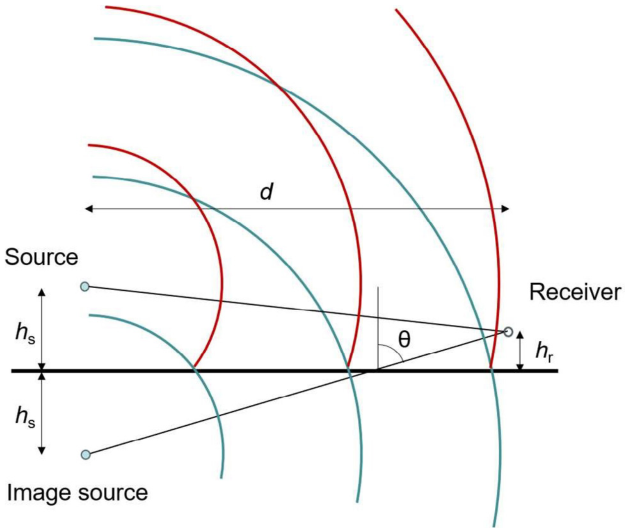

Figure 13: Spherical waves emitted from a point source and an image source. The receiver is a point in the height hr above the reflecting surface.

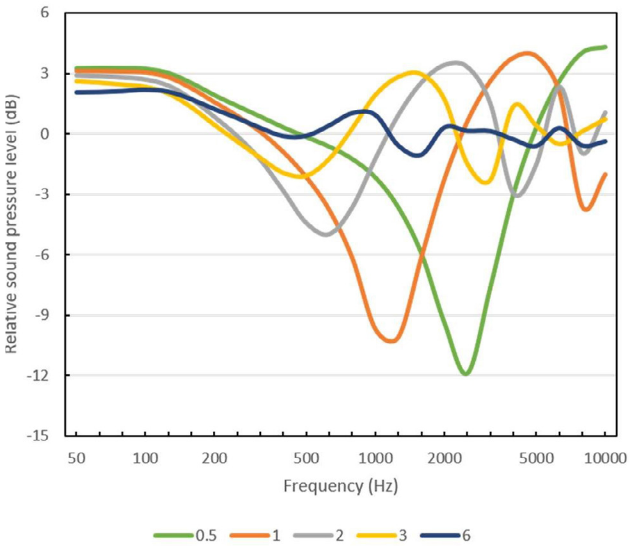

Fig. 14: The sound pressure level relative to the direct sound, calculated with different height hs of the source over the reflecting surface (0.5 m to 6 m). The surface material has acoustical properties typical for audience on upholstered seats. Horizontal distance is fixed at d = 20 m and height of receiver above the surface is hr = 0.4 m. Area of reflecting surface is 1000 m².

Recently, the author has derived an approximate solution that includes the complex radiation impedance of a surface with finite area [7]. An example of application of this method is seen in Figure 14. The reflecting surface has acoustical properties typical for an audience on upholstered seats. The seated audience is modelled as a large box with the height 0.8 m. The height of the receiver (the ear of a seated person) is assumed to be 1.2 m above the floor, and thus h_r = 0.4 m. The height of the sound source is varied while the horizontal distance to the receiver is d = 20 m. The results show a pronounced dip in the frequency curve when the height of the source is low (below 3 m). But at the source height 6 m the dip is no longer present and the frequency curve is relatively flat. At frequencies below 200 Hz the sound pressure level is around 2 dB to 3 dB above that in a free field (direct sound alone).

In the future it shall be interesting to see if the spherical wave reflection will be better understood in general, and to what extend room acoustic computer models can benefit from that.

REFERENCES

1. J.H. Rindel, Lydrefleksion fra konvekse og konkave cylinderflader. (In Danish). Proceedings of NAS-82, Stockholm, 1982, 71-74.

2. J.H. Rindel, Attenuation of Sound Reflections due to Diffraction. Proceedings of NAM-86, Aalborg, 1986, 257260.

3. P. Finne, Beregningsmodel for diffraktion. Akustiske anvendelser af Fresnel-Kirchhoffs approksimation. (In Danish). MSc Thesis, The Acoustics Laboratory, Kgs. Lyngby, Denmark 1987.

4. J.H. Rindel, The Design of an Array of Reflectors for Improved Ensemble on a Concert Hall Platform. Proceedings of NAM-90, Luleå, 1990, 129-134.

5. J.H. Rindel, A.C. Gade, N.V. Jordan, Radiohuset - Studio 1, Copenhagen, Denmark. Halls for music performance – Another two decades of experience 1982-2002. (Editors: I.B. Hoffman, C.A. Storch, T.J. Foulkes). Acoustical Society of America, 2003, 22-23.

6. J.H. Rindel, Modelling the directional characteristics of sound reflections. Proceedings of BNAM2004, Mariehamn, 2004.

7. J.H. Rindel, On the reflection of a spherical sound wave from a finite size surface. Submitted for Acoustics, Applied Sciences, MDPI, 2026.

Jens Holger Rindel
Professor emeritus, MSc, PhD
Senior researcher, Odeon A/S, Denmark
Senior acoustic consultant, Multiconsult, Norway

Short CV

2017

Jens Holger Rindel, b. 1947 in Copenhagen, Denmark. M.Sc. 1971 (civil engineering), Ph.D. 1977, both from the Technical University of Denmark. Until 2008 Professor in acoustics at the Technical University of Denmark. Senior researcher at the Norwegian Building Research Institute (1998-99). Visiting professor at the University of Sydney, the Nihon University, Japan, and the University of Auckland, New Zealand. Coordinator of European research projects (CAHRISMA, ERATO, DOREMI) and convenor of several ISO and CEN working groups. Author of textbooks, design guides in architectural acoustics, and more than 160 scientific papers. Short courses and master classes in architectural acoustics. Fellow of IOA and ASA. Since 2012 working part time with Odeon A/S and part time senior consultant in Multiconsult, Norway.

Work addresses:

Odeon A/S, Scion-DTU
Diplomvej 381
DK-2800 Kgs. Lyngby
Denmark

Multiconsult
Nedre Skøyen vei 2
P.O. Box 265 Skøyen
N-0213 Oslo
Norway

Telephone:

+45-5122 9870, +47-9801 5949
E-mail: jhr@odeon.dk, jehr@multiconsult.no

THE POSSIBILITY OF USING ELECTROACOUSTIC SOLUTIONS FOR ENHANCING ACOUSTIC PRIVACY IN PSYCHOTHERAPY PREMISES

[a] Illia Melnyk, [b] O. V. Bogdanov
[a]National Technical University of Ukraine "Igor Sikorsky Kyiv Polytechnic Institute", Kyiv, Ukraine, illia.melnyk90@gmail.com
[b]National Technical University of Ukraine "Igor Sikorsky Kyiv Polytechnic Institute", Kyiv, Ukraine, oleksiib@gmail.com

ABSTRACT

In the context of the growing demand for psychological assistance in Ukraine, especially in the post-war period, the quality of the acoustic environment in therapeutic offices is becoming a critical factor for treatment success. Ensuring complete confidentiality and low background noise levels (low Noise Criterion, NC) is a therapeutic requirement. Traditional passive sound insulation methods are often difficult to implement, particularly in existing buildings where doors and windows act as "weak links" with insufficient R'w indices. This paper presents an analysis of existing and prospective electroacoustic concepts to address this problem. To ensure the reliability of hybrid system control and reduce operational risks when integrating Artificial Intelligence algorithms, the paper proposes a controller model based on the Finite State Machine (FSM) method. A deep analysis of engineering, safety, and ethical risks is conducted, including physical actuator limitations, hardware limiters, and data privacy requirements (on-device processing) when integrating AI. The article presents a detailed experimental validation protocol. The authors conclude that a hybrid system — combining traditional architectural and electroacoustic methods — is optimal, and present a roadmap for prototype development.

KEYWORDS

Active Noise Control (ANC), Sound Masking, Architectural Acoustics, Psychotherapy, Sound Insulation, Artificial Intelligence (AI), Data Privacy.

1. INTRODUCTION

The scale of social and military challenges faced by Ukraine has caused an unprecedented increase in demand for mental health services [1], [2]. A significant number of cases of PTSD, anxiety, and depressive disorders are expected [3]. In this context, the psychotherapeutic office becomes an active therapeutic tool where trust and emotional safety are formed [4].

Two acoustic factors are key: acoustic comfort (low background noise and high speech intelligibility inside the room) [5] and confidentiality (unintelligibility of speech outside the office) [6]. The presence of extraneous sounds (footsteps, traffic, voices) can trigger traumatic experiences in clients [7], while a lack of confidentiality threatens the therapeutic alliance. One of the key problems is that in most existing buildings, doors and windows are "weak links" [8]. Traditional passive methods have physical limitations in efficiency, particularly in the low-frequency range (below 500 Hz) [9], [10].

The answer lies in the implementation of electroacoustic systems. Active Noise Control (ANC) technology purposefully attenuates background noise [9], while Sound Masking increases confidentiality by degrading the Speech Transmission Index (STI) outside the controlled zone [11]. This article clearly distinguishes between these two approaches and proposes hybrid concepts that integrate both.

Unlike existing single-domain approaches [12], [13], this work offers a comprehensive conceptual framework for hybrid electroacoustic systems, specifically tailored to the stringent ethical and privacy requirements of psychotherapeutic spaces.

The primary aim of this article is to synthesize classical active control approaches with AI-driven processing and a formal Finite State Machine (FSM) control logic to formulate a robust engineering architecture. By systematically evaluating hardware constraints, algorithmic behavior, and data privacy vectors (e.g., on-device processing constraints), this study establishes the theoretical and methodological foundation necessary for transitioning from conceptual design to hardware prototyping.

Furthermore, to bridge the gap between theoretical models and physical realization, the article introduces a rigorous experimental validation protocol (Section 7). While highly specific hardware-induced nonlinearities and high-variance secondary-path fluctuations inherent to real-world deployments represent subjects for subsequent empirical studies, the hybrid architecture and validation methodology formulated herein provide a structured, deterministic pathway for the development and assessment of active acoustic infrastructure.

2. ANALYSIS OF TECHNOLOGICAL PREREQUISITES AND EXISTING SOLUTIONS

2.1. HISTORICAL BACKGROUND OF ANC DEVELOPMENT

The concept of ANC was patented by P. Lueg in 1936 [14]. The patent described control in one-dimensional systems (ducts). Practical development began with L. Fogel's patent for aircraft cabins [15] and became possible due to the emergence of DSP in the 1970s-80s, which allowed for the implementation of adaptive algorithms [16]. Although Lueg's and Fogel's patents are foundational, their basic principles (interference, feedback) are well-known and do not hinder the development of modern systems based on FxLMS.

2.2. APPLICATION OF ANC/ASAC IN ARCHITECTURAL ACOUSTICS

In architecture, ANC is applied in targeted ways:

- Noise control in HVAC ducts [17].
- Active Structural Acoustic Control (ASAC) of "active windows," where actuators are attached to the glass [12], [13].
- Zonal ANC to create localized "zones of silence" [18].

2.3. ACOUSTIC REQUIREMENTS FOR THERAPEUTIC ROOMS

Based on international standards [19]—[21], the following targets have been defined:

Acoustic Parameter	Adapted Recommended Value[a.]	Basis for Adaptation
Background& HVAC Noise Level (***LAeq***)	35 dBA (NC 25)	BB93 recommends 30 dBA for SEN spaces and 35 dBA for standard learning environments [24]. LEED and healthcare acoustic guidelines support low background noise levels for confidential consultations [21]. Minimizes auditory distraction and supports concentration and emotional comfort.
Airborne Sound Insulation (***R'w / DnT,w***) walls	≥55 dB	STC/Rw ≈ 55 is commonly associated with high speech-privacy performance in sensitive consultation spaces (LEED v4, BB93-derived practice) [21, 24]. Supports confidentiality, speech privacy, and perceived safety.

Acoustic Parameter	Adapted Recommended Value[a.]	Basis for Adaptation
Airborne Sound Insulation (***R'w / DnT,w***) doors	≥42 dB	DGNB and BB93 emphasize the need for acoustically rated doors to preserve the overall sound insulation performance of the partition system. [20, 22, 24]
Impact Noise from Adjacent Corridors (***L'n,w***)	≤45 dB	BREEAM (Healthcare) / BB93 give strict criteria for quiet rooms. Reduces startle/distraction from footsteps or external activities.
Reverberation Time (***RT60***) for small rooms 125 Hz – 4 kHz	0.3–0.4 s	BB93 recommends RT60 values not exceeding approximately 0.4 s in SEN and other speech-critical support spaces [24]. DGNB SOC1.3 promotes comparable acoustic conditions aimed at achieving high speech intelligibility and acoustic comfort in small rooms [20]. Prevents echo, enhances clarity of speech and subtle emotional cues
Reverberation Time (***RT60***) for group rooms 125 Hz – 4 kHz	0.5–0.6 s	Values of 0.5–0.6 s are consistent with recommendations for meeting, consultation, and collaborative spaces where both speech intelligibility and acoustic comfort are required [20], [24]. Supports effective verbal communication without creating an over-damped acoustic environment.

*These values are proposed starting points for standardization and may require further refinement based on room size, specific therapeutic modality, and user feedback.

Tab. 1: Proposed Acoustic Requirements for Psychotherapy Spaces

The integration of HVAC noise into the overall background noise criterion ***(LAeq ≤ 35 dBA***) reflects the practical relationship between low ambient noise levels and compliance with the ***NC 25*** criterion commonly recommended for acoustically sensitive consultation spaces [20], [21], [24]. Evaluating both parameters within a single metric avoids redundancy, as mechanical and non-mechanical noise sources jointly determine the acoustic environment experienced by occupants and should remain below levels that could interfere with therapeutic communication. The reverberation-time targets are specified for the 125 Hz – 4 kHz octave-band range because this frequency region contains the most critical components for speech intelligibility and verbal interaction, which are fundamental to psychotherapeutic practice [24], [51], [52].

2.4. EMPIRICAL BASELINE: IN-SITU ASSESSMENT OF CONVENTIONAL DOORS

To empirically substantiate the designation of doors as critical acoustic "weak links", a series of in-situ measurements were conducted in operational modern office spaces. Office meeting rooms and psychotherapy consultation rooms within Ukraine's existing commercial building stock typically share an identical door construction, comprising the same standard interior door leaves (glass or solid wood), comparable frame and threshold installation practices, and supply from the same manufacturer base. As private psychotherapy practices are frequently established within precisely this class of retrofitted office space, the measured door performance is considered directly representative of the conditions found in psychotherapy premises. The measurements were performed according to ISO 16283-1 methodology to evaluate the apparent sound reduction index (***R'w***). As established in Section 2.3, ensuring speech confidentiality requires an isolation level of at least 42 dB. However, field data demonstrates a systematic failure of conventional architectural solutions to meet this criterion:

- **Standard single-pane glass doors (without specialized seals):** Demonstrated an ***R'w*** of 19 to 22 dB. The primary transmission paths are the lack of a mass, absence of threshold and unsealed perimeters.

- **Standard wooden doors (without drop-down seals):** Yielded an ***R'w*** of 24 to 25 dB. The lack of mass and structural acoustic decoupling restricts low-frequency attenuation.

- **"Acoustic" doors (with structural flaws):** Even heavy doors marketed with enhanced sound insulation provided an in-situ ***R'w*** of only 28 dB. Improper adjustment of drop-down seals (or even absence) and rigid frame mounting compromised the theoretical laboratory performance.

- These field measurements indicate a massive deficit of 14 to 23 dB between actual performance and the required target (***R'w ≥ 42 dB***). Achieving the required passive isolation solely through architectural means necessitates heavy, double-door vestibules, which are physically and ergonomically impossible to implement in most existing psychotherapy premises. This massive performance gap strictly dictates the necessity of active electroacoustic compensation. The full measurement protocol, equipment specifications, and complete per-door dataset are provided in Appendix A.

3. BASIC ANC ARCHITECTURES AND FXLMS

The idea of ANC is built on the generation of "anti-noise" [25]. A key part of constructing the correct "anti-noise" signal is the adaptive Filtered-X Least Mean Squares (FxLMS) algorithm, which requires an accurate model of the "secondary path" (***s(n)***) to ensure stability [26].

3.1. THE FXLMS ALGORITHM

Filtered-X LMS (FxLMS) is a modified variant of the LMS adaptive filtering algorithm, specifically designed for Active Noise Control (ANC) systems where the output signal passes through an additional physical path — the secondary path ***s(n)***. The presence of this path creates time delays and amplitude-phase distortions, causing the standard LMS to operate unstably [27], [28].

The Basic Problem: In classical LMS, the update of the adaptive filter weights is performed according to the equation:

$$\omega(n+1) = \omega(n) + \mu \cdot e(n) \cdot x(n) \tag{1}$$

Where ***e(n)*** is the error at the control point. However, in ANC, the output ***y(n)*** passes through an amplifier, loudspeaker, acoustic space, and reverberant interactions—i.e., through the secondary path ***s(n)***. As a result, the signal that actually reaches the control point differs from what the LMS "predicts." This leads to an incorrect gradient estimation, erroneous weight updates, and potential divergence of adaptation [27].

Where:
- ***n*** is the discrete time index (sample number). ***In*** digital signal processing, it reflects the sampled nature of the continuous time $t = nT_s$, where T_s is the sampling period. Therefore, ***n*** represents the current algorithmic iteration in the digital domain.

- ***ω(n)*** and ***ω(n+1)*** represent the coefficients (weights) of the adaptive filter at the current and the next discrete time step, respectively.

- ***μ*** is the step-size parameter (learning rate) governing the convergence speed and stability limit of the adaptation process.

- ***e(n)*** is the residual error signal measured by the error microphone at step ***n***.

- ***x(n)*** is the reference signal (primary noise) sampled at step ***n***.

- However, in ANC, the output ***y(n)*** passes through an amplifier, loudspeaker, acoustic space, and reverberant interactions—i.e., through the secondary path ***s(n)***. As a result, the signal that actually reaches the control point differs from what the LMS "predicts." This leads to an incorrect gradient estimation, erroneous weight updates, and potential divergence of adaptation [27].

3.2. THE CORE IDEA OF FXLMS

To account for the influence of the secondary path, the LMS cannot use the reference x(n) directly. FxLMS filters the reference signal through a model of the secondary path $\hat{s}(n)$:

$$\tilde{x}(n) = x(n) * \hat{s}(n) \qquad (2)$$

Where:

- $\hat{s}(n)$ is the estimated impulse response of the secondary path, acting as a fixed digital model of the physical electroacoustic environment.

- ******* denotes the discrete linear convolution operator in the time domain.

- $\tilde{x}(n)$ is the filtered reference signal, representing the reference noise mathematically processed through the digital secondary path model.

Using this filtered-x signal, the algorithm updates the weights as follows:

$$\omega(n+1) = \omega(n) + \mu \cdot e(n) \cdot \tilde{x}(n) \qquad (3)$$

Thanks to this modification, adaptation occurs taking into account the real delays and phase characteristics of the secondary path, making the algorithm stable in a physical system [28], [29].

3.3. STRUCTURE OF ANC WITH FXLMS

The system includes a reference microphone (measures primary noise ***d(n)***), an adaptive filter ***ω(n)***, a loudspeaker (generates ***y(n)***), the secondary path ***s(n)***, the model path $\hat{s}(n)$ in the DSP, the filtered-x block, and an error microphone that captures the residual signal ***e(n)***. FxLMS allows for a more accurate gradient calculation, compensating for the influence of the secondary path during the learning process [27], [28].

3.4. PURPOSE AND NECESSITY

Without secondary path compensation, the LMS receives an incorrect gradient vector. The system may:

- Diverge;

- Generate additional noise;

- Enter uncontrolled oscillations;

- Amplify the room's eigenmodes.

FxLMS eliminates this problem by pre-filtering the reference signal [28], [30].

3.5. MATHEMATICAL DESCRIPTION

Output of the adaptive filter:

$$y(n) = \sum_{k=0}^{M-1} \omega k(n) \cdot x(n-k) \qquad (4)$$

Where:

y(n) is the output signal of the adaptive filter (the digital "anti-noise") at the current discrete time step ***n***.

M is the length of the FIR (Finite Impulse Response) filter, representing the total number of filter coefficients (taps). This parameter defines the filter's memory window and directly impacts both the modeling accuracy and the computational complexity.

k is the summation index representing the discrete delay step within the filter's memory window.

ωk(n) is the ***k***-th weight coefficient of the adaptive filter at iteration ***n***.

x(n − k) is the reference signal sample delayed by ***k*** discrete time steps.

Signal at the control point (error signal):

$$e(n) = d(n) - y(n) * s(n) \tag{5}$$

Where:

d(n) is the primary acoustic noise (disturbance) at the location of the error microphone that the system aims to attenuate.

y(n) * s(n) represents the discrete time convolution of the controller's output ***y(n)*** with the impulse response of the actual physical secondary path ***s(n)***. Physically, this defines the anti-noise signal after it has propagated through the DAC, amplifier, loudspeaker, and the acoustic space to reach the error microphone.

FxLMS weight update:

$$\omega(n+1) = \omega(n) + \mu \cdot e(n) \cdot (x * \hat{s})(n) \tag{6}$$

Where:

$(x * \hat{s})(n)$ represents the convolution of the reference signal with the secondary path model at step ***n*** (which is mathematically equivalent to the filtered reference signal $\tilde{x}(n)$ introduced in Eq. 2). Using this term ensures the gradient estimation aligns with the phase delays and amplitude changes introduced by the physical secondary path.

The algorithm uses the secondary path estimate only in the gradient block, while the real ***s(n)*** is present in the physical system.

3.6. OBTAINING THE MODEL Ŝ(N)

The secondary path model is obtained using white or pink noise excitation. The transfer function between the loudspeaker and the error microphone is measured, after which an FIR model with a length of 50–300 coefficients is constructed. During ANC operation, this model is fixed (not updated), as changing it would lead to instability [28].

Advantages: FxLMS helps maintain stable ANC operation in real conditions, tolerates significant acoustic delays, can work with broadband and narrowband noises, and has low computational complexity for implementation on DSP or FPGA [27], [28], [31].

3.7. LIMITATIONS

The efficiency of FxLMS depends entirely on the accuracy of the secondary path model. If ***ŝ(n)*** does not correspond to ***s(n)***, attenuation efficiency drops significantly. The algorithm is less suitable for systems with strong non-linearity or conditions where the secondary path changes very rapidly (e.g., with a moving object) [30].

Although the FxLMS algorithm remains the de-facto baseline in feedforward ANC systems due to its simplicity and robustness, its performance can become constrained in scenarios characterized by strong nonlinearity, rapid changes in secondary-path dynamics, or highly nonstationary impulsive disturbances. In such cases, convergence speed, tracking accuracy, and overall stability may degrade, indicating that FxLMS does not always provide optimal control performance under more demanding acoustic conditions.

4. MATHEMATICAL MODEL OF THE SYSTEM

Any ANC system under consideration is based on the FxLMS architecture. The sound field at the error microphone point e(n) is described as:

$$e(n) = p(n) - s(n) * y(n) \tag{7}$$

Where:
p(n) is the penetrating primary noise. It is the result of the reference noise ***x(n)*** (from the corridor) convoluting with the impulse response of the primary acoustic path $p_{ir}(n)$ (slits, door leaf): $p(n) = p_{ir}(n) * x(n)$.

y(n) is the "anti-noise" generated by convoluting the reference signal with the controller's filter coefficients $\omega(n)$: $y(n) = \omega(n) * x(n)$.

s(n) is the physical secondary acoustic path impulse response (from speaker to error mic) convoluting with the anti-noise: ***s(n) * y(n)***.

The goal of the FxLMS algorithm is to update the coefficients of filter ***ω(n)*** to minimize the power of ***e(n)***. For the active retrofit frame concept, the perimeter slit of the door can be simply modeled as a 1D acoustic channel (pipe), for which the primary and secondary paths have relatively simple impulse responses, improving control stability [32].

5. ANALYSIS OF ELECTROACOUSTIC SOLUTION CONCEPTS

5.1. CONCEPT 1: „ACTIVE RETROFIT FRAME“ (ARF)

Description: Installation of a thin frame with arrays of microphones ($\boldsymbol{M_{ref}}$, $\boldsymbol{M_{err}}$) and actuators (loudspeakers) over the existing door frame to control leaks through slits [32].

Critical Analysis and Limitations:

- Physical Actuator Limitations. Integrating LF drivers capable of outputting the necessary SPL (approx. 70-80 dB in 1m for 50-300 Hz) into a “thin” frame (up to 5-7 cm) is quite complicated. This requires either significantly thickening the frame profile or using an external acoustic path (e.g., a compact subwoofer) near the base of the door.
- Bottom Slit Problem. The largest leak occurs under the door. If there is no threshold, actuator installation is impossible. The solution may require mechanical modification: installation of an automatic drop-down seal (for sealing) or a special floor module with an actuator.
- Physical Reliability. Components are vulnerable to impact. The design must include metal protective grilles and mechanical dampers.
- Privacy Efficiency. Classical FxLMS is ineffective against non-stationary signals (speech) [33]. ARF will reduce comfort issues (hum) well, but cannot guarantee confidentiality (speech intelligibility) without AI integration (see 6.8) or sound masking (see 5.3).
- External Radiation Risk. Any multi-channel ANC system located at the boundary of a room (such as an ANC) faces the risk that the generated “anti-noise” will itself radiate in an unwanted direction (e.g., out into a corridor) [49]. This creates additional acoustic pollution outside the controlled area. The design of the ANC should take this effect into account, and the control algorithms should include functions to suppress exterior radiation [49].

5.2. CONCEPT 2: „ACTIVE ACOUSTIC SCREEN“ (AAS)

Description: A mobile screen with a microphone/speaker array creating a local zone of silence (zonal ANC) [18], [34] in front of the door/window.

Critical Analysis and Limitations:

- Diffraction Problem. The screen creates only an “acoustic shadow,” but low-frequency sound will easily diffract around it.
- Privacy Problem. The solution is intended only to block incoming noise in the seating area and does not solve the problem of outgoing speech.
- Ergonomics. From a visual ergonomics perspective, bulky or visually intrusive equipment (e.g., a monitor) has the potential to negatively impact the therapeutic environment by creating a sense of technological presence that can be distracting to the client.

5.3. CONCEPT 3: „DISTRIBUTED STRUCTURAL LOUDSPEAKER NETWORK“ (DSLN)

Description: Integration of a network of loudspeakers into the suspended ceiling or wall cladding.

Critical Analysis and Limitations:

- Main Function – Sound Masking. The primary application is creating a uniform sound masking field [11] to increase the privacy of the therapy process [35]. This is the ideal solution for confidentiality, but it does not create silence.
- ANC Limitations. Using DSLN for global ANC (noise cancellation throughout the room) is practically unfeasible due to the need to control a complex 3D field (room modes) [36]. Only zonal ANC over chairs is possible [18].

- Risks. Masking efficiency requires synchronization with the corridor (masking must be present there too). Otherwise, the masking level required to drown out loud speech from the corridor will be uncomfortably high inside the office.

- Invasiveness. May require full or partial renovation.

6. PROSPECTS FOR ARTIFICIAL INTELLIGENCE (AI) INTEGRATION AND OTHER OPTIMIZATION METHODS

Limitations of classical DSP [33], [36] can be overcome using Deep Learning methods.

6.1. NONLINEAR AND ROBUST ANC CONTROL

Classical FxLMS exhibits limitations not only when dealing with speech [35], but also with other nonlinear or non-stationary signals, such as impulse noise (e.g., sudden loud sounds from the hallway, door slamming). Under such conditions, the stability of FxLMS can be compromised. To address this, "robust" algorithms are needed that dynamically modify the learning step size or the LMS logic to maintain stability under peak loads [47]. To overcome these nonlinear and non-stationary challenges, there are two promising directions:

- Deep Learning approaches. Replacing the linear filter ***ω(n)*** with a neural network (e.g., LSTM, CNN) [36, 37] to model complex nonlinear dependencies.

- Metaheuristic optimization. Using optimization algorithms such as Cuckoo Search (CS) to tune the LMS/NLMS filter coefficients. This approach has been shown to perform better in complex, nonlinear acoustic environments, potentially accelerating system convergence in real-world environments [48].

Advantage (for ARF and AAS): Improved efficiency and stability of non-stationary (speech, impulse) and nonlinear noise suppression.

6.2. ONLINE SECONDARY PATH IDENTIFICATION *s(n)*

AI Solution: Using an auxiliary neural network for online identification of ***ŝ(n)*** in real-time [37], [40].

Advantage (for ARF and AAS): Creating a system adaptive to environmental changes (movement of people), solving the main stability problem.

6.3. INTELLIGENT SOURCE SEPARATION

AI Solution: Training a neural network (e.g., Conv-TasNet [41]) for Blind Source Separation (BSS) [42], which "cleans" the reference signal ***x(n)***.

Advantage (for ARF): The ANC controller receives a clean signal containing only the target noise.

6.4. GENERATIVE ADAPTIVE SOUND DESIGN

AI Solution: (For DSLN) Using a generative AI model (e.g., WaveNet [43] or similar frameworks [44]) to create an adaptive, non-repetitive soundscape.

Advantage (for DSLN): Potentially enabling a transition from conventional noise cancellation toward the adaptive creation of a perceptually comfortable and more private acoustic environment, contingent on successful AI model validation and real-world implementation.

6.5. HARDWARE REQUIREMENTS AND AI LATENCY

AI integration is computationally expensive. Real-time neural network inference (with <5-10 ms latency) is unattainable for basic microcontrollers and requires specialized hardware accelerators (NPU - Neural Processing Unit) or powerful processors (e.g., ARM Cortex-A).

6.6. AI MODEL VALIDATION

Developing AI solutions requires a strict validation protocol:

- Training Data. Large datasets of real noises (corridors, speech, traffic).
- Metrics (BSS). SI-SDR (Signal-to-Distortion Ratio), PESQ, STOI to assess separation quality.

Metrics (ANC). MSE (Mean Squared Error) or energy reduction.

- Overfitting Prevention. The model must not "overfit" to a specific room; validation on unknown acoustic environments is required.

6.7. SPATIAL FIELD INTERPOLATION FOR SENSOR OPTIMIZATION

Zonal ANC, especially for AAS or DSLN concepts, may require a large number of error microphones to cover the entire zone, which significantly complicates and increases the cost of the system.

Use spatial sound field interpolation methods. Using signals from a reference microphone array, the system can mathematically interpolate (predict) the sound field at points where physical error microphones are absent [50]. Such a solution can serve as an effective way to solve the problem described above. This allows for a significant reduction in the number of error microphones required, while maintaining effective control over the "silent zone" [50]. This approach is also relevant for the ARF concept, where the physical space for mounting sensors in the frame is limited.

6.8. FINITE STATE MACHINE (FSM) MODEL FOR HYBRID CONTROLLER LOGIC

To manage the operational complexity and ensure the safety of this AI-driven hybrid system, we propose a Finite State Machine (FSM) model for the controller. This model provides a formal, verifiable logic for the system's behavior.

The FSM defines a finite set of operational states (Q), including:

- $\boldsymbol{q}_{IDLE}$ (Idle): System standby [ANC: Off, SM: Off].
- $\boldsymbol{q}_{ANC\_LOW}$ (Comfort): Activated by stable low-frequency hum. [FxLMS-ANC: On].
- $\boldsymbol{q}_{ANC\_AI}$ (Enhanced Comfort): Activated by non-stationary external noise (e.g., loud speech in the corridor). [NL-ANC (AI): On] [38].
- $\boldsymbol{q}_{MASKING}$ (Confidentiality): Activated by detection of internal speech. [Generative SM: On] [43].
- $\boldsymbol{q}_{HYBRID}$ (Full Privacy): Both external noise and internal speech are present. [ANC(AI): On, SM: On].
- $\boldsymbol{q}_{ADAPT}$ (Adaptation): Activated by environmental change; recalibrates the s(n) model [40].
- $\boldsymbol{q}_{FAULT}$ (Fail-safe): A critical error state (e.g., sensor failure or privacy breach risk). [SYSTEM HALTED].

The Transition Function (***δ***) defines the rules (e.g., ***δ*** (***qIDLE, noise_non_stationary***) → ***qANC_AI***). This FSM model provides the logical "skeleton" that improves operational predictability, while the AI modules act as the intelligent "brain" making decisions within that safe structure.

7. NUMERICAL SIMULATION, VALIDATION PROTOCOL AND USER TESTING

7.1. NUMERICAL SIMULATION OF THE ARF CONTROLLER

To technically validate the deterministic behavior of the FxLMS architecture within the Active Retrofit Frame (ARF) concept, a discrete-time numerical simulation was conducted. As formulated in Section 3, the door perimeter slit is modeled as a 1D acoustic channel.

The simulation parameterized the primary path $\boldsymbol{p_{ir}(n)}$ and secondary path as finite impulse response (FIR) filters representing physical electroacoustic delays and diffraction attenuation. A band-limited disturbance $\boldsymbol{x(n)}$ (50–300 Hz) was utilized to emulate typical low-frequency hallway hum, which conventional passive doors fail to attenuate (as demonstrated in Section 2.4). The FxLMS con-

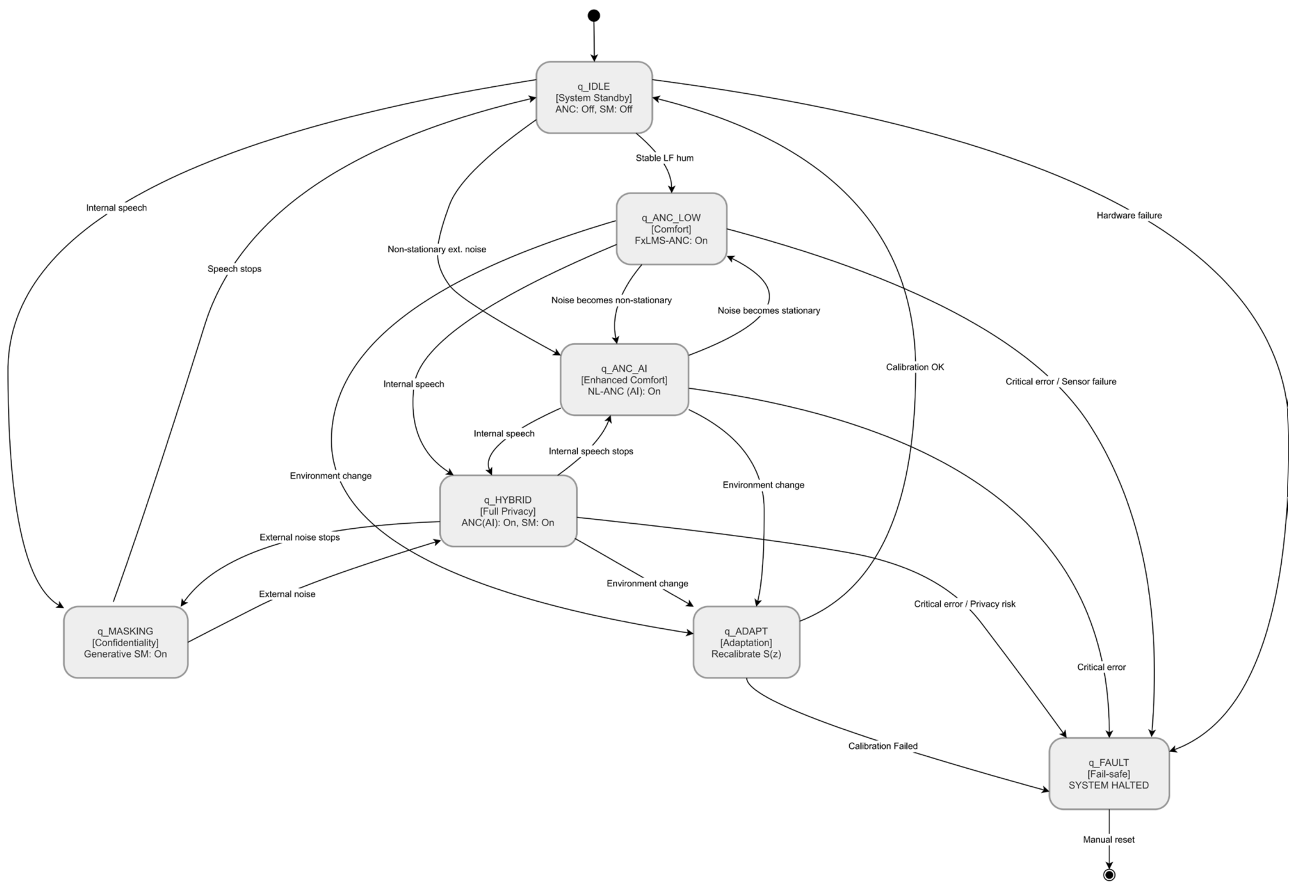

Fig. 1: Finite State Machine (FSM) Model for Hybrid Controller Logic

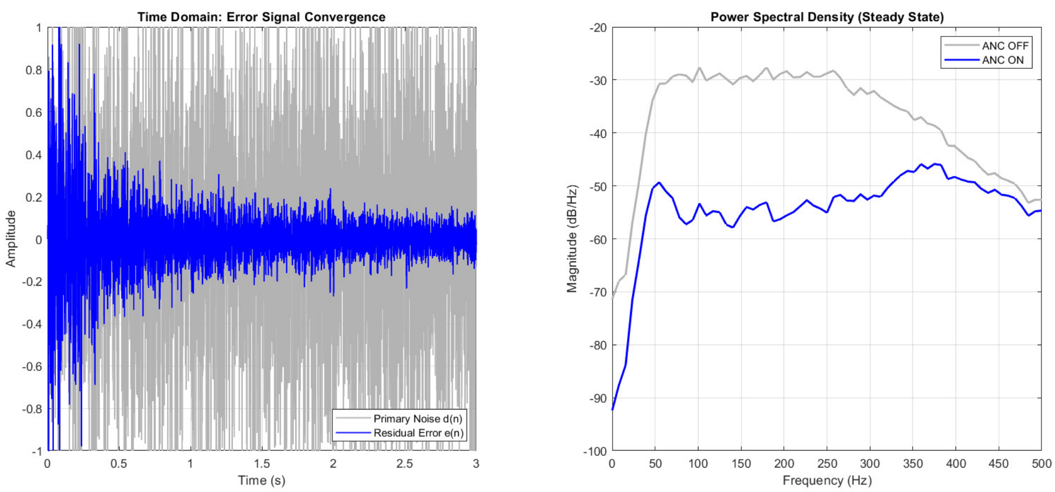

Fig 2. Time-domain convergence of the residual error signal e(n) (left) and the corresponding Power Spectral Density (PSD) attenuation in the steady state (right).

troller filter ***ω(n)*** was configured with ***M=128*** taps and a step size ***μ = 0.005***.

The numerical analysis (Fig. 2) demonstrates the theoretical feasibility of the proposed control strategy of the ARF concept. The adaptive algorithm achieved stable convergence within approximately 1.5 seconds, yielding an attenuation within the target low-frequency band exceeding 20 dB at the error microphone coordinate. This computational validation demonstrates that the 1D modelling approach for the door slit provides sufficient control stability, successfully linking the theoretical framework of Eq. 1-7 with the physical actuator requirements detailed in Section 3.1. The complete MATLAB source code, including all system parameters and impulse-response models used in this simulation, is provided in Appendix B.

7.2. EXPERIMENTAL VALIDATION PLAN

To transform the concept into an engineering product, a clear validation protocol is required.

1. Laboratory Measurements (ISO 10140-2 [45]). The prototype (e.g., ARF) is installed in a test aperture between two reverberation chambers.
2. Field Measurements (ISO 16283-1 [46]). The prototype is installed in a real office.
3. Noise Source. An omnidirectional source generating pink noise and a standardized speech signal (RASTI/STI).
4. Measuring Equipment. Precision Sound Pressure Level Meter (Class 1), calibrator, microphone arrays.
5. Test Scenarios:
   a. Test 1 (Passive): R'_w / ***NC*** / ***STI*** with the system off.
   b. Test 2 (Active): R'_w / ***NC*** / ***STI*** with the system on (FxLMS).
   c. Test 3 (Hybrid): R'_w / ***STI*** with the system on (FxLMS + Sound Masking).
6. Calibration $\hat{s}(n)$. Performed before tests by measuring impulse response (MLS or sine sweep) between each actuator and each error microphone.
7. Uncertainty Assessment: All R'_w measurements must be accompanied by measurement uncertainty calculations (±dB) according to ISO procedures to ensure result reliability.

7.3. SUBJECTIVE TESTING PROTOCOL

Parallel to technical measurements, subjective testing is conducted (N > 20, a group of therapists and volunteers) using questionnaires (Likert scale 1-5) to assess:

- Sense of privacy/confidentiality.
- Level of acoustic comfort and "naturalness" of the environment.
- Presence/absence of acoustic artifacts (artificiality, pressure).

8. ETHICAL, REGULATORY, AND ECONOMIC ASPECTS

8.1. DATA PRIVACY AND ETHICAL RISKS

A system using microphones in a therapy room poses a significant ethical risk.

1. **On-Device Processing**. All audio processing (FxLMS and AI inference) must occur exclusively on the device ("on-device"). No "raw" audio data or its derivatives should be transmitted to the cloud or stored in permanent memory.
2. **Data Minimization.** The system must not have permanent memory for audio; only temporary buffers (RAM) within a few milliseconds required for algorithm operation.
3. **Transparency.** The patient must be informed about the system's operation.
4. **Regulation**. The system must comply with GDPR standards and Ukrainian legislation on personal data protection.

8.2. FALLBACK' MECHANISMS AND AI RELIABILITY

The system must maintain fail-safe behavior under fault conditions.

In case of AI model failure (e.g., due to unpredictable input signal), the system must automatically transition ("fallback") to a conservative (safe) linear FxLMS controller.

In case of power failure or hardware fuse tripping, the system must switch to a fully passive mode.

8.3. REGULATORY REQUIREMENTS

Electrical Safety. A device installed in a public/medical room must comply with electrical safety standards (e.g., IEC 60601 for medical zones or EN 62368 for audio/IT equipment).

Electromagnetic Compatibility (EMC). The system must not create electromagnetic interference (EMI) for medical equipment or mobile phones.

8.4. ECONOMIC ANALYSIS AND FEASIBILITY

Although precise estimation requires a prototype, the estimated cost of hardware (DSP, MEMS mic array, LF actuators) for the ARF concept significantly exceeds the cost of passive solutions but is potentially lower than a complete renovation with replacement of the door units with a custom one etc.

The design (especially ARF) requires vandal-resistant execution. The system requires qualified maintenance (calibration, software updates).

9. CONCLUSION

The three concepts discussed address different aspects of the acoustic problem:

1. **"Active Retrofit Frame" (ARF)** is the only solution for local active blocking (noise reduction, NC). High engineering risks (LF drivers, bottom slit).

2. **"Active Acoustic Screen" (AAS)** is a flexible but inefficient solution that does not ensure confidentiality.

3. **"Distributed Structural Loudspeaker Network" (DSLN)** is the most invasive but most powerful solution for global confidentiality through sound masking.

No concept is ideal in isolation. ARF does not guarantee privacy. DSLN does not create localized attenuation zones.

The optimal solution is a hybrid system:

1. **Basic Level (Passive)**: Maximum possible passive isolation (including maximum sealing of gaps and thresholds).

2. **Active Level (ARF)**: Installation of a retrofit frame for active reduction of low-frequency hum (comfort).

3. **Privacy Level (DSLN)**: Installation of a distributed network to generate intelligent sound masking (AI-based [44]) (confidentiality).

Acoustic comfort and confidentiality are fundamental infrastructure requirements for psychotherapy in Ukraine [1], [3]. Existing doors [8] require innovative electroacoustic solutions. Moving beyond a comparative engineering analysis that defines the technical limitations, advantages, and risks of three concepts (ARF, AAS, DSLN), this work contributes a formal hybrid control logic based on a Finite State Machine (FSM).

Prior studies have shown that the limitations of classical digital signal processing algorithms (low efficiency for speech [33], instability [36]) can be mitigated by integrating AI (for non-linear control [38] and online adaptation [37]).

By establishing a deterministic operational skeleton, the proposed FSM-based architecture is designed to enhance system stability and address ethical concerns through robust fallback mechanisms. Furthermore, to safeguard data confidentiality, any viable system should rely on mandatory 'on-device' processing.

The most promising path is the development of a hybrid system (passive isolation + ARF + DSLN). This research lays the theoretical, engineering, and ethical foundation for further development, proposing a validation protocol (Section 7) that represents a clear progression from existing baseline solutions.

While the analysis provides insight into comparative algorithmic behavior, several implementation-level factors remain beyond the scope of this work.

REFERENCES

1. Goto, R., Pinchuk, I., Kolodezhny, O., Pimenova, N., Kano, Y., Skokauskas, N.: Mental Health of Adolescents Exposed to the War in Ukraine, JAMA PEDIATR., VOLUME 178, p. 480-488, 2024

2. Tolstoukhov, A., Matiash, M. M., Subbota, S., Lunov, V.: Ukrainian Syndrome. Behavioral and Functional Changes In Ukrainian Youth Under The Conditions of A 2022-Full-Scale Russian Invasion, SOCIAL SCIENCE RESEARCH NETWORK, SSRN Scholarly Paper ID 4319951, 2023

3. Ellis, E., Hazell, C. M., Mason, O.: The mental health of Ukrainian refugees: a narrative review, ACAD. MED., doi: 10.20953/AcadMed6232, 2024

4. Connellan, K., Gaardboe, M., Riggs, D., Due, G., Reinschmidt, A., Mustillo, L.: Stressed spaces: Mental health and architecture, HERD: HEALTH ENVIRONMENTS RES. & DESIGN J., VOLUME 6, p. 127-168, 2013

5. Passchier-Vermeer, W., Passchier, W. F.: Noise Exposure and Public Health, ENVIRON. HEALTH PERSPECT., VOLUME 108, p. 123-131, 2000

6. Ulrich, R. S., et al.: A review of the research literature on evidence-based healthcare design, HEALTH ENVIRONMENTS RESEARCH AND DESIGN JOURNAL, VOLUME 1, p. 61-125, 2008

7. Dijkstra, K., Pieterse, M., Pruyn, A.: Physical environmental stimuli that turn healthcare facilities into healing environments through psychologically mediated effects: Systematic review, J. ADV. NURS., VOLUME 56, p. 166-181, 2006

8. Fridlib, E., Melnyk, I., Maksymenko, A.: Comparison of objective acoustic criteria and subjective impressions in modern offices, PROC. 13TH ICBEN CONGRESS ON NOISE AS A PUBLIC HEALTH PROBLEM, Stockholm, Sweden, p. 1-5, 2021

9. Kajikawa, Y.: Recent advances on active noise control, IEICE ESS FUNDAM. REV., VOLUME 17, p. 36-43, 2023

10. Everest, F. A., Pohlmann, K. C.: Master Handbook of Acoustics, McGraw-Hill Education, 2015

11. Bradley, J. S.: The acoustical design of conventional open plan offices, CANADIAN ACOUSTICS, VOLUME 27, p. 23-31, 1999

12. Fuller, C. R., von Flotow, A. H.: Active control of sound and vibration, IEEE CONTROL SYSTEMS MAGAZINE, VOLUME 15, p. 9-19, 1995

13. Takeda, K., Kajikawa, Y., Nomura, Y.: Recent research and development of active noise control in Japan, INTER-NOISE 2005, Rio de Janeiro, Brazil, 2005

14. Lueg, P.: Process of silencing sound oscillations, U.S. Patent 2 043 416, 1936

15. Fogel, L. J.: System for elimination of sound, U.S. Patent 2 920 138, 1960

16. Elliott, S. J., Nelson, P. A.: Active noise control, IEEE SIGNAL PROCESSING MAGAZINE, VOLUME 10, p. 12-35, 1993

17. Kuo, S. M., Morgan, D. R.: Active noise control: a tutorial review, PROCEEDINGS OF THE IEEE, VOLUME 87, p. 943-973, 1999

18. Moreau, D., Celler, B., Cazzolato, B. S.: A review of virtual sensing algorithms for active noise control, ALGORITHMS, VOLUME 1, p. 69-99, 2008

19. DBN V.1.1-31:2013: Protection against noise in buildings, Minregionbud, Kyiv, Ukraine, 2013

20. DGNB e.V.: DGNB System – New Construction Buildings, Version 2014, SOC1.3 Acoustic Comfort, Stuttgart, Germany, 2014

21. U.S. Green Building Council: LEED v4 for Interior Design and Construction (ID+C), Acoustic Performance credit, Washington, DC, 2019

22. DGNB e.V.: DGNB System – New Construction Buildings, Version 2014, TEC1.2 Sound Insulation, Stuttgart, Germany, 2014

23. Order of the Ministry of Health of Ukraine No. 463: State sanitary norms of admissible noise levels in premises of residential and public buildings and in the territory of residential building, 2019

24. Department for Education: Building Bulletin 93: Acoustic Design of Schools – Performance Standards, TSO, London, 2014

25. Fuller, C. R., Elliott, S. J., Nelson, P. A.: Active Control of Vibration, Academic Press, 1996

26. Elliott, S. J.: Signal processing for active control, Academic Press, 2001

27. Burgess, J. C.: Active adaptive sound control in a duct: A computer simulation, JOURNAL OF THE ACOUSTICAL SOCIETY OF AMERICA, VOLUME 70, p. 715-726, 1981

28. Kuo, S. M., Morgan, D. R.: Active Noise Control Systems: Algorithms and DSP Implementations, Wiley, 1996

29. Widrow, B., Stearns, S. D.: Adaptive Signal Processing, Prentice-Hall, 1985

30. Takahashi, K., Kuo, S. M.: Modified filtered-X LMS algorithm for active noise control, PROC. IEEE ICASSP, p. 2633-2636, 1995

31. Morgan, D. R.: An analysis of multiple correlation cancellation loops with a filter in the auxiliary path, IEEE TRANSACTIONS ON ACOUSTICS, SPEECH, AND SIGNAL PROCESSING, VOLUME 28, p. 454-467, 1980

32. Zou, H., Shi, C., Gan, W. S., Lam, B.: Active control of sound transmission through a floor-level slit, THE JOURNAL OF THE ACOUSTICAL SOCIETY OF AMERICA, VOLUME 154, p. 2746-2755, 2023

33. Snyder, S. D.: Active control of the transmission of broadband, random sound through a finite double-panel partition, THE JOURNAL OF THE ACOUSTICAL SOCIETY OF AMERICA, VOLUME 112, p. 545-555, 2002

34. Elliott, S. J., Cheer, J.: Personal sound zones: a review, JSV-JOURNAL OF SOUND AND VIBRATION, VOLUME 331, p. 2567-2579, 2012

35. Venetjoki, N., Kaarlela-Tuomaala, A., Keskinen, E., Hongisto, V.: The effect of speech and speech intelligibility on task performance, ERGONOMICS, VOLUME 49, p. 1068-1091, 2006

36. Hansen, C., Snyder, S., Qiu, X., Brooks, L., Moreau, D.: Active control of noise and vibration, 2nd ed., CRC Press, 2012

37. Sun, H., Zhao, H., Zi, X., Gan, W. S.: A deep learning based online secondary path modeling method for active noise control, PROC. IEEE INT. CONF. ACOUST., SPEECH SIGNAL PROCESS. (ICASSP), Toronto, ON, Canada, p. 835-839, 2021

38. Zhang, H., Wang, D. L.: A deep learning approach to active noise control, PROC. INTERSPEECH 2020, Shanghai, China, p. 1141-1145, 2020

39. Huynh, M.-C., Chang, C.-Y., Kang, Z.: Nonlinear neural system for active noise controller to reduce narrowband noise, MATH. PROBL. ENG., VOLUME 2021, Art. no. 5555054, 2021

40. Yang, T., Sanada, H., Sakai, N., Kajikawa, Y., Nomura, Y.: A robust online secondary path modeling method with auxiliary noise power scheduling strategy and norm constraint manipulation, IEEE TRANS. AUDIO, SPEECH, LANG. PROCESS., VOLUME 16, p. 1680-1689, 2008

41. Luo, Y., Mesgarani, N.: Conv-TasNet: Surpassing Ideal Time-Frequency Masking for Speech Separation, IEEE/ACM TRANSACTIONS ON AUDIO, SPEECH, AND LANGUAGE PROCESSING, VOLUME 27, p. 1256-1266, 2019

42. Mishaly, Y., Wolf, L., Nachmani, E.: Deep Active Speech Cancellation with Mamba-Masking Network, ARXIV PREPRINT, arXiv:2502.01185, 2025

43. Birchfield, D., Mattar, N., Sundaram, H.: Design of a generative model for soundscape creation, PROC. INT. COMPUT. MUSIC CONF. (ICMC), Barcelona, Spain, 2005

44. Liu, H., et al.: AudioLDM: Text-to-audio generation with latent diffusion models, PROC. INT. CONF. MACH. LEARN. (ICML), Honolulu, HI, USA, p. 21976-22000, 2023

45. ISO 10140-2:2021: Acoustics — Laboratory measurement of sound insulation of building elements — Part 2: Measurement of airborne sound insulation, 2021

46. ISO 16283-1:2014: Acoustics — Field measurement of sound insulation in buildings and of building elements — Part 1: Airborne sound insulation, 2014

47. Liu, Y., Lei, Z.: Review of Advances in Active Impulsive Noise Control with Focus on Adaptive Algorithms, APPLIED SCIENCES, VOLUME 14, p. 1218, 2024

48. Liu, Y., Wang, Y., Zhao, H.: An Active Indoor Noise Control System Based on CS Algorithm, APPLIED SCIENCES, VOLUME 12, p. 9253, 2022

49. Kojima, T., Arikawa, K., Koyama, S., Saruwatari, H.: Multichannel Active Noise Control with Exterior Radiation Suppression Based on Riemannian Optimization, ARXIV PREPRINT, arXiv:2303.08396, 2023

50. Arikawa, K., Koyama, S., Saruwatari, H.: Spatial Active Noise Control Method Based on Sound Field Interpolation From Reference Microphone Signals, ARXIV PREPRINT, arXiv:2305.11276, 2023

Appendix A. In-Situ Acoustic Measurement Protocols for Conventional Doors

This appendix details the empirical acoustic measurements conducted in operational modern office spaces to evaluate the apparent sound reduction index (R'_w) of conventional doors. These measurements substantiate the empirical baseline described in Section 2.4 regarding the structural acoustic vulnerabilities of existing doors. The measurements were performed using a Class 1 precision sound level meter and an omnidirectional sound source, strictly adhering to the ISO 16283-1 methodology during years 2022...2026. The complete raw measurement protocols, including detailed frequency responses and site schematics, are openly available as a dataset in the repository [1].

The doors evaluated in this study can be subdivided into four different types based on their structural configuration and identified acoustic flaws:

Type 1: Standard single-pane glass doors

Location: BC tw12ve, 12 Novokostiantynivska Street, Kyiv, Ukraine.

Configuration: Single-pane glass door installed within a glass partition separating a corridor from an open-space area.

Measured Index: $R'_w = 19$ ***dB***.

Identified Deficiencies: Insufficient door perimeter sealing, complete absence of a threshold, and extremely low surface mass of the single-pane glass leaf.

Type 2: Glass doors with drop-down seals

Location: BC tw12ve, 12 Novokostiantynivska Street, Kyiv, Ukraine.

Configuration: Door equipped with a mechanical drop-down seal, installed within a double-glazed partition.

Measured Index: $R'_w = 21$ ***dB***.

Identified Deficiencies: The drop-down seal lacked proper mechanical engagement and pressure against the floor. Additionally, the perimeter rubber seals were loosely fitted, completely negating the theoretical acoustic benefits of the double-glazed partition.

Type 3: Standard wooden doors in combined partitions

Location: BC Spaces, 18/2 Maidan Nezalezhnosti, Kyiv, Ukraine.

Configuration: Solid wooden door installed in a combined gypsum board and glass partition.

Measured Index: $R'_w = 25$ ***dB***.

Identified Deficiencies: Lack of adequate mass and poor structural acoustic decoupling between the door frame and the partition, facilitating significant low-frequency flanking transmission.

Type 4: "Acoustic" doors with installation flaws

Location: BC Unit.City, 8 Sim'i Khokhlovykh Street, Kyiv, Ukraine.

Configuration: Heavy doors explicitly designed and marketed for enhanced sound insulation (theoretical laboratory rating $R'_w = 32$ ***dB***.).

Measured Index: $R'_w = 28$ ***dB***.

Identified Deficiencies: Low surface mass of the door leaf, absence of a double rebate (second quarter) in the frame, poor sealing of the perimeter contour, and a complete absence of a drop-down or stationary threshold.

Confidentiality Requirement: To ensure proper speech confidentiality in highly sensitive environments (such as meeting or therapy rooms), it is strictly recommended that the entrance door possesses an inherent apparent sound reduction index of $R'_w \geq 42$ ***dB***. The measured deficit of 14 dB demonstrates that conventional door constructions alone may be insufficient for achieving the target level of speech privacy, thereby motivating investigation of supplementary electroacoustic solutions.

REFERENCES

[1] 10.6084/m9.figshare.32866445

Appendix B. MATLAB Source Code for Numerical Simulation of the FxLMS Controller

This appendix provides the complete MATLAB source code utilized for the discrete-time numerical simulation of the Active Retrofit Frame (ARF) concept, as presented in Section 7.1. The script models the door perimeter slit as a 1D acoustic channel and implements the Filtered-X Least Mean Squares (FxLMS) algorithm to attenuate band-limited low-frequency noise (50–300 Hz). The adaptation logic rigorously conforms to the standard digital signal processing (DSP) sign convention (error subtraction approach), ensuring algorithmic stability and strict mathematical correspondence with Equations (5), (6), and (7) formulated in the manuscript.

```
% ==============================================================================

% Numerical Simulation of FxLMS for Active Retrofit Frame (1D Acoustic Slit)

% ==============================================================================

clear; clc; close all;


% 1. System parameters initialization

fs = 8000;        % Sampling frequency (8 kHz is sufficient for LF noise)

T = 3;            % Simulation duration (3 seconds)

N = fs * T;        % Total number of samples

mu = 0.005;       % Adaptation step size (Learning rate)

M = 128;          % Length of the adaptive FIR filter W(n)


% 2. Primary noise generation x(n) (low-frequency corridor hum, 50-300 Hz)

x = randn(N, 1);

[b_bp, a_bp] = butter(4, [50 300]/(fs/2), 'bandpass');

x = filter(b_bp, a_bp, x); % Band-limiting the spectrum to realistic LF noise

x = x / max(abs(x));      % Amplitude normalization


% 3. Modeling of physical acoustic paths (Impulse Responses)

% Primary Path P(z) - sound propagation through the slit (delay + attenuation)

Pw = zeros(64, 1);

Pw(12) = 1; Pw(13) = 0.8; Pw(14) = 0.4; Pw(15) = 0.1; % Diffraction emulation

d = filter(Pw, 1, x); % Target noise at the error microphone e(n)
```

```
% Secondary Path S(z) - from ARF loudspeaker to the error microphone e(n)
Sw = zeros(32, 1);
Sw(5) = 0.5; Sw(6) = -0.2; Sw(7) = 0.05; % Acoustic delay of ~5 samples
S_hat = Sw; % Secondary path model (assuming perfect estimation for baseline simulation)

% 4. FxLMS variables initialization
W = zeros(M, 1);        % Weight vector of the adaptive controller
e = zeros(N, 1);        % Error signal (residual noise)
y = zeros(N, 1);        % Anti-noise signal (controller output)

% Pre-filtering the reference signal through S_hat(z) -> x_prime(n)
x_prime = filter(S_hat, 1, x);

% State buffers (delay lines)
x_state = zeros(M, 1);
y_state = zeros(length(Sw), 1);
xp_state = zeros(M, 1);

% 5. Main FxLMS adaptation loop
disp('Running FxLMS Simulation...');
for n = 1:N
  % Update reference signal buffer
  x_state = [x(n); x_state(1:end-1)];

  % Generate anti-noise via controller y(n) = w(n) * x(n)
  y(n) = W' * x_state;

  % Propagate anti-noise through the physical secondary path S(z)
```

```
    y_state = [y(n); y_state(1:end-1)];
    anti_noise_at_mic = Sw' * y_state;

    % Sound field at the error microphone: e(n) = d(n) - s(n)*y(n)
    e(n) = d(n) - anti_noise_at_mic;

    % Update filtered reference signal buffer
    xp_state = [x_prime(n); xp_state(1:end-1)];

    % Update adaptive filter weights (gradient descent)
    W = W + mu * e(n) * xp_state;
end
disp('Simulation Complete.');

% ==========================================================================
% 6. Results visualization (Plots for the manuscript)
% ==========================================================================
figure('Position', [100, 100, 900, 400], 'Color', 'w');

% Plot 1: Time domain (Algorithm convergence)
subplot(1,2,1);
t = (0:N-1)/fs;
plot(t, d, 'Color', [0.7 0.7 0.7], 'LineWidth', 1); hold on;
plot(t, e, 'b', 'LineWidth', 1);
title('Time Domain: Error Signal Convergence');
xlabel('Time (s)'); ylabel('Amplitude');
legend('Primary Noise d(n)', 'Residual Error e(n)', 'Location', 'SouthEast');
grid on; axis([0 T -1 1]);
```

```
% Plot 2: Frequency domain (Power Spectral Density attenuation)
subplot(1,2,2);
[P_d, F] = pwelch(d(N/2:end), 1024, 512, 1024, fs); % Spectrum without ANC
[P_e, ~] = pwelch(e(N/2:end), 1024, 512, 1024, fs); % Spectrum with ANC
plot(F, 10*log10(P_d), 'Color', [0.7 0.7 0.7], 'LineWidth', 1.5); hold on;
plot(F, 10*log10(P_e), 'b', 'LineWidth', 1.5);
title('Power Spectral Density (Steady State)');
xlabel('Frequency (Hz)'); ylabel('Magnitude (dB/Hz)');
legend('ANC OFF', 'ANC ON', 'Location', 'NorthEast');
grid on; xlim([0 500]);
```

Illia Melnyk

PhD student at the Faculty of Electronics, National Technical University of Ukraine "Igor Sikorsky Kyiv Polytechnic Institute". He holds a Master of Science in Civil Engineering from the Kyiv National University of Construction and Architecture (2012) and a Master of Psychology from the Interregional Academy of Personnel Management (2024). His professional and academic profile operates at the intersection of engineering and architectural acoustics, psychoacoustics, and clinical psychology. In addition to his multidisciplinary academic background, he is a practicing psychologist, a certified Gestalt therapist, and the founder of Isophon, a company specializing in architectural acoustics and professional soundproofing. His current doctoral research is focused on the acoustic requirements for premises designed for personal and group psychotherapy. This work addresses the critical need for objective acoustic criteria — including sound insulation, reverberation time, and background noise control — specifically tailored for trauma-sensitive environments. Furthermore, his research explores the implementation of hybrid electroacoustic solutions, combining passive architectural measures with Active Noise Control (ANC) and sound masking technologies to ensure strict speech privacy and confidentiality. His broader research interests include the evaluation of subjective acoustic comfort versus objective criteria in modern offices, as well as the acoustic optimization of public infrastructure, such as metro stations.

O. V. Bogdanov

Graduated NTUU "KPI" in 2004 in the specialty "Acoustic equipment and systems." From 2004 to 2012 - assistant of Department of Acoustics and Acoustoelectronics. Since 2012 - associate professor of Department of Acoustics and Acoustoelectronics.

The patent of Ukraine owner number 51439 - "Method of determining the depth and thickness of the inner layer of the three-layer package"

In 2011 defended thesis for the degree of PhD, specialty 05.09.08 "Applied Acoustics and Sound technics" on "Apply for photothermoacoustic conversion tasks flaw"

NUMERICAL INVESTIGATION OF VIBRATIONAL MODES AND SOUND RADIATION IN A GAMELAN GONG

[a)]Laurentius Kevin Hendinata

[a)]Centrale Méditerranée, Aix Marseille Université, 13013 Marseille, France,
laurentius-kevin.hendinata@etu.univ-amu.fr

ABSTRACT

The gamelan gong holds a central place in Javanese musical and cultural traditions, serving both as a sonic landmark and a symbol within ritual performances. This study numerically investigates the gong's vibrational behavior and acoustic radiation using a finite element model that captures the coupled structural-acoustic dynamics under realistic boundary conditions. Structural dynamics and coupled acoustic simulations uncover a fundamental mode at 233 Hz, where motion concentrates in the central boss and yields a deep, slowly decaying tone that underpins the ensemble's cycle. Two higher resonances at 1546 Hz and 2738 Hz exhibit increasingly intricate nodal patterns, producing sharply peaked sound pressure levels up to 150 dB and generating the inharmonic partials that give the gong its characteristic shimmer. Quantitative comparison with ethnomusicological measurements confirms frequency ratios of approximately 6.6 and 11.8 relative to the fundamental.

KEYWORDS

Gong, Javanese gamelan, vibrational modes, acoustic radiation

1. INTRODUCTION

Gamelan is a traditional musical ensemble from Indonesia, known for its unique sound and layered rhythmic structure. It consists mainly of tuned percussion instruments made from bronze or iron [1], [2], [3]. It exists in several regional forms, including Javanese, Balinese, Sundanese, and others, each with unique styles, tunings, and cultural meanings. The ensemble is not only a musical system but a symbolic expression of communal and spiritual values.

Within the gamelan ensemble, a variety of percussion instruments coexist. A standard gamelan ensemble typically includes metallophones, xylophones, kendang (drums), saron, bonang, gender, rebab (bowed string instrument), suling (bamboo flute), and gongs [3], [4]. These physical differences lead to a distinctive range of fundamental frequencies and overtone structures, creating a rich sonic palette.

Among its instruments, the gong occupies a central role, both sonically and symbolically. In Javanese gamelan, large gongs with a central raised boss (called *penclon*) serve as temporal anchors. Their function is not melodic but structural: they mark the culmination of musical cycles, known as gongan, and signal key moments in performance [5]. The striking of a gong signifies a transition, often aligning with ritual time or the turning of a narrative phrase. The instrument is deeply embedded in cultural practice and is often associated with ideas of cosmic balance, ancestral presence, and sacred space [6], [7], [8]. Its resonant, slowly decaying tone is considered essential for grounding the ensemble and connecting the physical and spiritual realms during performance.

From a physical perspective, the gong presents a compelling object of study. It combines a curved shell geometry with nonuniform thickness, leading to a rich and complex vibrational response. When struck, it supports a range of vibrational modes, some of which couple efficiently with the surrounding air to produce strong acoustic radiation. The vibrational energy is initially concentrated in the central boss, then propagates across the body of the gong [9], [10], [11]. The resulting acoustic field reflects both the structural dynamics of the plate and its interaction with air as a radiating surface [12].

This study applies FEM to analyze the vibroacoustic response of a traditional Javanese gong. It identifies natural frequencies and mode shapes under support conditions resembling physical suspension. The study also simulates forced vibration at the gong's central boss and evaluates the resulting acoustic pressure field. Through this approach, the work aims to connect structural vibration patterns with audible features such as pitch salience and overtone richness.

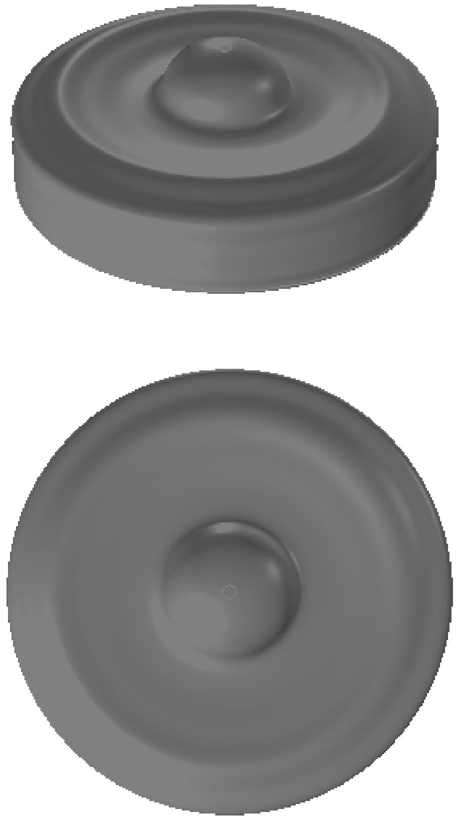

2. GEOMETRIC AND MATERIAL CONFIGURATION

2.1. GEOMETRY DEFINITION

The gong analyzed in this study is a moderately sized example from the Javanese gamelan family, selected to represent typical structural features while maintaining computational efficiency. The model geometry is based on a direct measurement of a physical instrument. The overall radius of the gong is set at 10.5 cm, with a central boss (or penclon) radius of 2.2 cm. The gong's thickness is not uniform, varying from approximately 0.20 cm at the rim to 0.30 cm at the boss, following a gradual contour that is typical of handcrafted gongs.

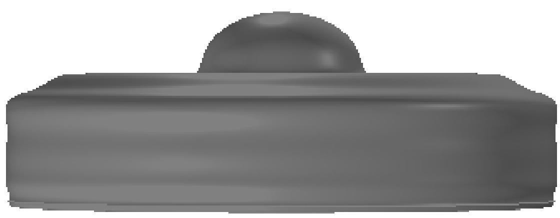

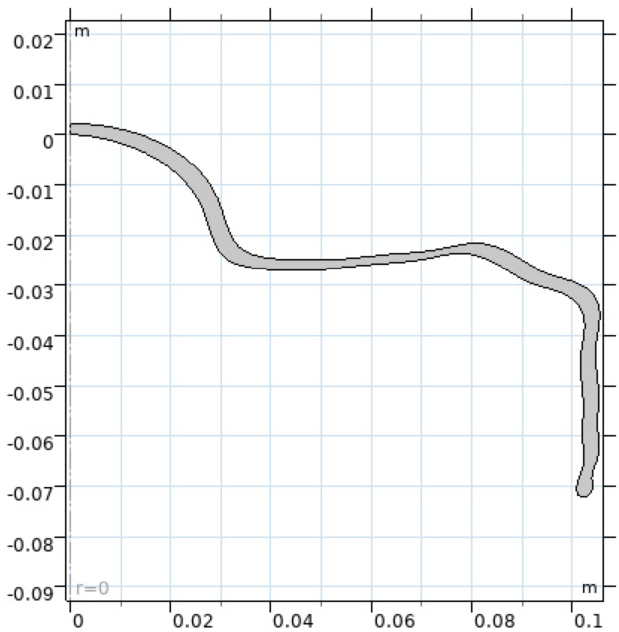

Fig. 1: Illustration of the traditional gamelan gong (a) orthogonal views and the top-side plane perspectives, and (b) cross-sectional profile modeled in 2D axisymmetric coordinates.

The geometry is represented using a 2D axisymmetric model (Figure 1b), which captures the essential profile of the gong while assuming perfect rotational symmetry. This approach simplifies computation and is appropriate for capturing the dominant radial and circumferential modes in an idealized structure. However, it does not account for three-dimensional irregularities such as local warping, material anisotropy, or slight asymmetries introduced during traditional casting and manual tuning.

2.2. MATERIAL PROPERTIES

Traditional Javanese gongs are cast from a high-tin bronze alloy, typically comprising 78% copper and 22% tin by weight. This alloy selection balances high stiffness and acoustic brightness with the castability required for detailed shaping. Tin increases the alloy's hardness and elevates its elastic modulus, while copper ensures sufficient density and ductility. In some cases, trace elements such as zinc or lead are included in small amounts to improve fluidity during casting or influence internal damping. The specific alloy composition used in gamelan manufacturing has been refined over generations to optimize both mechanical stability and tonal richness.

This specific alloy composition forms the basis for our simulation parameters. The density of 8800 kg/m³ reflects the heavy copper content. Young's modulus of 110 GPa captures the combined stiffness of copper and tin in the alloy. Poisson's ratio of 0.34 characterizes its lateral contraction under load. These values are consistent with published data for high-tin bronzes used in musical applications. The material is assumed to be isotropic and homogeneous, a simplification that ignores potential grain orientation or segregation effects, which may arise during solidification or manual finishing.

To represent internal energy loss, an isotropic structural loss factor of 0.04 is applied. This damping term accounts for internal friction, arising primarily from dislocation motion, grain boundary sliding, and minor inelastic effects within the metallic microstructure. It does not include radiation damping, which is treated separately in the acoustic simulation.

3. MODAL ANALYSIS

3.1. MARKING OF IMAGES

The finite element model is developed using a 2D axisymmetric approach to capture the gong's cross-sectional geometry. The solid domain is assigned bronze material properties based on the alloy specifications described earlier. An eigenfrequency solver based on the Arpack method is used to extract the natural frequencies and associated mode shapes.

The boundary condition applied is a simply supported outer edge, implemented by constraining radial displacement at the rim (u_r = 0), while allowing vertical motion and rotation. This setup approximates the real-world suspension of a gong by cords at discrete points around its edge, which imposes minimal constraint on its vertical motion but provides support in the plane of the plate. The central boss remains entirely free, mimicking how the striking zone moves during performance.

The mesh is constructed using a swept triangular element scheme, with quadratic Lagrange elements to improve accuracy in capturing curvature and localized bending. The mesh is refined significantly near the boss and shoulder transitions, where mode localization and curvature effects dominate. A mesh convergence study was conducted by systematically refining the element size and observing the change in the first few natural frequencies. Convergence was achieved with less than 0.5% deviation in frequency values upon further refinement, confirming mesh-independence of the results.

No pre-stress or residual stress conditions were included in this initial analysis. While residual stresses from casting and tuning could influence real-world frequencies slightly, they are neglected here to focus on geometry-driven modal behavior.

3.2. RESULTS

The finite element model is developed using a 2D axisymmetric approach to capture the gong's cross-sectional geometry. The solid domain is assigned bronze material properties based on the alloy specifications described

The computed mode shapes reveal distinct nodal circles and diameters that correspond to the gong's harmonic spectrum. The fundamental mode concentrates displacement in the central boss, matching the deep bass resonance valued in Javanese ceremonies. Higher modes form complex patterns that distribute vibrational energy across the plate, enriching overtone content.

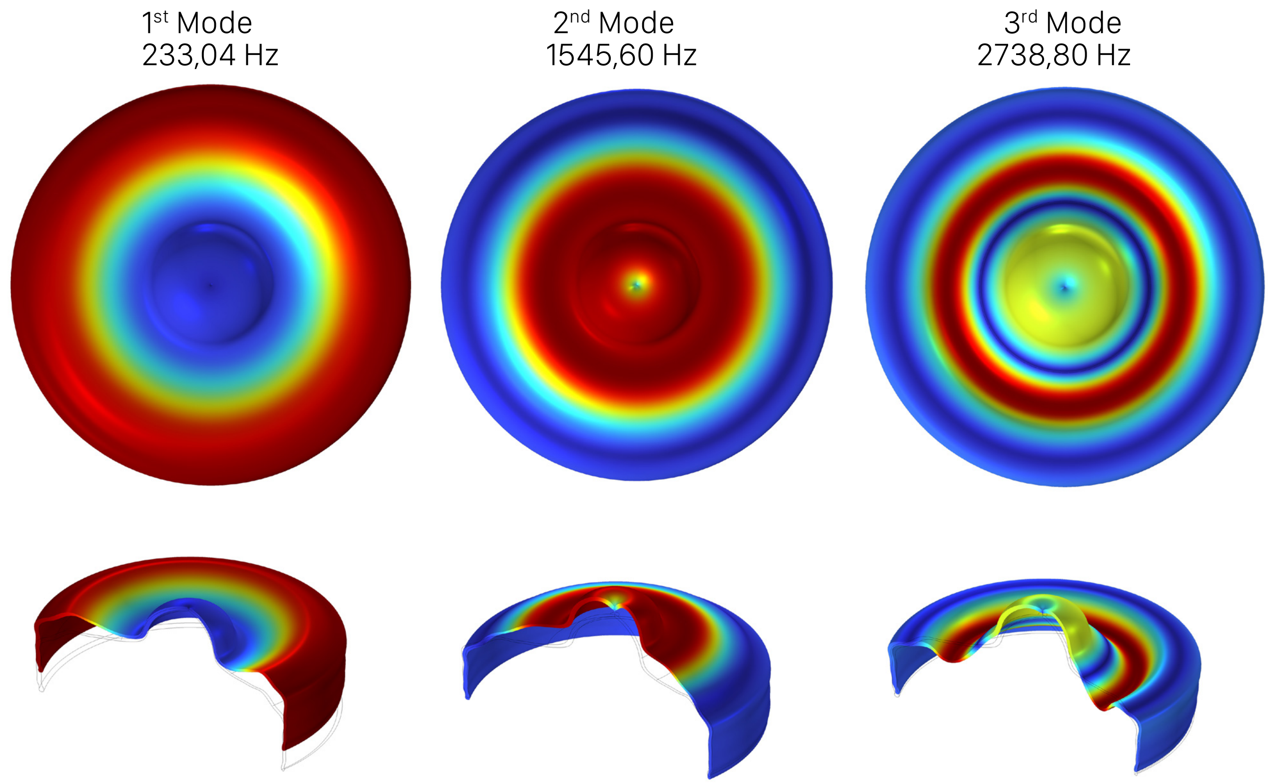

Fig. 2: First three modes of the gamelan gong.

The simulated natural frequencies and mode shapes of the gong show clear vibrational patterns consistent with the behavior of circular plates that have non-uniform thickness. Table 1 presents the first three modes from the results. The lowest frequency is 233.04 Hz, followed by 1545.60 Hz and 2737.80 Hz. This wide frequency range reflects the contrast in stiffness between the central boss and the rest of the plate.

The first mode at 233.04 Hz shows strong displacement localized at the central boss, with minimal movement in the outer regions. This is a typical piston-like mode, where the boss moves in and out while the surrounding plate acts as a relatively rigid support. Physically, the boss behaves as a mass-loaded center, reducing the system's effective stiffness in the region and lowering the frequency. The outer plate's thickness and radial stiffness suppress significant motion, resulting in a deep, sustained tone with relatively low radiation efficiency.

The second mode, near 1545.60 Hz, features a large vibrating region across much of the plate surface, including the dome and shoulder areas. Several nodal diameters and one or two nodal circles can be identified. This pattern allows more efficient coupling with the surrounding air, and as such, this mode corresponds to the most acoustically prominent pitch of the gong. It produces the sharp, striking tone often used to mark phrase boundaries in Javanese musical cycles.

At 2737.80 Hz, the third mode exhibits a more fragmented pattern, with multiple nodal circles and diameters. The vibrational energy is distributed in smaller lobes across the plate, contributing to inharmonic overtones and the rich metallic timbre of the gong.

The frequency ratios of the modes deviate significantly from those expected for an ideal circular plate with uniform thickness. In theory, for a thin isotropic plate with clamped or simply supported boundaries, the second and third frequencies would occur at approximately 2.0 and 3.5 times the first mode, depending on boundary conditions and aspect ratio. However, in this case, the second mode occurs at 6.6 times the first, and the third at 11.7 times, indicating strong modal inharmonicity.

The inharmonicity observed in the modal frequencies arises from a combination of geometric and material factors. First, the plate's non-uniform thickness introduces variations in local bending stiffness, which causes certain higher-order modes to shift upward more significantly than others. In contrast, the central boss acts as a concentrated mass, lowering the fundamental frequency more than it affects the higher modes, thus widening the gap between them. Additionally, the combined influence of internal damping and the complex curvature of the gong disrupts the regular spacing of natural frequencies typically found in idealized circular plates, further reinforcing the inharmonic structure that characterizes the gong's acoustic signature.

Such inharmonic spacing is intentional and musically significant in gamelan instruments. The perceived intervals and pitch centers differ from Western scales, and the modal structure here supports that cultural usage. In practice, the asymmetry and minor imperfections in the real instrument further split these modes, leading to beating phenomena and spectral richness that are prized in performance.

4. FORCED VIBRATION AND TRANSFER FUNCTION ANALYSIS

4.1. EXCITATION SETUP

To study the gong's response under external loading, a forced vibration analysis was carried out using a harmonic excitation approach. The excitation was applied as a point force directly at the center of the dome, which is the usual striking point during a performance. Although percussive impacts happen in the time domain, a harmonic sweep in the frequency domain was chosen because it allows detailed observation of the system's steady-state response at each frequency. This method is useful for identifying resonances, and its results can later be related to time-domain behavior through Fourier analysis.

The excitation force was set with a fixed amplitude and zero phase shift. Because the model assumes linear behavior, the response scales proportionally with the force, and only the relative amplitude and phase are important. A sweep from 50 Hz to 2000 Hz was used to cover both the fundamental mode and several higher modes that contribute to the gong's sound. This range was chosen to capture the bass and overtone content typically heard in performance and to stay within the lower part of the human hearing range, where most of the gong's energy lies.

Displacement results were monitored at three locations: the dome rim, the shoulder (where the dome transitions to the flat plate), and the outer edge of the gong. These points were selected to track how vibrations spread from the impact point across the surface. They also provide useful data for evaluating transfer functions, which show how energy moves through the structure and where it tends to concentrate or fade out.

4.2. TRANSFER FUNCTION EVALUATION

The transfer function describes how much motion occurs at one point on the gong in response to a force applied at another. It is defined as the ratio between the displacement magnitude at a given location and the applied harmonic force. Mathematically, it takes the form as in Eq. (1).

$$H(f) = \frac{U_{resp}(f)}{F_{input}(f)} \tag{1}$$

where $U_{resp}(f)$ represents the frequency-dependent displacement amplitude at the observation point and $F_{input}(f)$ is the magnitude of the applied excitation force. This formulation allows quantification of how effectively vibrations propagate from the excitation site to other parts of the gong's structure.

By plotting both the magnitude and phase of the transfer function over the swept frequency range, resonant peaks corresponding to natural vibration modes can be identified. These peaks indicate frequencies at which the gong responds strongly to excitation, highlighting modal contributions to the overall vibro-acoustic behavior. The phase information provides insight into the relative timing of displacement responses, which is important for understanding wave propagation and mode coupling within the instrument.

more coherent motion across the plate, leading to stronger radiation and a clearer peak in the sound pressure spectrum.

The spacing between these peaks does not follow simple harmonic ratios, which is typical for plates and shells with curved and non-uniform geometry. In these systems, the modal frequencies are determined by complex relationships involving stiffness, mass distri-

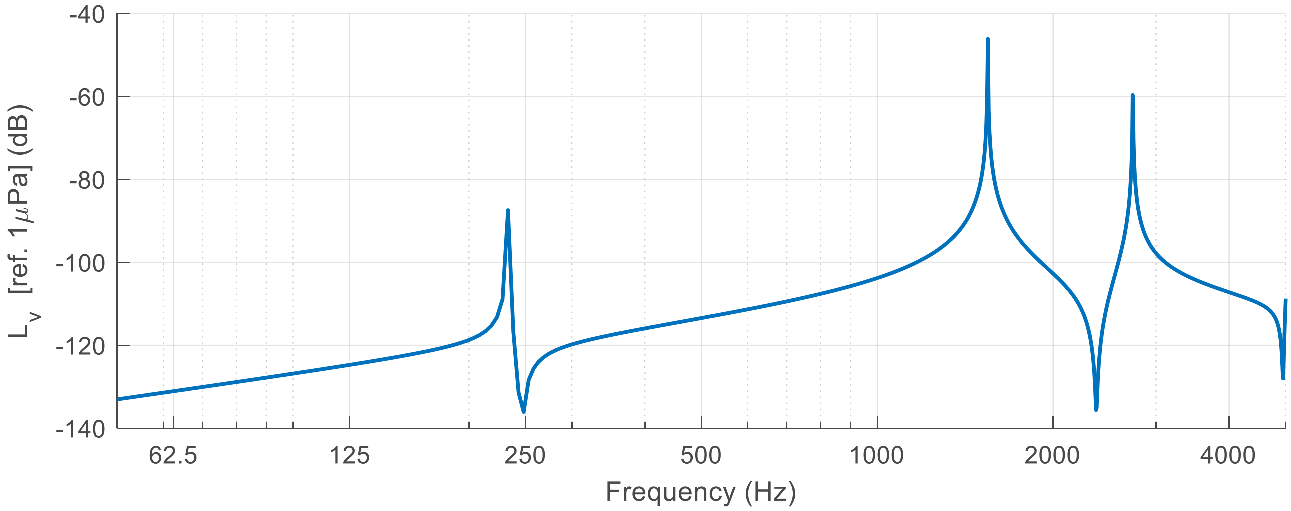

Fig. 3: Vibration level distribution on the gong arm.

bution, and boundary conditions. As a result, the gong produces a rich set of inharmonic overtones that contribute to its unique timbre, different from the harmonic series found in string or air column instruments.

Figure 3 shows the vibration levels recorded at the outer region of the gong. The first clear resonance appears around 250 Hz, but the amplitude is relatively low, about −85 dB. In contrast, the strongest response is found near 1700 to 1800 Hz, where the displacement level rises to about −45 dB. Other peaks appear around 2500 Hz and close to 4000 Hz, but with lower intensity, typically near −60 dB. These frequencies correspond to the system's natural modes and reflect how the structure responds to excitation, based on its shape and material properties.

The variation in peak amplitudes shows that not all modes radiate sound equally well. The low-frequency mode near 250 Hz causes mostly localized movement in the central dome. While this motion is strong within the plate, it often leads to weak sound radiation due to destructive interference. Opposite parts of the surface may move out of phase, cancelling each other's acoustic output. In contrast, the higher-frequency mode near 1700 Hz appears to couple better with the surrounding air. Its vibration pattern may involve

5. ACOUSTIC COUPLING AND SPL ESTIMATION

To simulate the conversion of mechanical vibration into radiated sound, a coupled structural-acoustic analysis is performed in the frequency domain. The solid domain represents the gong's bronze shell, governed by the Navier-Cauchy equations for linear elasticity. The surrounding air domain is modeled using the Helmholtz equation for time-harmonic pressure fields. The two domains are coupled through boundary conditions that ensure physical continuity at their interface. Specifically, the normal velocity of the vibrating shell must match the fluid particle velocity, and the stress in the solid must balance the pressure-induced traction in the fluid.

The air domain extends approximately 2 meters from the center of the gong in all directions. To simulate an unbounded acoustic space, radiation boundary conditions are applied at the outer boundaries. These are implemented using perfectly matched layers (PML) that absorb outgoing waves without reflection, mimicking open-air conditions. This treatment avoids artificial interference from wave reflections at the domain edge and improves the accuracy of radiated sound predictions.

The coupled problem is solved using the finite element method, where the solid and fluid domains are meshed and computed simultaneously. The FEM solver handles the direct coupling of degrees of freedom at the solid-fluid boundary, ensuring energy transfer across the interface is correctly modeled. This approach captures the mutual interaction between vibration and sound radiation.

To evaluate sound radiation quantitatively, pressure is monitored at several points placed on a circular probe line 1 meter above the gong apex. The selected distance approximates a typical listening position and ensures measurements are taken in the acoustic far field. Probe points are evenly distributed along the circumference to capture angular variations in pressure and avoid bias from directional radiation. The pressure magnitude at each frequency $p(r,f)$ is recorded and converted to sound pressure level (SPL) using the standard expression, as in Eq. (2).

$$SPL\ (f) = 20\log_{10}\left(\frac{|p(r,f)|}{p_{ref}}\right) \tag{2}$$

where p_{ref} = 20μPa is the reference sound pressure. An average SPL over all probe points is taken to provide a representative measure of the radiated acoustic energy at each frequency.

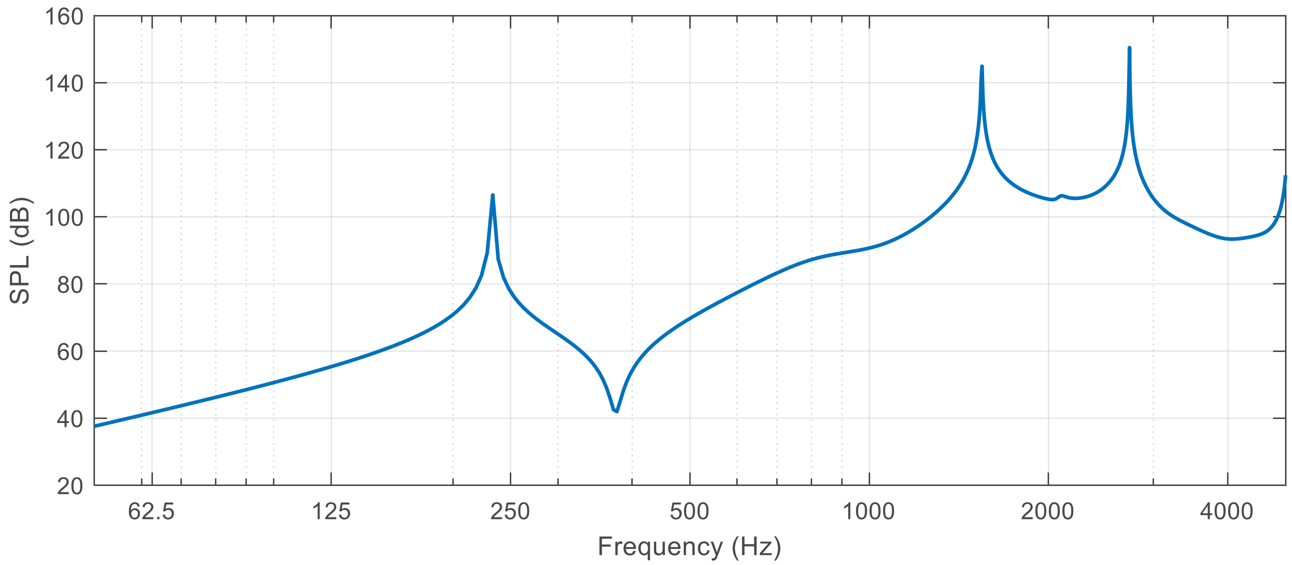

Fig. 4: SPL measured at 1 meter above the gong apex during shell excitation.

Figure 4 presents the SPL measured at 1 meter above the gong following harmonic excitation. The spectrum shows several peaks, each indicating a strong acoustic response. These peaks align with structural resonances where surface motion efficiently couples to the surrounding air. The most prominent peak appears between 1700 and 1800 Hz, corresponding to a vibration mode that radiates sound effectively due to its coherent surface motion.

The third peak, at 2737 Hz, arises from a more fragmented mode with several nodal lines. While less efficient than the second mode, it still contributes to the overall sound character. A fourth peak appears near 3500 to 4000 Hz and likely represents higher-order patterns that radiate due to their higher frequency and surface area involvement.

Between these peaks, distinct dips are visible in the SPL. At 377 Hz, 1997 Hz, and 4058 Hz,

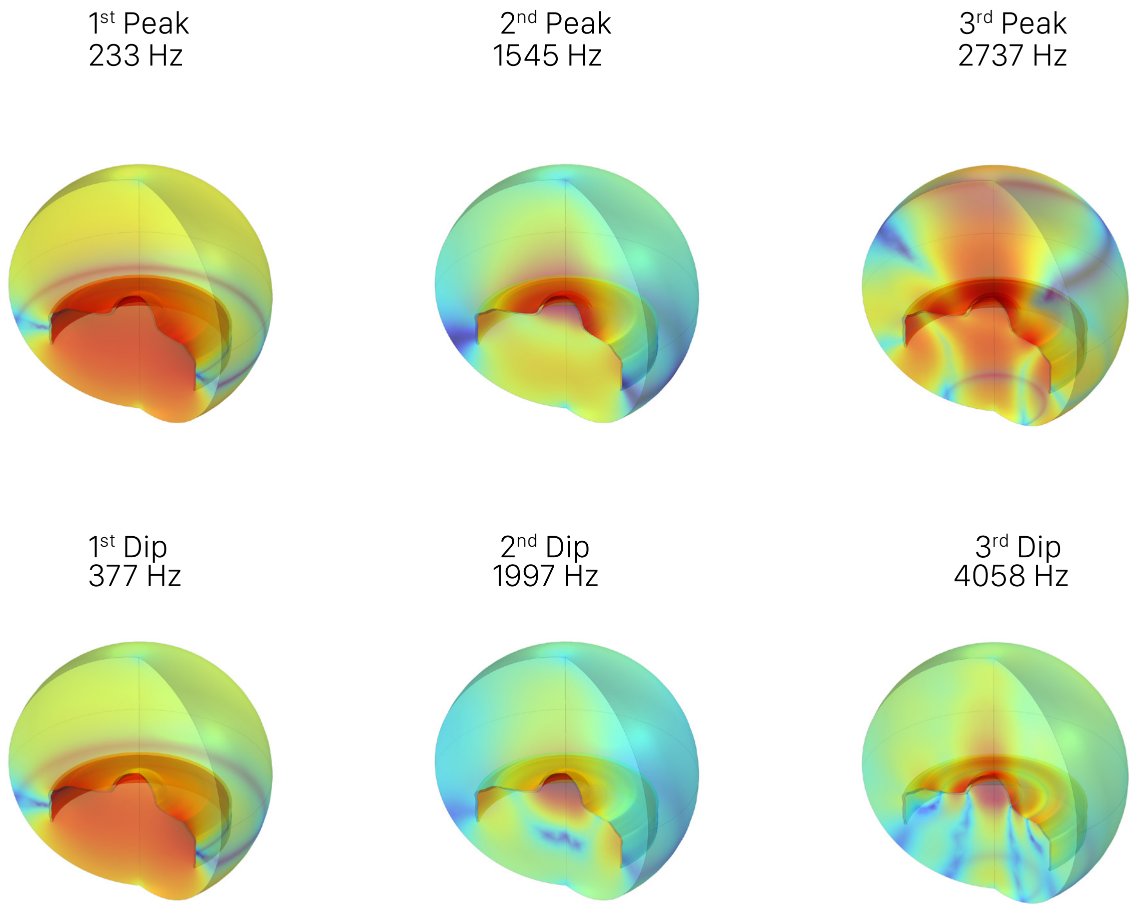

Fig. 5: Mode shapes of the gong shell at key resonance frequencies corresponding to peaks and dips in the SPL spectrum.

Figure 5 shows the mode shapes associated with key SPL features. For example, the first peak at 233 Hz corresponds to a low-order mode concentrated near the boss. Although structurally dominant, this mode produces limited sound because surface motion is mostly localized and generates minimal net air displacement. The second peak near 1546 Hz displays a broader pattern with most of the shell moving in phase. This mode behaves like a monopole source, pushing air uniformly and maximizing radiation efficiency.

the measured pressure drops sharply. These dips correspond to modes where adjacent regions on the gong surface move out of phase. This leads to destructive interference in the radiated field, a phenomenon similar to dipole or quadrupole cancellation. In such cases, the radiated sound waves cancel each other in certain directions, reducing net sound output despite significant vibration.

The correlation between mode shapes and SPL behavior highlights the role of radiation impedance. At peak frequencies, the gong's surface impedance matches well with the acoustic load, allowing efficient energy transfer. At dip frequencies, mismatched impedance and out-of-phase motion hinder radiation. These observations explain the uneven SPL response and the rich, inharmonic timbre of the gong.

Lastly, the slight discrepancy between the first vibration mode at 233 Hz and the first SPL peak near 250 Hz likely results from damping and coupling effects in the full system. While the modal analysis identifies the structural resonance, actual sound radiation depends on how effectively that mode excites pressure waves in air.

6. DISCUSSION

The gong's vibration behavior is shaped by its geometry, material distribution, and mass loading at the boss. The lowest mode, observed near 233 Hz, is mainly concentrated around the central boss. The added mass in this area reduces the natural frequency significantly. Most of the peripheral surface remains nearly stationary in this mode, which limits its ability to transfer energy into the air. As a result, this mode does not radiate sound efficiently. However, it plays an important perceptual role. It adds a tactile sensation when the gong is played and forms a deep spectral foundation that supports the higher components of the sound. While not clearly audible as a pitch, this mode adds depth and a sense of physical presence to the sound.

The mode at approximately 1546 Hz shows a much broader and more coherent motion across the shell. Its simple nodal pattern allows large surface regions to move in phase, making this mode highly efficient in radiating sound. This efficiency explains the prominent peak in the SPL spectrum. In performance, this mode produces the most clearly perceived pitch. It behaves as the "singing mode" of the gong and is often interpreted by listeners as the fundamental tone, even though it is not the lowest in frequency. This auditory dominance is due to its strong acoustic output and the human ear's sensitivity to frequencies in this range.

At higher frequencies, such as 2737 Hz and above, the mode shapes become increasingly complex. These higher modes contain multiple radial and circumferential nodal lines, breaking the shell into many segments that move in alternating directions. This fragmented motion causes the radiated pressure field to include a set of inharmonic overtones. These partials are not evenly spaced in frequency, unlike those from simple vibrating plates. Their irregular distribution contributes to the shimmering, evolving quality of the gong's sound. Though they carry less acoustic energy than the main mode at 1546 Hz, they are crucial for the instrument's timbre and richness.

These acoustic properties are closely linked to the cultural function of the gong. The prominent mode near 1546 Hz is tuned to match an interval in the Javanese slendro scale, rather than a note from Western tuning systems. In gamelan music, this pitch helps define musical structure. It marks time divisions within the gong and supports the ensemble's coordination. The deep 233 Hz component, while not clearly melodic, helps create a background sound that supports the ceremonial or meditative context of performance. Together, the inharmonic spectrum and sustained resonance of the gong support its role in both musical and spiritual dimensions.

From a design perspective, the gong's acoustic behavior reflects deliberate shaping of its physical structure. The thickness varies across the surface, and the boss adds asymmetry and mass, both of which shift the frequencies of key modes. These features seem intentionally designed to produce a complex, inharmonic spectrum suited to the instrument's function in gamelan music. The combination of structural and acoustical features supports ideas of balance, depth, and sonic presence, which are valued in the cultural context.

7. CONCLUSIONS

The finite element analysis identified the gamelan gong's natural frequencies and mode shapes. The fundamental mode near 233 Hz localizes vibration in the central boss, producing the culturally significant deep tone.

Higher modes at approximately 1546 Hz and 2738 Hz create inharmonic overtone patterns that enrich the sonic texture. The predicted sound pressure level spectrum matches well with known acoustic behavior, showing resonant peaks at these frequencies. These results quantitatively explain the gong's inharmonicity and modal distribution, confirming that its geometry and material properties critically shape its vibrational and acoustic response.

REFERENCES

1. R. A. Sutton, "Gamelan: The Traditional Sounds of Indonesia (review)," *Asian Music,* vol. 38, no. 1, pp. 142–144, 2007, Accessed: Jul. 25, 2025. [Online]. Available: https://muse.jhu.edu/pub/15/article/216426
2. H. Spiller and E. A. Clendinning, *Focus: Gamelan Music of Indonesia*, 3rd ed. New York: Routledge, 2022. doi: 10.4324/9781003014836.
3. D. W. Krueger, K. L. Gee, and J. Grimshaw, "Acoustical and vibrometry analysis of a large Balinese gamelan gong," *J. Acoust. Soc. Am.*, vol. 128, no. 1, pp. EL8–EL13, Jun. 2010, doi: 10.1121/1.3425742.
4. Sumarsam, "Inner Melody in Javanese Gamelan Music," *Asian Music,* vol. 7, no. 1, pp. 3–13, 1975, doi: 10.2307/833922.
5. J. Becker and A. Becker, "14. A Musical Icon: Power and Meaning in Javanese Gamelan Music," in *The Sign in Music and Literature*, W. Steiner, Ed., University of Texas Press, 2014, pp. 203–215. Accessed: Jul. 25, 2025. [Online]. Available: https://www.degruyterbrill.com/document/doi/10.7560/775633-014/html
6. D. Simons, *Gong Culture: A Survey of East Asian Gong Traditions*. 2009.
7. S. P. Walton, "Aesthetic and Spiritual Correlations in Javanese Gamelan Music," *J. Aesthet. Art Crit.*, vol. 65, no. 1, pp. 31–41, Sep. 2007, doi: 10.1111/j.1540-594X.2007.00235.x.
8. J. Becker, "Earth, Fire, Śakti, and the Javanese Gamelan," *Ethnomusicology,* vol. 32, no. 3, pp. 385–391, 1988, doi: 10.2307/851938.
9. D. W. Krueger, K. L. Gee, and J. Grimshaw, "Acoustical and vibrometry analysis of a large Balinese gamelan gong," *J. Acoust. Soc. Am.*, vol. 128, no. 1, pp. EL8–EL13, Jun. 2010, doi: 10.1121/1.3425742.
10. G. Tsai, B. Wang, Y. Lee, and Z. Chang, "Study of vibration and sound characteristics of a copper gong," *J. Chin. Inst. Eng.,* vol. 28, no. 4, pp. 713–719, Jun. 2005, doi: 10.1080/02533839.2005.9671038.
11. N. McLachlan, R. Adams, and C. Burvill, "Tuning natural modes of vibration by prestress in the design of a harmonic gong," *J. Acoust. Soc. Am.*, vol. 131, no. 1, pp. 926–934, Jan. 2012, doi: 10.1121/1.3651255.
12. G. Tsai, B. Wang, Y. Lee, and Z. Chang, "Study of vibration and sound characteristics of a copper gong," *J. Chin. Inst. Eng.,* vol. 28, no. 4, pp. 713–719, Jun. 2005, doi: 10.1080/02533839.2005.9671038.

Laurentius Kevin Hendinata

Laurentius Kevin Hendinata is an Acoustic Engineer at an engineering, climate, and performance consulting firm. He holds an Erasmus Mundus Joint Master's Degree in Waves, Acoustics, Vibrations, Engineering and Sounds (WAVES), jointly awarded by the University of Coimbra, the Polytechnic University of Valencia, and Aix-Marseille University. He received his Bachelor's degree in Engineering Physics from Universitas Gadjah Mada, Indonesia. His professional and research interests include building acoustics, environmental acoustics, noise and vibration control, and numerical modelling for acoustic applications.

USING IMPULSE ACOUSTIC RESPONSE TO EVALUATE THE EFFICIENCY OF RAIL ABSORBERS

VYUŽITÍ IMPULSNÍ AKUSTICKÉ ODEZVY PRO HODNOCENÍ ÚČINNOSTI KOLEJNICOVÝCH ABSORBÉRŮ

Smutný J., Pazdera L. Štukavec M.

Brno University of Technology, Faculty of Civil Engineering, Veveří 95, 602 00 Brno
Vysoké učení technické v Brně, Fakulta stavební, Veveří 95, 602 00 Brno

Abstract

The paper deals with laboratory measurements and analysis of the acoustic response of a rail equipped with various rail absorbers during impulse excitation by mechanical shock. The aim of the research was to design and verify an experimental methodology enabling an objective comparison of the acoustic properties of various design solutions of rail absorbers in controlled laboratory conditions. The excitation of the test sample was realized by the impact of a steel ball of defined mass from a constant height onto the rail head, while the resulting acoustic response was recorded using a measuring system with a calibrated measuring path. The measured signals were subsequently evaluated in the time, frequency and time-frequency domains using the analysis of the measured impulse response. Particular attention was paid to the evaluation of the maximum sound pressure levels, the course of the response attenuation and changes in spectral characteristics after the installation of the absorbers. The results demonstrate that the proposed methodology allows for reliable identification of differences in the acoustic behavior of individual absorbers and provides a suitable tool for their laboratory evaluation, development and optimization before deployment in railway operations.

Keywords: rail absorbers, laboratory measurements, acoustic response, impulse excitation, mechanical shock, steel ball, FFT analysis, vibroacoustics, railway infrastructure

Anotace

Příspěvek se zabývá laboratorním měřením a analýzou akustické odezvy kolejnice vybavené různými kolejnicovými absorbéry při impulsním buzení mechanickým rázem. Cílem výzkumu bylo navrhnout a ověřit experimentální metodiku umožňující objektivní porovnání akustických vlastností různých konstrukčních řešení kolejnicových absorbérů v kontrolovaných laboratorních podmínkách. Buzení zkušebního vzorku bylo realizováno dopadem ocelové koule definované hmotnosti z konstantní výšky na hlavu kolejnice, přičemž vzniklá akustická odezva byla zaznamenávána pomocí měřícího systému s kalibrovanou měřící cestou. Naměřené signály byly následně vyhodnoceny v časové, frekvenční a časově frekvenční oblasti s využitím analýzy naměřené impulsní odezvy. Pozornost byla věnována zejména hodnocení maximálních hladin akustického tlaku, průběhu útlumu odezvy a změnám spektrálních charakteristik po instalaci absorbérů. Výsledky prokazují, že navržená metodika umožňuje spolehlivě identifikovat rozdíly v akustickém chování jednotlivých absorbérů a poskytuje vhodný nástroj pro jejich laboratorní hodnocení, vývoj a optimalizaci před nasazením v železničním provozu.

Klíčová slova: kolejnicové absorbéry, laboratorní měření, akustická odezva, impulsní buzení, mechanický ráz, ocelová koule, FFT analýza, vibroakustika, železniční infrastruktura

1. INTRODUCTION TO THE ISSUE

The noise generated by rail transport represents a significant environmental problem, especially in urbanized areas and in the vicinity of intensively used railway lines. With increasing train speeds and growing demands for the comfort of the population, the issue of reducing noise pollution is becoming increasingly important. The dominant sources of railway noise include noise generated by the interaction of the wheel and rail, which is considered to be a decisive component of the total noise emission of rail vehicles in the speed range of approximately 50 km·h⁻¹ and above [1, 2]. This noise arises as a result of the dynamic excitation of the wheel and rail by the irregularities of their surface and the subsequent radiation of acoustic energy into the surrounding environment.

One of the effective measures for reducing noise emitted by tram and railway lines are rail absorbers [3]. These are passive vibroacoustic elements installed on the rail web or even the rail heel, whose task is to increase the structural damping of the rail and limit the amplitude of its vibrations in critical frequency bands. By reducing the vibration level, the acoustic power radiated by the rail is also reduced, which leads to a reduction in the overall noise emission of rail transport. Currently, a number of design solutions for rail absorbers are available on the market, differing in the materials used, weight, mounting method and frequency range of effectiveness.

Operational noise measurements during the passage of train sets or vibration measurements directly on the rail are commonly used to assess the effectiveness of rail absorbers. However, these methods are time-consuming, require appropriate operating conditions and their results can be influenced by a number of external factors, such as vehicle speed, rail surface condition, meteorological conditions or railway traffic composition [4, 5].

For this reason, increasing attention is being paid to laboratory methods that enable reproducible evaluation of the vibroacoustic properties of rail absorbers under controlled conditions. Laboratory methods represent an important tool for the development, optimization and comparison of rail absorbers before their deployment in railway operations. Com-

1. ÚVOD DO PROBLEMATIKY

Hluk generovaný železniční dopravou představuje významný environmentální problém zejména v urbanizovaných oblastech a v okolí intenzivně využívaných železničních tratí. Se zvyšujícími se rychlostmi vlakových souprav a rostoucími požadavky na komfort obyvatelstva nabývá problematika snižování hlukové zátěže stále většího významu. Mezi dominantní zdroje železničního hluku patří zejména hluk vznikající interakcí kola a kolejnice, který je v rychlostním pásmu přibližně od cca 50 km·h⁻¹ výše považován za rozhodující složku celkové hlukové emise kolejových vozidel [1, 2]. Tento hluk vzniká v důsledku dynamického buzení kola a kolejnice nerovnostmi jejich povrchu a následným vyzařováním akustické energie do okolního prostředí.

Jedním z účinných opatření ke snižování hluku vyzařovaného tramvajovou a železniční tratí jsou kolejnicové absorbéry [3]. Jedná se o pasivní vibroakustické prvky instalované na stojinu nebo i patu kolejnice, jejichž úkolem je zvýšit strukturální útlum kolejnice a omezit amplitudu jejích vibrací v kritických frekvenčních pásmech. Snížením úrovně vibrací dochází současně ke snížení akustického výkonu vyzařovaného kolejnicí, což vede ke snížení celkové hlukové emise železniční dopravy. V současné době je na trhu k dispozici řada konstrukčních řešení kolejnicových absorbérů, lišících se použitými materiály, hmotností, způsobem uchycení i frekvenčním rozsahem účinnosti.

Pro posouzení účinnosti kolejnicových absorbérů jsou běžně využívána provozní měření hluku při průjezdu vlakových souprav nebo vibrační měření přímo na kolejnici. Tyto metody však bývají časově náročné, vyžadují vhodné provozní podmínky a jejich výsledky mohou být ovlivněny řadou externích faktorů, například rychlostí vozidla, stavem povrchu kolejnice, meteorologickými podmínkami nebo složením železničního provozu [4, 5].

Z tohoto důvodu se stále větší pozornost věnuje laboratorním metodám umožňujícím reprodukovatelné hodnocení vibroakustických vlastností kolejnicových absorbérů v kontrolovaných podmínkách. Laboratorní metody představují důležitý nástroj pro vývoj, optimalizaci a porovnávání kolejnicových absorbérů ještě před jejich nasazením do žepared to operational measurements on the track, they offer a number of advantages that allow for more accurate and better reproducible results [6].

The most significant advantage of laboratory measurements is the high repeatability of the experiment. In laboratory conditions, the excitation force, excitation position, microphone placement, test sample geometry and boundary conditions can be precisely defined. Each measurement is thus carried out under practically the same conditions, which allows for an objective comparison of individual absorber variants. Another significant advantage is the elimination of the influence of railway operations. In operational measurements, the results are influenced by a number of variables, such as train speed, vehicle type, wheel condition, train load or immediate operating conditions. In the laboratory, these effects are removed and only the properties of the rail and absorber system itself can be monitored [7].

Another significant benefit is the possibility of detailed analysis of the causes of noise and vibrations. In laboratory conditions, the acoustic response, rail vibrations, frequency characteristics, natural frequencies and attenuation parameters can be measured simultaneously. This allows a better understanding of the mechanism of action of the absorber and identification of the frequency bands in which its efficiency is highest.

Laboratory measurements are also less time-consuming and economically demanding. There is no need to organize track closures or coordinate measurements with train operations. Individual absorber variants can be quickly changed and a large number of experiments can be performed in a short time. This is particularly advantageous when developing new design solutions or optimizing absorber parameters. Another advantage is the possibility of using standardized excitation. For example, a mechanical impact with a steel ball or modal hammer represents a well-defined broadband impulse, which allows results to be compared between different laboratories or different experimental campaigns. This increases the objectivity of the assessment [8].

lezničního provozu. Ve srovnání s provozními měřeními na trati nabízejí řadu výhod, které umožňují získat přesnější a lépe reprodukovatelné výsledky [6].

Nejvýznamnější výhodou laboratorního měření je vysoká opakovatelnost experimentu. V laboratorních podmínkách lze přesně definovat budicí sílu, polohu buzení, umístění mikrofonů, geometrii zkušebního vzorku i okrajové podmínky. Každé měření tak probíhá za prakticky stejných podmínek, což umožňuje objektivní porovnávání jednotlivých variant absorbérů. Další významnou výhodou je eliminace vlivu železničního provozu. Při provozních měřeních jsou výsledky ovlivňovány řadou proměnných, jako jsou rychlost vlaku, typ vozidla, stav kol, zatížení soupravy nebo okamžité provozní podmínky. V laboratoři jsou tyto vlivy odstraněny a lze sledovat pouze vlastnosti samotného systému kolejnice a absorbéru [7].

Významným přínosem je také možnost detailní analýzy příčin vzniku hluku a vibrací. V laboratorních podmínkách lze současně měřit akustickou odezvu, vibrace kolejnice, frekvenční charakteristiky, vlastní frekvence i útlumové parametry. To umožňuje lépe pochopit mechanismus působení absorbéru a identifikovat frekvenční pásma, ve kterých je jeho účinnost nejvyšší.

Laboratorní měření jsou rovněž časově a ekonomicky méně náročná. Není nutné organizovat výluky tratí ani koordinovat měření s provozem vlaků. Jednotlivé varianty absorbérů lze rychle střídat a během krátké doby provést velké množství experimentů. To je výhodné zejména při vývoji nových konstrukčních řešení nebo při optimalizaci parametrů absorbérů. Další výhodou je možnost použití standardizovaného buzení. Například mechanický ráz ocelovou koulí nebo modálním kladivem představuje dobře definovaný širokopásmový impuls, který umožňuje porovnávat výsledky mezi různými laboratořemi nebo různými experimentálními kampaněmi. Tím se zvyšuje objektivita hodnocení [8].

Laboratorní podmínky rovněž umožňují omezení vlivu okolního hluku. Měření lze provádět v akusticky upravených prostorech, případně v bezdozvukových nebo polobezdozvukových komorách, kde je minimalizován vliv odrazů a rušivých zvuků. Výsledky tak lépe odrážejí

Laboratory conditions also allow limiting the influence of ambient noise. Measurements can be performed in acoustically modified rooms, or in anechoic or semi-anechoic chambers, where the influence of reflections and disturbing sounds is minimized. The results thus better reflect the real properties of the measured system.

An important aspect is also the safety and simplicity of the implementation of experiments. It is not necessary to enter the track during operation or to handle measuring equipment near passing trains. All measurements can be performed in a controlled laboratory environment.

In addition, laboratory methods allow the testing of prototype solutions that have not yet been approved for operational use. Manufacturers and research organizations can thus verify new materials, absorber geometries or mounting methods without the need for their immediate installation on the railway infrastructure.

Although laboratory measurements cannot fully replace verification operational tests, they represent a necessary intermediate step between absorber design and its application in practice. They enable the rapid identification of prospective design variants, reduce development costs and provide detailed information on the vibroacoustic behavior of the system, which is often difficult to obtain during operational measurements. For these reasons, laboratory methods are now considered a standard part of the development and evaluation of rail absorbers.

skutečné vlastnosti měřeného systému.

Významným aspektem je také bezpečnost a jednoduchost realizace experimentů. Není nutné vstupovat do kolejiště za provozu ani manipulovat s měřicí technikou v blízkosti projíždějících vlaků. Veškerá měření lze provádět v kontrolovaném laboratorním prostředí.

Laboratorní metody navíc umožňují testování prototypových řešení, která ještě nebyla schválena pro provozní použití. Výrobci a výzkumné organizace tak mohou ověřovat nové materiály, geometrie absorbérů nebo způsoby uchycení bez nutnosti jejich okamžité instalace na železniční infrastrukturu.

Přestože laboratorní měření nemohou plně nahradit ověřovací provozní zkoušky, představují nezbytný mezikrok mezi návrhem absorbéru a jeho aplikací v praxi. Umožňují rychlou identifikaci perspektivních konstrukčních variant, snižují náklady na vývoj a poskytují podrobné informace o vibroakustickém chování systému, které bývá při provozních měřeních obtížné získat. Z těchto důvodů jsou laboratorní metody dnes považovány za standardní součást vývoje a hodnocení kolejnicových absorbérů.

2. METHODS USED FOR THE EVALUATION OF RAIL ABSORBERS

Evaluation of the effectiveness of rail absorbers is an important part of the development and verification of noise control measures in rail transport. The aim of these methods is to determine the ability of the absorber to reduce rail vibrations and subsequently the noise emitted into the surrounding environment.

Currently, several approaches are used, which differ in complexity, accuracy and areas of application [9].

2. METODY POUŽÍVANÉ PRO HODNOCENÍ KOLEJNICOVÝCH ABSORBÉRŮ

Hodnocení účinnosti kolejnicových absorbérů představuje důležitou součást vývoje a ověřování protihlukových opatření v železniční dopravě. Cílem těchto metod je stanovit schopnost absorbéru snižovat vibrace kolejnice a následně i hluk vyzařovaný do okolního prostředí. V současné době se používá několik přístupů, které se liší náročností, přesností i oblastí použití [9].

Nejpřímější metodou je provozní měření hluku při průjezdu vlakových souprav. Při této

The most direct method is the operational measurement of noise during the passage of train sets. In this method, the noise emitted by the railway track before and after the absorber installation is recorded using precise measuring microphones. The result is a comparison of equivalent sound pressure levels, maximum levels or spectral characteristics of the noise. The advantage of this method is the direct evaluation of the actual benefit of the absorber in real operation. The disadvantage is a significant dependence on operating conditions, train speed, vehicle type, wheel condition and meteorological influences.

Another frequently used method is the measurement of rail vibrations. Vibrations are usually detected by piezoelectric accelerometers placed on the rail web or head. The vibration level before and after the installation of absorbers is compared, and the frequency response of the vibrations is evaluated. This method provides information directly about the mechanism of action of the absorber, since its main function is to increase the attenuation of the rail and limit the amplitude of its vibrations. In the case of measuring rails with absorbers, the problem of attaching the accelerometer can be a problem.

A significant group of methods is represented by modal and dynamic rail tests. In these, the rail is excited, for example, by a modal hammer, an electrodynamic exciter or a mechanical impulse. Based on the response, the natural frequencies, vibration shapes and damping characteristics of the system are determined. The information obtained allows the evaluation of changes in the dynamic properties of the rail caused by the installation of absorbers.

Laboratory methods based on impulse response have been increasingly used in recent years. The rail is excited by a short mechanical impulse, for example by the impact of a steel ball or a modal hammer. The acoustic or vibration response is then analyzed in the time and frequency domain. The advantages of this method are high repeatability of the measurement, simple experimental setup and the possibility of quick comparison of different absorber design variants without the need for operational tests.

Another option is to measure frequency transfer functions (FRF). This method analyzes the

metodě se pomocí přesných měřicích mikrofonů zaznamenává hluk vyzařovaný železniční tratí před instalací absorbéru a po jeho instalaci. Výsledkem bývá porovnání ekvivalentních hladin akustického tlaku, maximálních hladin nebo spektrálních charakteristik hluku. Výhodou této metody je přímé hodnocení skutečného přínosu absorbéru v reálném provozu. Nevýhodou je značná závislost na provozních podmínkách, rychlosti vlaků, typu vozidel, stavu kol a meteorologických vlivech.

Další často používanou metodou je měření vibrací kolejnice. Vibrace jsou zpravidla snímány piezoelektrickými akcelerometry umístěnými na stojině nebo hlavě kolejnice. Porovnává se úroveň vibrací před a po instalaci absorbérů, případně se vyhodnocuje frekvenční průběh vibrací. Tato metoda poskytuje informace přímo o mechanismu působení absorbéru, protože jeho hlavní funkcí je zvýšení útlumu kolejnice a omezení amplitudy jejích vibrací. V případě měření kolejnic s absorbéry může být problémem uchycení akcelerometru.

Významnou skupinu metod představují modální a dynamické zkoušky kolejnic. Při nich je kolejnice buzena například modálním kladivem, elektrodynamickým budičem nebo mechanickým impulsem. Na základě odezvy se stanovují vlastní frekvence, tvary kmitání a útlumové charakteristiky systému. Získané informace umožňují hodnotit změny dynamických vlastností kolejnice způsobené instalací absorbérů.

V posledních letech se stále častěji využívají laboratorní metody založené na impulsní odezvě. Kolejnice je buzena krátkým mechanickým impulsem, například dopadem ocelové koule nebo úderem modálního kladiva. Následně se analyzuje akustická nebo vibrační odezva v časové a frekvenční oblasti. Výhodou této metody je vysoká opakovatelnost měření, jednoduché experimentální uspořádání a možnost rychlého porovnání různých konstrukčních variant absorbérů bez nutnosti realizace provozních zkoušek.

Další možností je měření frekvenčních přenosových funkcí (FRF). Při této metodě se analyzuje vztah mezi budicí silou a odezvou konstrukce. Frekvenční přenosové funkce poskytují podrobné informace o rezonančních frekvencích, úrovni útlumu a dynamické tuhosti relationship between the excitation force and the response of the structure. Frequency transfer functions provide detailed information about the resonant frequencies, the level of attenuation and the dynamic stiffness of the system. The method is often used in the development of new absorbers and in the validation of numerical models. It should be noted that more expensive specific equipment is needed for this type of test.

In addition to experimental methods, numerical simulations are also widely used, in particular the finite element method (FEM) and the boundary element method (BEM). These approaches allow the analysis of the vibration and acoustic behavior of the rail and absorber before the prototype is manufactured. Numerical models are used to optimize the absorber mass, its geometry, material composition or frequency tuning. In practice, the simulation results are verified by laboratory or operational measurements.

For the evaluation of acoustic properties, frequency analysis in the time domain is commonly used, followed by FFT, one-third octave analysis and impulse response analysis, or the application of modern time-frequency analysis methods. These procedures allow to determine the frequency bands in which the absorber shows the highest efficiency. One-third octave analysis in particular is important for comparing the results with the requirements of technical standards and regulations used in the field of railway acoustics.

Therefore, a comprehensive evaluation of rail absorbers usually combines several methods simultaneously. Laboratory measurements provide detailed information on the acoustic behavior of the absorber under controlled conditions, while operational measurements verify its real benefit in real railway operation. The combination of experimental methods with numerical modeling today represents the most effective approach to the development, optimization and objective evaluation of rail absorbers [9].

One of the advantageous options is the use of pulsed excitation of the rail by mechanical shock. A short pulse represents a broadband energy source capable of exciting a significant part of the natural frequencies of the rail-absorber system. The subsequent analysis of the systému. Metoda je často využívána při vývoji nových absorbérů a při validaci numerických modelů. Podotkněme, že pro tento typ zkoušek je potřeba dražší specifické vybavení.

Vedle experimentálních metod se široce uplatňují také numerické simulace, zejména metoda konečných prvků (FEM) a metoda hraničních prvků (BEM). Tyto přístupy umožňují analyzovat vibrační i akustické chování kolejnice a absorbéru ještě před výrobou prototypu. Numerické modely se využívají k optimalizaci hmotnosti absorbéru, jeho geometrie, materiálového složení nebo frekvenčního naladění. V praxi bývají výsledky simulací ověřovány laboratorními nebo provozními měřeními.

Pro hodnocení akustických vlastností se běžně používá frekvenční analýza v časové rovině, dále pomocí FFT, třetinooktávová analýza a analýza impulsní odezvy, případně aplikace moderních metod časově frekvenční analýzy. Tyto postupy umožňují určit frekvenční pásma, ve kterých absorbér vykazuje nejvyšší účinnost. Zejména třetinooktávová analýza je důležitá pro porovnání výsledků s požadavky technických norem a předpisů používaných v oblasti železniční akustiky.

Komplexní hodnocení kolejnicových absorbérů proto zpravidla kombinuje několik metod současně. Laboratorní měření poskytují detailní informace o akustickém chování absorbéru v kontrolovaných podmínkách, zatímco provozní měření ověřují jeho skutečný přínos v reálném železničním provozu. Spojení experimentálních metod s numerickým modelováním dnes představuje nejefektivnější přístup k vývoji, optimalizaci a objektivnímu hodnocení kolejnicových absorbérů [9].

Jednou z výhodných možností je využití impulsního buzení kolejnice mechanickým rázem. Krátký impuls představuje širokopásmový zdroj energie schopný excitovat významnou část vlastních frekvencí systému kolejnice–absorbér. Následná analýza akustické odezvy poskytuje informace o dynamických vlastnostech měřeného systému, jeho útlumových schopnostech a frekvenční charakteristice [10]. Výhodou této metody je jednoduchost experimentálního uspořádání, vysoká opakovatelnost měření a možnost rychlého porovnání různých konstrukčních variant absorbérů.

acoustic response provides information about the dynamic properties of the measured system, its attenuation capabilities and frequency characteristics [10]. The advantage of this method is the simplicity of the experimental arrangement, high repeatability of measurements and the possibility of quick comparison of different design variants of absorbers.

The rest of the article deals with the design and verification of a laboratory methodology for evaluating rail absorbers based on measuring the acoustic response of the rail caused by the mechanical impact of a steel ball. Attention is paid to the description of the experimental arrangement, the measurement methodology and the methods of processing the measured data in the time and frequency domains. The aim of the conclusion of the article is to assess the usability of the proposed procedure for objectively comparing the acoustic properties of rail absorbers and to create a basis for their further development and optimization.

Další text příspěvku se zabývá návrhem a ověřením laboratorní metodiky hodnocení kolejnicových absorbérů založené na měření akustické odezvy kolejnice vyvolané mechanickým rázem ocelové koule. Pozornost je věnována popisu experimentálního uspořádání, metodice měření a způsobům zpracování naměřených dat v časové i frekvenční oblasti. Cílem závěru článku je posoudit využitelnost navrženého postupu pro objektivní porovnávání akustických vlastností kolejnicových absorbérů a vytvořit podklady pro jejich další vývoj a optimalizaci.

3. DESCRIPTION OF TEST MEASUREMENTS

The aim was not only to perform laboratory measurements of the acoustic parameters of a rail sample without and with two types of sidewalls in order to compare their acoustic parameters, but also to verify the reliability of the method in question. A total of three types of measurements were performed. The first measurement was performed on a grooved NT3 rail without rail absorbers, the next two using two types of rail absorber fastening, one of which was attached with steel clips and the other was glued and with an SBR heel profile. It should be noted that the SBR heel profile is a flexible profile located in the area of the rail heel, made of SBR (Styrene-Butadiene Rubber). This is one of the most widely used synthetic rubbers in railway construction, especially for anti-vibration and acoustic applications. The SBR profile is installed along the rail foot and performs several functions:

- Reduces the transmission of vibrations from the rail to the fasteners and sleepers,
- Increases the material damping of the rail-fastening system,

3. POPIS TESTOVACÍCH MĚŘENÍ

Cílem bylo nejen laboratorní měření akustických parametrů vzorku kolejnice bez a s dvěma typy bokovnic za účelem srovnání jejich akustických parametrů, ale i ověření spolehlivosti předmětné metody. Celkem byly provedeny tři typy měření. První měření bylo provedeno na žlábkové kolejnici NT3 bez kolejnicových absorbérů, další dvě s využitím dvou typů upevnění kolejnicových absorbérů, kdy jeden byl připevněn ocelovými sponami a druhý byl nalepený a s patním profilem SBR. Podotkněme, že SBR patní profil je pružný profil umístěný v oblasti paty kolejnice, vyrobený z materiálu SBR (Styrene-Butadiene Rubber), tedy styren-butadienového kaučuku. Jedná se o jeden z nejpoužívanějších syntetických kaučuků v železničním stavitelství, zejména pro antivibrační a akustické aplikace. SBR profil se instaluje podél paty kolejnice a plní několik funkcí:

- Snižuje přenos vibrací z kolejnice do upevňovadel a pražce,
- Zvyšuje materiálové tlumení soustavy kolejnice—upevnění,

- Limits noise radiation through the rail,
- Protects the rail from direct contact with some parts of the absorber,
- Serves as an elastic element when attaching rail absorbers.

When a train passes through, bending, longitudinal and torsional vibrations occur in the rail. Due to its elasticity, the SBR profile allows for small deformations and at the same time converts part of the vibration energy into heat. This phenomenon is referred to as internal hysteretic damping of rubber. From the point of view of rail dynamics, the SBR foot profile is actually a viscoelastic damper, which together with the rail mass and any steel core of the absorber creates a mass-spring-damper system.

The mechanical shock was realized by the impact of a steel ball (Fig. 1) lowered from a special holder (with adjustable heights) in the vertical direction. A steel ball with a diameter of 38 mm was used. The microphone was placed 1 m from the measured samples (rail posts). The measuring microphone was directed perpendicular to the samples and was placed at a height of 17 cm above the surface. The excitation ball was lowered onto the running part of the rail from a height of 60 cm. Each measurement in each variant was performed 10 times. The values obtained were averaged.

The dynamic-acoustic response parameters were recorded by a microphone. The B&K 3053-B-120 measuring set from Brüel&Kjaer and the Labshop B&K measuring software were used to measure the acoustic parameters. The dynamic-acoustic response parameters were measured when applying shock excitation, i.e. when the ball hit once. After the analysis, control measurements and calculations were carried out, the following methods and parameters were used to analyze the response to mechanical shock:

- Time display of the instantaneous sound pressure value,
- Short-term equivalent sound pressure level, one-third octave spectrum,

- Omezuje vyzařování hluku kolejnicí,
- Chrání kolejnici před přímým kontaktem s některými částmi absorbéru,
- Slouží jako pružný prvek při uchycení kolejnicových absorbérů.

Při průjezdu vlaku vznikají v kolejnici ohybové, podélné i torzní kmity. SBR profil díky své pružnosti umožňuje malé deformace a současně přeměňuje část vibrační energie na teplo. Tento jev je označován jako vnitřní hysteretické tlumení pryže. Z pohledu dynamiky kolejnice je SBR patní profil vlastně viskoelastický tlumič, který společně s hmotou kolejnice a případným ocelovým jádrem absorbéru vytváří systém hmota—pružina—tlumič.

Mechanický ráz byl realizován dopadem ocelové koule (Obr 1) spouštěné ze speciálního držáku (s nastavitelnými výškami) ve svislém směru. Byla použita ocelová koule o průměru 38 mm. Mikrofon byl umístěn od měřených vzorků (stojny kolejnic) ve vzdálenosti 1 m. Měřící mikrofon byl nasměrován kolmo ke vzorkům a byl umístěn ve výšce 17 cm nad povrchem. Budící koule byla spouštěna na pojezdovou část kolejnice z výšky 60 cm. Každé měření v dané variantě bylo provedeno 10x. Získané hodnoty byly průměrovány.

Parametry dynamicko-akustické odezvy byly snímány mikrofonem. K měření akustických parametrů byla využita měřící souprava B&K 3053-B-120 od společnosti Brüel&Kjaer a měřící software Labshop B&K. Parametry dynamicko-akustické odezvy byly měřeny při aplikaci rázového buzení, tj. při jednom dopadu koule. Po provedeném rozboru, realizovaných kontrolních měřeních a výpočtech byly k analýze odezvy na mechanický ráz použito následujících metod a parametrů:

- Časového zobrazení průběhu okamžité hodnoty akustického tlaku,
- Krátkodobé ekvivalentní hladiny akustického tlaku, třetinooktávové spektrum,
- třetino-oktávových spekter akustického tlaku,
- Frekvenční analýzy Welchovou metodou,

- Third-octave sound pressure spectra,
- Frequency analysis by the Welch method, this method is based on the use of a discrete Fourier transform applied to the measured data and subsequent appropriate averaging,
- Time-frequency analysis (for the transition from the time to the time-frequency domain, the Short-term Fourier transform algorithm was used).

The author-developed software implemented in the Python programming language was used to analyze and evaluate the measured data. This software allows for effective processing, analysis and visualization of the obtained data.

tato metoda je založena na použití diskrétní Fourierovy transformace aplikované na naměřená data a na následném vhodném průměrování,

- Časově-frekvenční analýzy (pro přechod z časové do časově-frekvenční oblasti byl využít algoritmus Krátkodobé Fourierovy transformace).

K analýze a vyhodnocení naměřených dat byl použit autorsky vyvinutý software implementovaný v programovacím jazyce Python. Tento software umožňuje efektivní zpracování, analýzu i vizualizaci získaných dat.

Fig. 1 View of the measurement location, absorber attached to the rail with clips

Obr. 1 Pohled na místo měření, absorbér uchycený ke kolejnici sponami

Fig. 2 View of the measurement location, absorber attached to the rail by gluing

Obr. 2 Pohled na místo měření, absorbér uchycený ke kolejnici lepením

4. RESULTS

For the calculation of the short-term equivalent sound pressure level, an interval of 100 ms from the beginning of the measured signal was selected due to the nature of the response signals. This is the interval in which the most significant attenuation of the sound pressure occurs. The calculated values were averaged. The average values of the short-term sound pressure level for the investigated signal interval of 200 ms are given in Table Tab. 1. Furthermore, from the measured data in the given interval, the third-octave spectra were calculated for each variant. These were again averaged. The average third-octave spectra are shown in Figure Fig. 3.

4. ZÍSKANÉ VÝSLEDKY

Pro výpočet krátkodobé ekvivalentní hladiny akustického tlaku byl vzhledem k charakteru odezvových signálů vybrán interval 100 ms od začátku naměřeného signálu. Jde o interval, v kterém dochází k nejvýraznějšímu útlumu akustického tlaku. Vypočtené hodnoty byly zprůměrovány. Průměrné hodnoty krátkodobé hladiny akustického tlaku pro vyšetřovaný interval signálu délky 200 ms jsou uvedeny v tabulce Tab. 1.

Dále byla z naměřených dat v daném intervalu vypočtena pro každou variantu třetino-oktávová spektra. Tyto byla opět průměrovány. Průměrná třetino-oktávová spektra jsou uvedena v obrázku Obr. 3.

Měřený vzorek / Measured sample	**L_{eqv} [dB(A)]**
Kolejnice NT3, bez absorbéru / NT3 rail, without acoustic absorber	93.5
Kolejnice NT3, s absorbérem a se sponami / NT3 rails, with side rails with clips	84.8
Kolejnice NT3, s nalepeným absorbérem a s SBR patním profilem / NT3 rail, with glued absorber and SBR heel profile	83.2

Table 1 Comparison of short-term equivalent level values for individual variants

Tab. 1 Srovnání hodnot krátkodobé ekvivalentní hladiny pro jednotlivé varianty

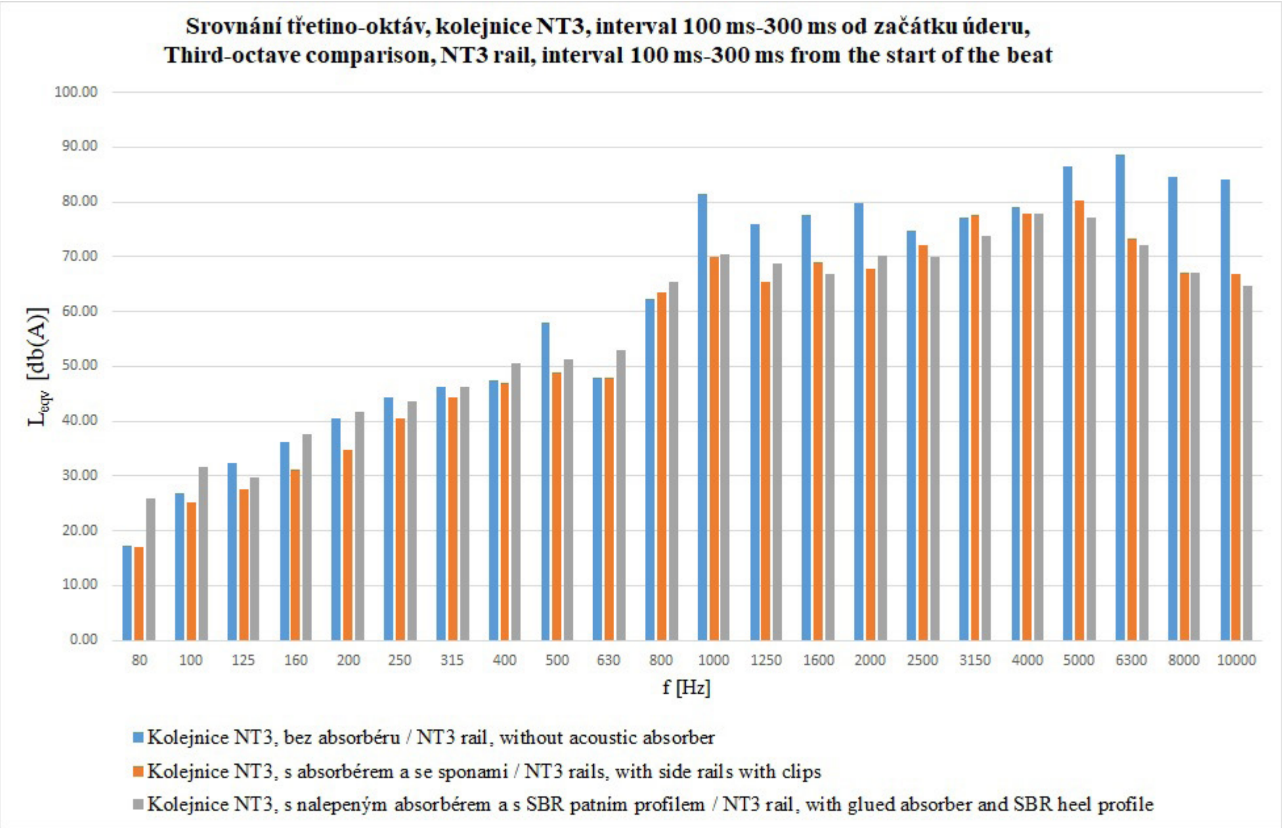

Fig. 3 Comparison of third-octave spectra for the measured variants

Obr. 3 Srovnání třetino-oktávových spekter pro měřené varianty

According to Table Tab. 1, the sound pressure values in the case of a separate NT3 rail are almost ten decibels higher than when using sidewalls. When comparing both types of sidewalls, it is possible to state from this table that the equivalent sound pressure level values are slightly more favourable for the rail with glued sidewalls including SBR foot profile. The difference here is 1.6 dB.

The third-octave characteristic of the equivalent noise levels using the A filter is shown in Fig. 3 for the measurement of all three variants, i.e. without sidewall rails, rails with sidewalls fastened with steel clips and rails with

Dle tabulky Tab. 1 jsou hodnoty akustického tlaku v případě samostatné kolejnice NT3 o téměř deset decibelů vyšší než při použití bokovnic. Při srovnání obou typů bokovnic je možné z této tabulky konstatovat nepatrně výhodnější ekvivalentní hodnoty hladiny akustického tlaku u kolejnice s nalepovacími bokovnicemi včetně SBR patním profilem. Rozdíl zde činí 1.6 dB.

Třetino-oktávová charakteristika ekvivalentních hladin hluku s použitím filtru A je pro měření všech tří variant, tedy bez kolejnice bokovnic, kolejnice s bokovnicemi upevněnými ocelovými sponami a kolejnice s nalepenými bokovnicemi a SBR glued sidewalls and SBR foot profile. Significant values in the measurement variant on the rail without sidewalls were found at a frequency 500 Hz and further especially in the intervals 800 Hz to 2500 Hz and 5 kHz to 10 kHz. Both types of sidewalls, both with clips and with adhesive sidewalls including the SBR heel profile, significantly attenuate frequency components in the intervals of 800 Hz to 2500 Hz and 5 kHz to 10 kHz compared to the variant without sidewalls. Slightly more favourable attenuation was achieved in the rail sample with adhesive sidewalls with an SBR heel profile. It should be noted that the frequency range up to 800 Hz is less significant in terms of the total Short-term equivalent sound pressure level, since in this interval its values are approximately below 60 dB(A). Therefore, from the point of view of the effect of noise on humans, attenuation in the area of 800 Hz is important. It should be noted that these are third-octave waveforms, i.e. from the point of view of calculating a discontinuous frequency range. For this reason, bar graphs were used.

For a more detailed evaluation and comparison of individual samples, an analysis was performed using the time, frequency and time-frequency domains. Images were created for the time-frequency analysis, which consist of three graphs (Fig. 3 to Fig. 6). The upper graph shows the time course of the instantaneous acoustic pressure value. It shows in particular global extremes and attenuation within the entire signal with time. The left graph shows the amplitude spectrum of the acoustic response as a function of frequency calculated by direct application of the Fourier transform to the measured signal. Significant frequency components contained in the entire measured signal are visible here. The middle graph shows a 3D display of the time-frequency course of the acceleration amplitude spectrum. The dependence of the amplitude spectrum at individual time and frequency moments is shown here, i.e. the time and frequency course are combined. In simple terms, time-frequency graphs provide information about how long a given frequency component occurs in the measured signal. The sound pressure values in the decibel scale are shown in different colors in the middle graphs. Note that the maximum value is black, the lowest is white.

The time course of the sound pressure for a rail without sidewalls shows a maximum sound pressure value of around ±20 Pa on average.

patním profilem, zobrazena v obr. 3. Výrazné hodnoty ve variantě měření na kolejnici bez bokovnic byly zjištěny na frekvenci 500 Hz a dále zejména v intervalech 800 Hz až 2500 Hz a 5 kHz až 10 kHz. Oba typy bokovnic, jak se sponami, tak s nalepovacími bokovnicemi včetně SBR patního profilu výrazně tlumí frekvenční složky v intervalech 800 Hz až 2500 Hz a 5 kHz až 10 kHz oproti variantě bez bokovnic. Nepatrně výhodnějšího útlumu bylo dosaženo u vzorku kolejnice s nalepovacími bokovnicemi s SBR patním profilem. Podotkněme, že frekvenční oblast do 800 Hz je méně významná z hlediska výše celkové Krátkodobé ekvivalentní hladiny akustického tlaku, neboť v tomto intervalu jsou její hodnoty cca pod 60 dB(A). Tedy z hlediska vlivu hluku na člověka je důležité tlumení v oblasti na 800 Hz. Poznamenejme, že se jedná o třetino-oktávové průběhy, tedy z hlediska výpočtu nespojité frekvenční oblasti. Z uvedeného důvodu byly použity sloupcové grafy.

K detailnějšímu vyhodnocení a srovnání jednotlivých vzorků byla provedena analýza s využitím časové, frekvenční a časově frekvenční oblasti. K časově frekvenční analýze byly vytvořeny obrázky, které jsou tvořeny trojicí grafů (Obr. 3 až Obr. 6). V horním grafu je zobrazen časový průběh okamžité hodnoty akustického tlaku. V něm jsou patrné zejména globální extrémy a útlum v rámci celého signálu s časem. V levém grafu je zobrazeno amplitudové spektrum akustické odezvy v závislosti na frekvenci vypočítané přímou aplikací Fourierovy transformace na naměřený signál. Zde jsou patrny význačné frekvenční složky obsažené v celém naměřeném signále. V prostředním grafu je 3D zobrazení časově frekvenčního průběhu amplitudového spektra zrychlení. Je zde zobrazena závislost amplitudového spektra v jednotlivých časových a frekvenčních okamžicích, tj. spojuje se časový a frekvenční průběh. Zjednodušeně je možné říci, že časově frekvenční grafy poskytují informaci o tom, jak dlouho se daná frekvenční složka vyskytuje v naměřeném signále. Hodnoty akustického tlaku v decibelové stupnici jsou znázorněny u prostředních grafů odlišnými barvami. Poznamenejme, že maximální hodnota je barvy černé, nejnižší je pak barvy bílé.

Z časového průběhu akustického tlaku u kolejnice bez bokovnic je patrná maximální hodnota akustického tlaku v průměru kolem

The attenuation of the response signal is very gradual, reaching values 10x lower in about 0.5 s. The amplitude spectrum calculated by the Welch method shows significant values at frequencies 1020 Hz, 2010 Hz, 2900 Hz, 4100 Hz, 4380 Hz, 4540 Hz, 5280 Hz, 6690 Hz, 6880 Hz, 7740 Hz, 8600 Hz, 9440 Hz, and 9700 Hz. The calculated values of the key components of the spectrum range from 110 dB to 130 dB. The same key components of the spectrum are visible from the amplitude spectrum created using the short-term Fourier transform. At the same time, it is evident that the key components of the spectrum have a relatively long duration from the excitation pulse (up to 0.5 s), with a decrease of 30 dB.

The time course of the acoustic pressure for a rail with sidewalls attached with steel clips shows a maximum acoustic pressure value of around ±13 Pa on average. Compared to the variant without sidewalls, the signal attenuation is significantly faster, reaching values 10x lower in approximately 0.2 s. The amplitude spectrum calculated by the Welch method shows significant values at frequencies of 1020 Hz, 2010 Hz, 2900 Hz, 4100 Hz, 4380 Hz, 4540 Hz, 5280 Hz, 6690 Hz, 7740, Hz, 8600 Hz, 9440, 9700 Hz. The calculated values of the key components of the spectrum range from 102 dB to 116 dB. It is clear that these are significantly lower than in the case of measuring a rail without sidewalls. The amplitude spectrum created using the short-term Fourier transform shows the same key components of the spectrum. At the same time, it is clear that the key components of the spectrum have a higher attenuation compared to the measurement variant of the rail without sidewalls, from the excitation shock (maximum 0.3 s – 0.35 s), with a decrease of 30 dB.

From the time course of the acoustic pressure for the rail with glued sidewalls including the application of the SBR foot profile, the maximum acoustic pressure value is visible on average around ±11 Pa. The attenuation of the signal is again relatively fast compared to the measurement on the rail without sidewalls, to values 10x lower in about 0.2 s. When compared to the variant of the rail with sidewalls attached with steel clips, it is approximately the same. The amplitude spectrum calculated by the Welch method shows significant values at frequencies of 990 Hz, 2430 Hz, 4100 Hz, 4540 Hz, 5760 Hz, 7500 HZ, 850 Hz and 9100 Hz. The calculated values of the key

±20 Pa. Útlum odezvového signálu je velmi pozvolný, na hodnoty 10x nižší je za cca 0.5 s. Amplitudové spektrum vypočtené Welchovou metodou vykazuje význačné hodnoty na frekvencích 1020 Hz, 2010 Hz, 2900 Hz, 4100 Hz, 4380 Hz, 4540 Hz, 5280 Hz, 6690 Hz, 6880 Hz, 7740 Hz, 8600 Hz, 9440 Hz, a 9700 Hz. Vypočtené hodnoty klíčových složek spektra se pohybují v intervalu 110 dB do 130 dB. Z amplitudového spektra vytvořeného pomocí krátkodobé Fourierovy transformace jsou patrné stejné klíčové složky spektra. Současně je patrné, že klíčové složky spektra mají poměrně dlouhou dobu svého trvání od budícího rázu (až 0.5 s), při poklesu o 30 dB.

Z časového průběhu akustického tlaku u kolejnice s bokovnicemi připevněnými ocelovými sponami je patrná maximální hodnota akustického tlaku v průměru kolem ±13 Pa. Oproti variantě bez bokovnic je útlum signálu výrazně rychlejší, na hodnoty 10x nižší za cca 0.2 s. Amplitudové spektrum vypočtené Welchovou metodou vykazuje význačné hodnoty na frekvencích 1020 Hz, 2010 Hz, 2900 Hz, 4100 Hz, 4380 Hz, 4540 Hz, 5280 Hz, 6690 Hz, 7740, Hz, 8600 Hz, 9440, 9700 Hz. Vypočtené hodnoty klíčových složek spektra se pohybují v intervalu 102 dB do 116 dB. Je zřejmé, že tyto jsou výrazně nižší než v případě měření kolejnice bez bokovnic. Z amplitudového spektra vytvořeného pomocí krátkodobé Fourierovy transformace jsou patrné stejné klíčové složky spektra. Současně je patrné, že klíčové složky spektra mají vyšší útlum v porovnání s variantou měření kolejnice bez bokovnic, od budícího rázu (maximálně 0.3 s – 0.35 s), při poklesu o 30 dB.

Z časového průběhu akustického tlaku u kolejnice s lepenými bokovnicemi včetně aplikace SBR patního profilu je patrná maximální hodnota akustického tlaku v průměru kolem ±11 Pa. Útlum signálu je opět poměrně rychlý oproti měření na kolejnici bez bokovnic, na hodnoty 10x nižší za cca 0.2 s. Při srovnání s variantou kolejnice s bokovnicemi uchycenými ocelovými sponami je přibližně stejný. Amplitudové spektrum vypočtené Welchovou metodou vykazuje význačné hodnoty na frekvencích 990 Hz, 2430 Hz, 4100 Hz, 4540 Hz, 5760 Hz, 7500 HZ, 850 Hz a 9100 Hz. Vypočtené hodnoty klíčových složek spektra se pohybují v intervalu 86 dB až 114 dB. Je zřejmé, že tyto jsou výrazně components of the spectrum range from 86 dB to 114 dB. It is clear that these are significantly lower than in the case of measuring a rail without sidewalls.

When compared with the variant of a rail with sidewalls attached with steel clips, the results are similar. The amplitude spectrum created using the short-term Fourier transform shows the same key components of the spectrum as in the frequency analysis. At the same time, it is clear that the key components of the spectrum have a higher attenuation compared to the variant of measuring a rail without sidewalls, from the excitation shock (maximum 0.3 s – 0.35 s), with a decrease of 30 dB. When comparing the measurements of the rail and both types of sidewalls, it is clear that the rail with adhesive sidewalls and SBR heel profile has more favourable time, frequency and time-frequency characteristics.

nižší než v případě měření kolejnice bez bokovnic.

Při srovnání s variantou kolejnice s bokovnicemi uchycenými ocelovými sponami jde o podobné výsledky. Z amplitudového spektra vytvořeného pomocí krátkodobé Fourierovy transformace jsou patrné stejné klíčové složky spektra jako u frekvenční analýzy. Současně je patrné, že klíčové složky spektra mají vyšší útlum v porovnání s variantou měření kolejnice bez bokovnic, od budícího rázu (maximálně 0.3 s – 0.35 s), při poklesu o 30 dB. Při srovnání měření kolejnice a obou typů bokovnic je zřejmé, že výhodnější časové, frekvenční i časově frekvenční charakteristiky vykazuje kolejnice s nalepovacími bokovnicemi a SBR patním profilem.

4. CONCLUSIONS

Within the framework of the obtained results, it can be stated that the best damping properties are exhibited by the rail sample with adhesive sidewalls and SBR heel profile. However, it is worth noting that the difference in measured values for the rail sample with adhesive sidewalls and SBR heel profile compared to the rail with sidewalls fastened with steel clips is relatively small.

Based on the measurements and analyses performed, it can be stated that the methodology of laboratory measurements and analyses used provides suitable results and conclusions for assessing the attenuation of the measured samples in the laboratory. The measured and calculated quantities are characterized by sufficient accuracy and informativeness. They allow for very good qualitative differentiation of individual samples. The obtained results will need to be verified during field measurements.

Based on the laboratory measurements and subsequent analyses, it can be stated that the proposed methodology for evaluating rail absorbers using acoustic response to mechanical impact by a steel ball represents a suitable tool for rapid and reproducible assessment of their acoustic properties. The use of standard-

4. ZÁVĚRY

V rámci získaných výsledků je možné konstatovat, že nejlepší tlumící vlastnosti vykazuje vzorek kolejnice s nalepovacími bokovnicemi a SBR patním profilem. Je však vhodné podotknout, že rozdíl naměřených hodnot u vzorku kolejnice s nalepovacími bokovnicemi a SBR patním profilem ve srovnání s kolejnicí s bokovnicemi upevněnými ocelovými sponami je poměrně malý.

Na základě provedených měření a analýz lze konstatovat, že použitá metodika laboratorních měření a analýz poskytuje vhodné výsledky a závěry pro posouzení útlumu měřených vzorků v laboratoři. Měřené i vypočítané veličiny se vyznačují dostatečnou přesností a vypovídající schopností. Umožňují od sebe velmi dobře kvalitativně odlišit jednotlivé vzorky. Získané výsledky bude nutné ověřit při měřeních v terénu.

Na základě provedených laboratorních měření a následných analýz lze konstatovat, že navržená metodika hodnocení kolejnicových absorbérů prostřednictvím akustické odezvy na mechanický ráz ocelovou koulí představuje vhodný nástroj pro rychlé a reprodukovatelné posuzování jejich akustických vlastností. Použití standardizovaného impulsního buzení umožnilo vytvořit opakovatelné podmínky ized impulse excitation made it possible to create repeatable experimental conditions and ensure mutual comparability of the results obtained for individual tested absorber variants.

The analyses performed in the time and frequency domains demonstrated that the measured acoustic response reacts sensitively to changes in the dynamic properties of the rail-absorber system. The obtained impulse responses, frequency spectra, one-third octave characteristics and the use of time-frequency analysis made it possible to identify differences between individual design solutions and assess their ability to limit rail vibrations and reduce acoustic energy radiation. At the same time, it was confirmed that the efficiency of the absorbers is manifested not only by a decrease in the amplitude of the acoustic response, but also by a faster attenuation of vibrations and therefore of the acoustic pressure by changing the spectral distribution of energy in the crucial frequency bands.

A significant advantage of the proposed methodology is its simplicity, low time consumption and minimal requirements for experimental equipment compared to extensive operational measurements on the railway infrastructure. The method allows for a large number of repeated tests to be carried out in controlled laboratory conditions and provides sufficiently sensitive data for the development, optimization and mutual comparison of rail absorbers before their installation into service.

The obtained results confirm that the acoustic response induced by mechanical shock can be used as a relevant indicator of the vibroacoustic behaviour of the rail and the efficiency of the absorbers used. The proposed procedure thus represents a suitable addition to standard vibration and acoustic tests and can serve as an effective tool for laboratory screening of new design solutions. At the same time, it creates the prerequisites for further development of the methodology, for example by some connection of acoustic parameter measurements with vibration measurements using accelerometers, modal analysis or numerical modelling using the finite element method. It can therefore be stated that the proposed methodology has met the expected goals and has proven its applicability for objective evaluation of the acoustic properties of rail absorbers. Its use can contribute to streamlining the process

experimentu a zajistit vzájemnou porovnatelnost výsledků získaných pro jednotlivé zkoušené varianty absorbérů.

Provedené analýzy v časové i frekvenční oblasti prokázaly, že měřená akustická odezva citlivě reaguje na změny dynamických vlastností systému kolejnice–absorbér. Získané impulzní odezvy, frekvenční spektra, třetinooktávové charakteristiky i použití časově frekvenční analýzy umožnily identifikovat rozdíly mezi jednotlivými konstrukčními řešeními a posoudit jejich schopnost omezovat vibrace kolejnice a snižovat vyzařování akustické energie. Současně bylo potvrzeno, že účinnost absorbérů se projevuje nejen poklesem amplitudy akustické odezvy, ale také rychlejším útlumem vibrací a tedy i akustického tlaku změnou spektrálního rozložení energie v rozhodujících frekvenčních pásmech.

Významnou předností navržené metodiky je její jednoduchost, nízká časová náročnost a minimální požadavky na experimentální vybavení ve srovnání s rozsáhlými provozními měřeními na železniční infrastruktuře. Metoda umožňuje realizovat velké množství opakovaných zkoušek v kontrolovaných laboratorních podmínkách a poskytuje dostatečně citlivé podklady pro vývoj, optimalizaci a vzájemné porovnávání kolejnicových absorbérů ještě před jejich instalací do provozu.

Získané výsledky potvrzují, že akustická odezva vyvolaná mechanickým rázem může být využita jako relevantní indikátor vibroakustického chování kolejnice a účinnosti použitých absorbérů. Navržený postup tak představuje vhodný doplněk ke standardním vibračním a akustickým zkouškám a může sloužit jako efektivní nástroj pro laboratorní screening nových konstrukčních řešení. Současně vytváří předpoklady pro další rozvoj metodiky, například určitým propojením měřením akustických parametrů s měřením vibrací pomocí akcelerometrů, modální analýzou nebo numerickým modelováním metodou konečných prvků.

Lze proto konstatovat, že navržená metodika splnila očekávané cíle a prokázala svou použitelnost pro objektivní hodnocení akustických vlastností kolejnicových absorbérů. Její využití může přispět k zefektivnění procesu vývoje protihlukových opatření a ke zvyšování účinnosti technických prostředků určených of developing noise-reducing measures and increasing the efficiency of technical means intended to reduce the noise load of railway transport.

ke snižování hlukové zátěže železniční dopravy.

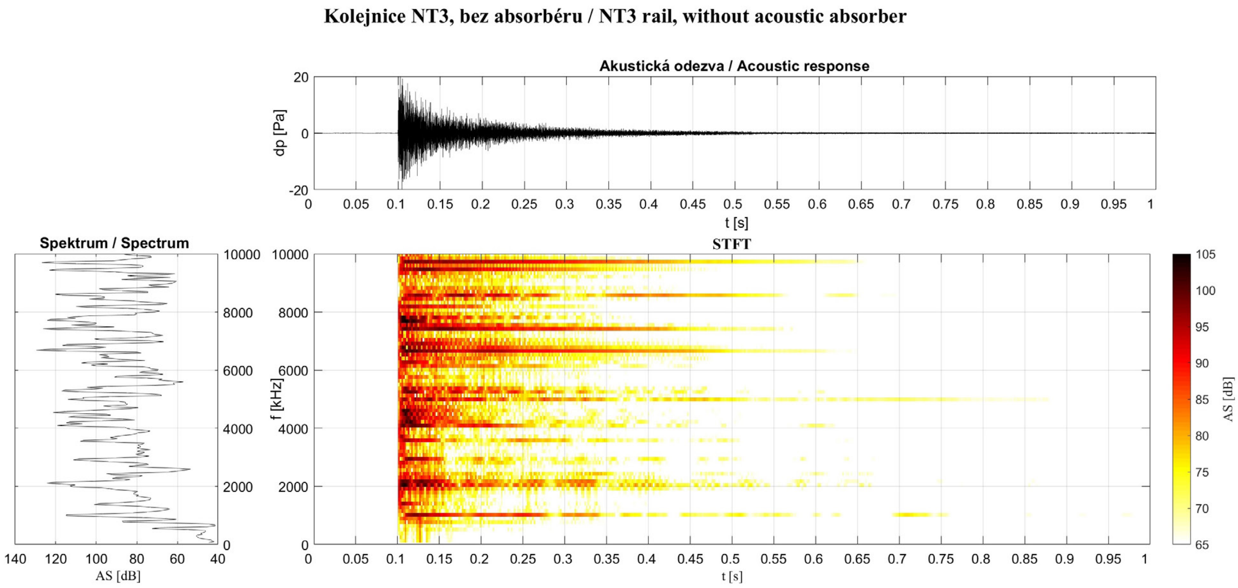

Fig. 4 Rail without absorber

Obr. 4 Kolejnice bez absorbéru

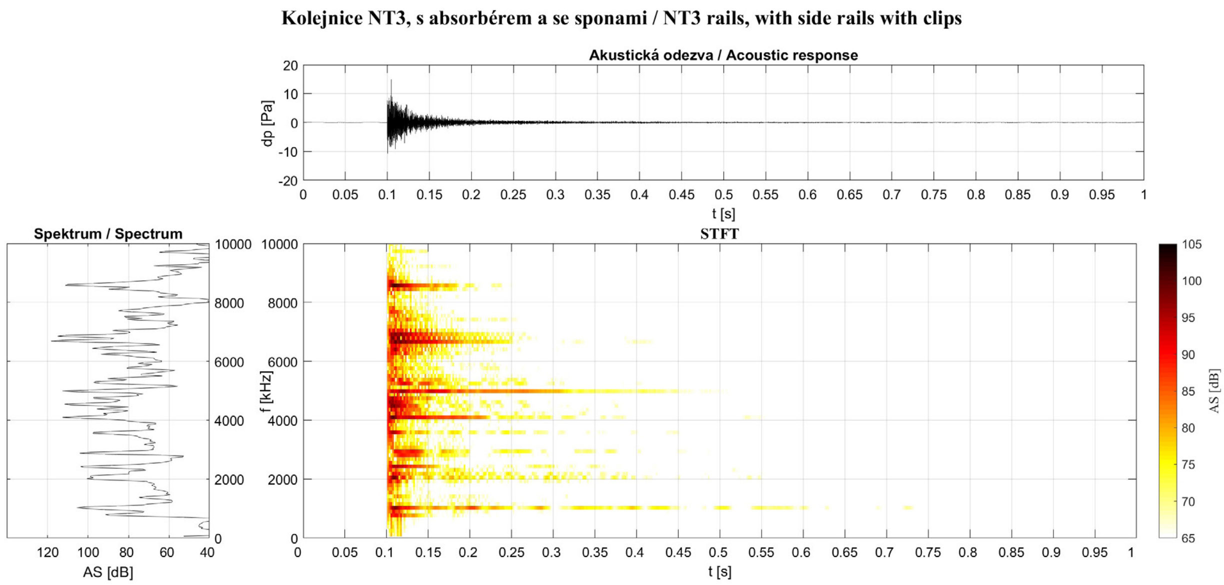

Fig. 5 Rail with absorber attached with steel clips

Obr. 5 Kolejnice s absorbérem uchyceným ocelovými sponami

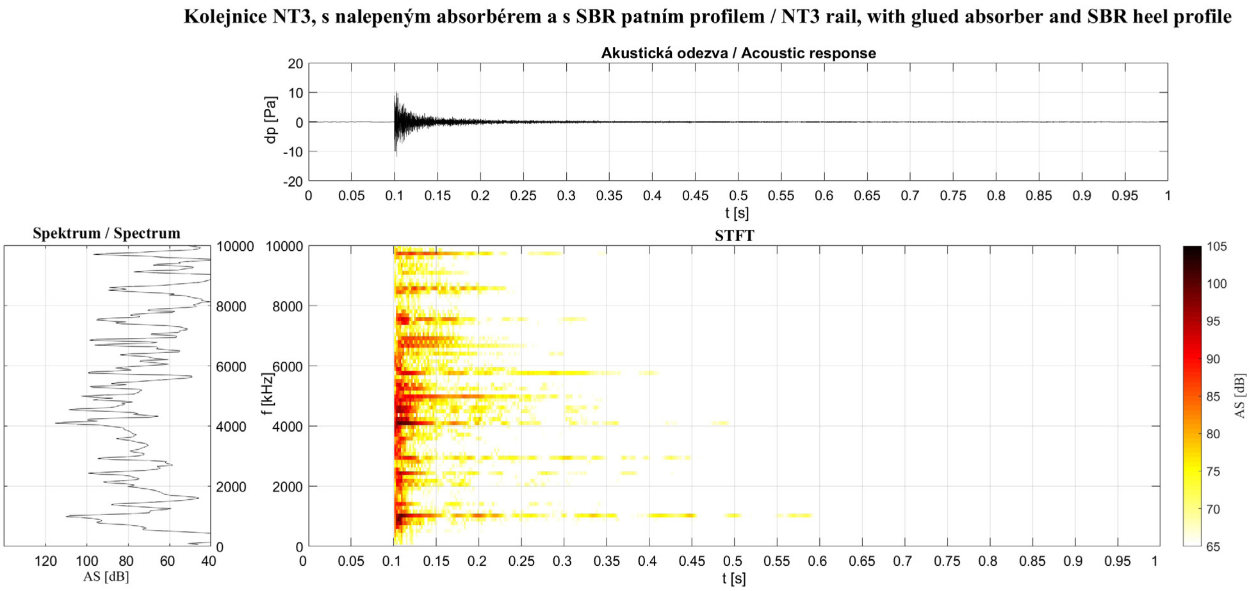

Fig. 6 Rail with glued absorber including SBR foot profile

Obr. 6 Kolejnice s nalepeným absorbérem včetně SBR patního profilu

In the future, the authors plan to expand the research by designing and implementing a large-scale model of a railway/tram track, which will allow for a more detailed study of vibration propagation, interaction of individual structural elements and evaluation of the effectiveness of various anti-vibration measures under laboratory conditions. Further development will also include the implementation of an electrodynamic exciter, which will enable precisely defined and repeatable excitation of the structure in a wide frequency range. The use of an electrodynamic exciter will provide the opportunity to perform advanced dynamic tests, identify natural frequencies and shapes of structural oscillations, determine frequency transfer functions and perform a detailed analysis of the effectiveness of the proposed anti-noise and anti-vibration measures. The experimental facility created in this way should contribute to a deeper understanding of the mechanisms of vibration generation and propagation in the railway infrastructure and at the same time enable verification of the results of numerical models and simulation calculations.

In future research, the authors also want to pay great attention to the development of modern methods of signal processing and analysis and their connection with artificial intelligence tools. The goal is to implement advanced methods of time, frequency and

Do budoucna autoři plánují rozšířit výzkum o návrh a realizaci velkoprostorového modelu železniční/tramvajové tratě, který umožní podrobnější studium šíření vibrací, interakce jednotlivých konstrukčních prvků a hodnocení účinnosti různých antivibračních opatření za laboratorních podmínek. Součástí dalšího vývoje bude rovněž implementace elektrodynamického budiče, jenž umožní přesně definované a opakovatelné buzení konstrukce v širokém frekvenčním rozsahu. Využití elektrodynamického budiče poskytne možnost realizovat pokročilé dynamické zkoušky, identifikaci vlastních frekvencí a tvarů kmitání konstrukce, stanovení frekvenčních přenosových funkcí a detailní analýzu účinnosti navržených protihlukových a protivibračních opatření. Takto vytvořené experimentální zařízení by mělo přispět k hlubšímu pochopení mechanismů vzniku a šíření vibrací v železniční infrastruktuře a současně umožnit ověřování výsledků numerických modelů a simulačních výpočtů.

Velkou pozornost chtějí autoři v budoucím výzkumu věnovat také rozvoji moderních metod zpracování a analýzy signálů a jejich propojení s nástroji umělé inteligence. Cílem je implementace pokročilých metod časové, frekvenční a časově-frekvenční analýzy, které umožní podrobnější identifikaci dynamických jevů probíhajících v železniční infrastruktuře. Současně bude pozornost zaměřena na time-frequency analysis, which will allow for a more detailed identification of dynamic phenomena occurring in the railway infrastructure. At the same time, attention will be focused on the use of machine learning methods and deep neural networks for automatic classification, anomaly detection, damage identification and prediction of the future technical condition of structures.

It is expected that the combination of modern signal analysis methods with artificial intelligence algorithms will significantly increase the accuracy of structural condition assessment, streamline the diagnostic process and create the prerequisites for the introduction of predictive maintenance systems for railway infrastructure. The result should be tools capable of automatically evaluating large volumes of measured data, identifying incipient degradation processes and providing support in decision-making on the optimal timing of maintenance and repairs. The process will be completed with a certified methodology.

využití metod strojového učení a hlubokých neuronových sítí pro automatickou klasifikaci, detekci anomálií, identifikaci poškození a predikci budoucího technického stavu konstrukcí.

Očekává se, že kombinace moderních metod signálové analýzy s algoritmy umělé inteligence umožní výrazně zvýšit přesnost hodnocení stavu konstrukcí, zefektivnit proces diagnostiky a vytvořit předpoklady pro zavedení systémů prediktivní údržby železniční infrastruktury. Výsledkem by měly být nástroje schopné automaticky vyhodnocovat rozsáhlé objemy měřených dat, identifikovat počínající degradační procesy a poskytovat podporu při rozhodování o optimálním načasování údržby a oprav. Daný proces bude zakončen zakončen certifikovanou metodikou.

REFERENCES/ POUŽITÁ LITERATURA

1. THOMPSON, D. J. Railway Noise and Vibration: Mechanisms, Modelling and Means of Control. Oxford: Elsevier, 2009. ISBN 978-0-08-045147-3.

2. THOMPSON, D. J. Railway Noise and Vibration. Amsterdam: Elsevier, 2009.

3. DUMITRIU, M.; CRUCEANU, I. C. On the Rolling Noise Reduction by Using the Rail Damper. Journal of Engineering Science and Technology Review, 2017, 10(6), s. 87–95.

4. HANSSEN, B.; JONES, C.; CROFT, J. Laboratory Methods for Testing the Performance of Acoustic Rail Dampers. In: Internoise Proceedings, 2013.

5. KUCHAK, A. J. T.; MARINKOVIC, D.; ZEHN, M. Parametric Investigation of a Rail Damper Design Based on a Lab-Scaled Model. Journal of Vibration Engineering & Technologies, 2021, 9(5), s. 1009–1024.

6. ZOONTJENS, L.; WELSH, A.; CROFT, J. Predicting and Managing Rolling Noise Emissions from Trains Using Rail Dampers. Proceedings of Acoustics Australia, 2017.

7. SUN, F. et al. Experimental Study on the Rail Damper for Vibration and Noise Reduction. Railway Engineering Science, 2025.

8. ISO 3095. Railway Applications – Acoustics – Measurement of Noise Emitted by Railbound Vehicles. Geneva: International Organization for Standardization.

9. EN 15461. Railway Applications – Noise Emission – Characterisation of the Dynamic Properties of Track Sections for Pass-By Noise Measurements.

10. SMUTNÝ J., PAZDERA L.: New Techniques in Analysis of Dynamic Parameters Rail

Fastening, InSight, The Journal of The British Institute of Non-Destructive Testing. Vol 46. No 10. October. 2004. pp. 612-615. ISSN 13542575.

Acknowledgements/ Poděkování

This contribution was supported by the project FAST-S-26-9099, Development of multimodal diagnostics of railway infrastructure using vibration analysis and visual identification of trainsets.

Tento příspěvek byl podpořen projektem FAST-S-26-9099, Rozvoj multimodální diagnostiky železniční infrastruktury využívající vibrační analýzu a vizuální identifikaci vlakových souprav.

Prof. Ing. Jaroslav Smutný, Ph.D.

He graduated from the Faculty of Electrical Engineering, TU Brno, specialisation technology of radio and communication devices. He works as a researcher-teacher at the Department of railway constructions and structures. He was graduated Ph.D. at the specialisation Theory of structures (Ph.D. thesis Modern Method of Noise and Vibration Analysis Applied on Railway Structures). College lecturer – 2002 ("Time Frequency Analysis of Constructional Structures and Materials"). 2009 - Professor – Constructions and Transport Structures. He is member of Czech association for geo-information, Czech acoustic society and Time frequency user club. Within the framework of the scientific and research and pedagogical activities he devotes his activities especially to the problems of geographical information systems, the experimental analysis of structures, the analysis of noise and vibrations, the problems of applying the methods of the artificial intelligence in experimental analysis of structures, the modelling of structures etc.

e-mail: smutny.j@fce.vutbr.cz

Prof. Ing. Pazdera, CSc.

He graduated from Technical University of Brno. Since 2009 he is a professor. He is the Member of the Czech Association for Non-Destructive Testing - a professional group for Acoustic Emission and the member of the RS 07 regional group committee. Since 1988, he is on The Department of Physics, Faculty of Civil Engineering, Brno University of Technology. He is in charge of theoretical exercises and laboratory sessions in Physics. He is conducting research and development in the field of physical phenomenon measurement and measurement automation, with particular focus on the application of computers in measurements and evaluation. His research is focused on the acoustic and vibration areas.

He published over 40 papers in foreign periodicals, in the field of engineering source signal measurement and analysis, dealing above all, with nondestructive testing, noise and vibrations.

e-mail: pazdera.l@fce.vutbr.cz

Milan Štukavec

He graduated from the Faculty of Civil Engineering, TU Brno, specialisation Structural design. He gained his Ph.D. in the specialisation Theory of structures (Ph.D. thesis Mitigating Noise and Vibrations Using Recycled Elastomers). Certified Engineer in the field of Statics and Dynamics of Structures. Court expert in the field of Structural Engineering. A member of the Czech Chamber of Authorized Engineers and Technicians. He has been working as a structural engineer at Manhire Associates, K2 project and ZIPP Brno. Several projects of concrete railway structures with strong interest in experimental analysis and measuring real behaviour and response of the structures.

Akustika, odborný časopis o akustice a vibracích
Šéfredaktorka: Ing. Jana Dolejší (Studio D-akustika s.r.o., České Budějovice, Česká republika)

Redakce a administrace:	Studio D- akustika, s. r. o., U Sirkárny 467/2a, 370 04 České Budějovice
Adresa webové schránky:	www.journalakustika.com,
e-mailová adresa:	akustikad@akustikad.com,
Vydává:	Studio D-akustika, s. r. o., České Budějovice,
Distribuce:	online

Registrace: ISSN 2570-8775 (Online), MK ČR E 18950